Smart Materials and Structures

**TOPICAL REVIEW**

# A review of modeling techniques for advanced effects in shape memory alloy behavior

IOP Publishing
Smart Materials and Structures
Smart Mater. Struct. 25 (2016) 103001 (36pp)
doi:10.1088/0964-1726/25/10/103001

Topical Review

# A review of modeling techniques for advanced effects in shape memory alloy behavior

**Cheikh Cisse[1], Wael Zaki[1] and Tarak Ben Zineb[1,2,3]**

[1] Khalifa University of Science, Technology, and Research, PO Box 127788, Abu Dhabi, UAE
[2] Université de Lorraine, LEMTA, UMR 7563, Vandoeuvre-lès-Nancy F-54500, France
[3] CNRS, LEMTA, UMR 7563, Vandoeuvre-lès-Nancy F-54500, France

E-mail: cheikh.cisse@kustar.ac.ae, wael.zaki@kustar.ac.ae and tarak.ben-zineb@univ-lorraine.fr

Received 20 October 2015, revised 14 February 2016
Accepted for publication 14 March 2016
Published 16 September 2016

**Abstract**

The paper reviews and discusses various techniques used in the literature for modeling complex behaviors observed in shape memory alloys (SMAs) that go beyond the core pseudoelastic and shape memory effects. These behaviors, which will be collectively referred to herein as 'secondary effects', include mismatch between austenite and martensite moduli, martensite reorientation under nonproportional multiaxial loading, slip and transformation-induced plasticity and their influence on martensite transformation, strong thermomechanical coupling and the influence of loading rate, tensile–compressive asymmetry, and the formation of internal loops due to incomplete phase transformation. In addition, because of their importance for practical design considerations, the paper discusses functional and structural fatigue, and fracture mechanics of SMAs.

Keywords: shape memory alloys, modeling, review

(Some figures may appear in colour only in the online journal)

## 1. Introduction

Early models for shape memory alloys (SMAs) focused exclusively on their pseudoelastic and shape memory effects (Tanaka 1986, Liang and Rogers 1990), which constitute the most prominent and well-studied features of SMA behavior. A review of constitutive models accounting for these effects was presented by e.g. Lagoudas *et al* (2006), Lexcellent (2013) and more recently by Cissé *et al* (2016).

In addition to the core pseudoelastic and shape memory effects, experimental observations reveal a number of secondary effects that are important to consider for a realistic description of SMA behavior. The techniques used for modeling these effects are the subject of a rich body of knowledge that we attempt to summarize and discuss in the present manuscript.

A common assumption of early SMA models, such as (Liang and Rogers 1990), is that austenite and martensite share the same elastic stiffness. However, experimental work by Ford and White (1996) and more recently Šittner *et al* (2014) and Zhu *et al* (2014) suggests that austenite can be twice as stiff as martensite. This issue is mostly addressed nowadays by the introduction of equivalent elastic stiffness measures for SMAs that depend on the phase fraction of martensite (Zaki and Moumni 2007a, Zhou 2012, Auricchio *et al* 2014, Savi 2015). Moreover, experimental work on SMAs led to the observation of tensile–compressive asymmetry (Wasilewski 1971, Orgéas and Favier 1995), which, while similar to some extent, is unrelated to the Bauschinger effect observed in some metals. An explanation was given according to which different mechanisms of energy dissipation are active in tension and compression. This explanation motivated the derivation of constitutive models featuring unsymmetric loading surfaces and evolution rules for phase transformation depending on the loading direction. The asymmetric stress–strain behavior of SMAs results in asymmetric dissipation of energy in a loading cycle, which is further influenced by the loading rate (Shaw and Kyriakides 1995). This influence is interpreted as the consequence of viscous effects or of strong thermomechanical coupling, with experiemtnal evidence favoring the latter intepretation (Van Humbeeck and Delaey 1981, Leo *et al* 1993, Grabe and Bruhns 2008, He and Sun 2010). The amount of dissipated energy, as well as other features of SMA behavior, is dependent on the type of martensite obtained during phase transformation, which many authors dissociated into thermal-induced and stress-induced fraction (Bekker and Brinson 1998, Popov and Lagoudas 2007). The behavior is also senstive to changes in local load orientation, which result in detwinning and reorientation of martensite variants and has attracted significant interest to modeling SMAs subjected to nonproportional loading conditions (Arghavani *et al* 2010, Yu *et al* 2015). The dissipative processes involved in the reorientation and transformation of martensite, as well as plastic deformation of the SMA, result in significant heat exchange that may have observable consequences on SMA response through thermomechanical coupling. In particular, the amount of energy dissipated by the material in a complete loading cycle is relatedto the size of the hysteresis loop. The loop is largest if the loading cycle leads to complete martensite transformation followed by full recovery, otherwise minor loops may form (Ivshin and Pence 1994, Bouvet *et al* 2004, Nascimento *et al* 2009). On the other hand, the influence of plasticity results from slip dislocations interfering with the phase change process (Strnadel *et al* 1995, Auricchio *et al* 2007a). This influence is especially significant in SMAs subjected to cyclic loading in which transformation-induced plasticity (TRIP) is responsible for the formation of residual stress and strain fields at the origin of the two-way shape memory effect (TWSME). It is also important in high-temperature SMAs (HTSMAs) (Hartl *et al* 2010, Chemisky *et al* 2014) and in iron-based SMAs (Fe-SMAs) in which slip dislocation severely impedes or suppresses the formation and recovery of inelastic strains due to phase transformation (Nishimura and Tanaka 1998, Jemal *et al* 2009, Khalil *et al* 2012). In addition to the secondary effects introduced above, the structural behavior of SMAs is affected by the presence of structural defects, such as cracks where the near-field loading is strongly non-proportional and presents strong gradients (Freed and Banks-Sills 2007, Wang 2007, Creuziger *et al* 2008, Maletta *et al* 2009, Ramaiah *et al* 2011, Baxevanis *et al* 2014, Hazar *et al* 2015, Moumni *et al* 2015). It is also influenced by the degradation, referred to as functional fatigue, of SMA performance under the influence of repeated cyclic loading which may preceed fatigue-induced failure (Moumni 1995, McKelvey and Ritchie 2001, Wagner *et al* 2004, Runciman *et al* 2011).

The present review of secondary effects in SMAs and their models is organized into topical sections: section 2 addresses modeling techniques to account for variable elastic stiffness in SMAs, section 3 discusses the separation of thermal and mechanical effects and martensite reorientation, section 4 considers the influence of loading rate and TRIP on phase transformation, section 5 focuses on thermomechanical coupling, section 6 on tensile–compressive asymmetry, section 7 on modeling hysteresis subloops, and the last two sections that preceed the conclusion are dedicated to modeling fracture and fatigue in SMAs.

## 2. Dependence of the elastic stiffness on phase transformation

Most of the early models for SMAs consider identical elastic stiffnesses for austenite and martensite in order to simplify the derivation of constitutive equations and their subsequent time integration (Liang and Rogers 1990, Leclercq and Lexcellent 1996, Huang and Brinson 1998, Souza *et al* 1998). Experimental evidence, however, shows significant variation in stiffness between the two phases. For instance, the ratio of Young's modulus of austenite $E_A$ to that of martensite $E_M$ is reported to be in the range [2, 3] for NiTi alloys (Thamburaja and Anand 2001, Helbert *et al* 2014, Šittner *et al* 2014, Zhu *et al* 2014) and up to 5 if one considers twinned martensite in $Ni_{55}Ti_{45}$ (Ford and White 1996). This observation is generally accounted for in constitutive models through the introduction of an effective Young's modulus $E_{eq}$ for the SMA that depends on the volume fraction of martensite $\xi$ such that $E_{eq} = E_A$ for $\xi = 0$ and $E_{eq} = E_M$ for $\xi = 1$. The equivalent modulus is constructed using homogenization schemes, the most common of which are those of Reuss, Voigt and Mori–Tanaka (Auricchio and Sacco 1997).

The Reuss model (Reuss 1929) considers the SMA as a composite in which austenite and martensite are arranged in series. In this case, the effective Young's modulus for the alloy is given by

$$\frac{1}{E_{eq}^{R}} = \frac{1-\xi}{E_A} + \frac{\xi}{E_M}. \tag{1}$$

This model was adopted among others by Ivshin and Pence (1994), Auricchio *et al* (2003), Ikeda *et al* (2004), Zaki and Moumni (2007a), Auricchio *et al* (2008, 2009), Morin *et al* (2011a), Lagoudas *et al* (2012), Meraghni *et al* (2014), Mehrabi *et al* (2014a) and Depriester *et al* (2014). Sedlak *et al* (2012) and Auricchio *et al* (2014) used the same bulk modulus for austenite, twinned martensite and oriented martensite but considered a Reuss equivalent shear modulus $G_{eq}^{R}$ for the SMA given by

$$\frac{1}{G_{eq}^{R}} = \frac{1-\xi_T-\xi_\sigma}{G_A} + \frac{\xi_T}{G_T} + \frac{\xi_\sigma}{G_\sigma}, \tag{2}$$

where $G_A$ is the shear modulus of austenite, $G_T$ is the shear modulus of temperature-induced martensite of volume fraction $\xi_T$ and $G_\sigma$ is the shear modulus of stress-induced martensite (SIM) of volume fraction $\xi_\sigma$.

The Voigt model (Voigt 1889), on the other hand, was utilized by Tanaka (1986), Sato and Tanaka (1988) and Liang (1990). It considers austenite and martensite to be arranged in strips parallel to the loading direction. The effective Young's modulus of the SMA is then given by

$$E_{\mathrm{eq}}^{\mathrm{V}} = (1 - \xi)E_{\mathrm{A}} + \xi E_{\mathrm{M}}. \tag{3}$$

This model was used among others by Brinson (1993), Bo and Lagoudas (1999), Yan *et al* (2003), Zhao *et al* (2005), Wang *et al* (2008), and Zhou (2012). Savi *et al* (2002) and Paiva *et al* (2005) used the Voigt scheme for the determination of both the elastic and plastic moduli of the SMA. The same model was also utilized by Savi (2015) who extended the work of Paiva *et al* (2005) to describe nonlinear dynamics and chaos in SMA oscillators and vibration absorbers. While the Voigt scheme may be easier to implement, the underlying assumption of parallel arrangement of austenite and martensite strips in a volume element of SMA is not supported by experimental evidence. In addition, the Voigt and Reuss schemes assume either uniform strain or stress fields in a volume element, thereby ignoring grain interactions that are accounted for in more advanced homogenization methods such as Mori–Tanaka.

The Mori–Tanaka scheme considers the SMA as a metal matrix of one phase containing Eshelby inclusions of the other phase (Auricchio and Sacco 1997). In this case, the equivalent elastic modulus is given by

$$E_{\mathrm{eq}}^{\mathrm{MT}} = \frac{E_{\mathrm{A}}E_{\mathrm{M}}}{2}\left[\frac{(1 - \xi) + \xi E^{\mathrm{MA}}}{E_{\mathrm{M}}(1 - \xi) + \xi E^{\mathrm{MA}}E_{\mathrm{A}}} + \frac{(1 - \xi)E^{\mathrm{AM}} + \xi}{E_{\mathrm{M}}(1 - \xi)E^{\mathrm{AM}} + \xi E_{\mathrm{A}}}\right], \tag{4}$$

where

$$E^{\mathrm{MA}} = \frac{E_{\mathrm{M}}}{E_{\mathrm{A}} + p(E_{\mathrm{M}} - E_{\mathrm{A}})} \text{ and } E^{\mathrm{AM}} = \frac{E_{\mathrm{A}}}{E_{\mathrm{M}} + p(E_{\mathrm{A}} - E_{\mathrm{M}})} \tag{5}$$

In (4), $p$ is a parameter depending on the geometry of the inclusion. For example, $p = \frac{1}{2}$ for penny-shaped inclusions and $p = \frac{4 - 5\nu}{15(1 - \nu)}$ for spherical inclusions, where $\nu$ is Poisson's ratio considered to be identical for both phases. This scheme is accurate for values of the volume fraction of martensite $\xi < 0.2$, corresponding to martensite inclusions in an austenite matrix, or $\xi > 0.8$, corresponding to austenite inclusions in a martensite matrix. Among others, Gong *et al* (2011) used an extended Mori–Tanaka scheme to predict the effective elastic modulus of CuAlMn SMA with oriented oblate spheroid pores. Auricchio and Sacco (1997) compared the predictions of the Reuss and Mori–Tanaka schemes to experimental data taken from Auricchio (1995) and reported better accuracy using the Reuss model as shown in figure 1(b). It can also be seen in figure 1(a) that the Reuss scheme gives a lower bound on the effective elastic modulus, whereas the Voigt scheme gives an upper bound. The homogenization models described above, lose accuracy in case of highly anisotropic materials, for which accurate averaging requires more statistical information. It is also worth noting that most SMA constitutive models consider higher elastic stiffness for austenite, which appears to be in contradiction with first-principles calculations (Wagner and Windl 2008, Hatcher *et al* 2009, Saitoh and Liu 2009) and *in situ* neutron diffraction measurements (Rajagopalan *et al* 2005, Qiu *et al* 2011), both of which predicting higher stiffness for martensite. In this regard, Wang and Sehitoglu (2014) recently used density function theory calculations to prove that austenite is stiffer than twinned martensite but softer than oriented martensite. The lower stiffness of twinned martensite used in modeling SMAs therefore corresponds to an apparent measure, affected by detwinning and other deformation processes that give the impression of lower martensite stiffness (Wagner and Windl 2008). It may be important, in addressing this issue in constitutive models, to distinguish twinned and oriented martensite as separate phases.

## 3. Decoupling between transformation and reorientation processes

Early models for SMAs, such as the work of Tanaka (1986), use a single scalar variable to represent the amount of martensite in a SMA volume element. Experimental evidence, however, shows that the macroscopic transformation strain in SMAs is due to SIM ($M_\sigma$) and is not affected by the formation of self-accommodated variants ($M_{\mathrm{T}}$). In order to accomodate this observation, Brinson (1993) proposed an additive split of the total martensite volume fraction $\xi$ into temperature-induced and stress-induced parts, $\xi_{\mathrm{T}}$ and $\xi_\sigma$, such that

$$0 \leqslant \xi_{\mathrm{T}} \leqslant 1, \; 0 \leqslant \xi_\sigma \leqslant 1, \text{ and } 0 \leqslant \xi = \xi_\sigma + \xi_{\mathrm{T}} \leqslant 1. \tag{6}$$

Brinson's approach was adopted by Brinson and Lammering (1993), Leclercq and Lexcellent (1996), Bekker and Brinson (1998), Auricchio and Sacco (1999) and Lagoudas and Shu (1999). It was then further improved by Govindjee and Kasper (1999), Paiva *et al* (2005) and Rizzoni and Marfia (2015) who wrote the volume fraction of oriented martensite as the sum of tension-induced and compression-induced fractions, $\xi_\sigma^{\mathrm{t}}$ and $\xi_\sigma^{\mathrm{c}}$. Using these two scalar variables, however, may be insufficient to properly account for change in the transformation flow direction, which may require specifying distinct flow rules for forward and reverse transformations (RTs). For example, Boyd and Lagoudas (1996) considered the rate of inelastic strain in forward phase transformation to be proportional to the deviatoric stress. In order to avoid having no phase transformation at zero stress, the authors defined an alternate flow direction for RT. Later, Popov and Lagoudas (2007) developed a 3D model in which additive split is applied to the rate of total inelastic strain $\dot{\varepsilon}^{\mathrm{ine}}$, written as the sum of phase transformation and martensite orientation parts, $\dot{\varepsilon}^{\mathrm{tr}}$ and $\dot{\varepsilon}^{\mathrm{ori}}$, such that

$$\dot{\varepsilon}^{\mathrm{ine}} = \dot{\varepsilon}^{\mathrm{tr}} + \dot{\varepsilon}^{\mathrm{ori}}. \tag{7}$$

In a subsequent work, Arghavani *et al* (2010) extended the model of Souza *et al* (1998) by introducing a multiplicative split of the inelastic strain tensor into a magnitude $q$ and an

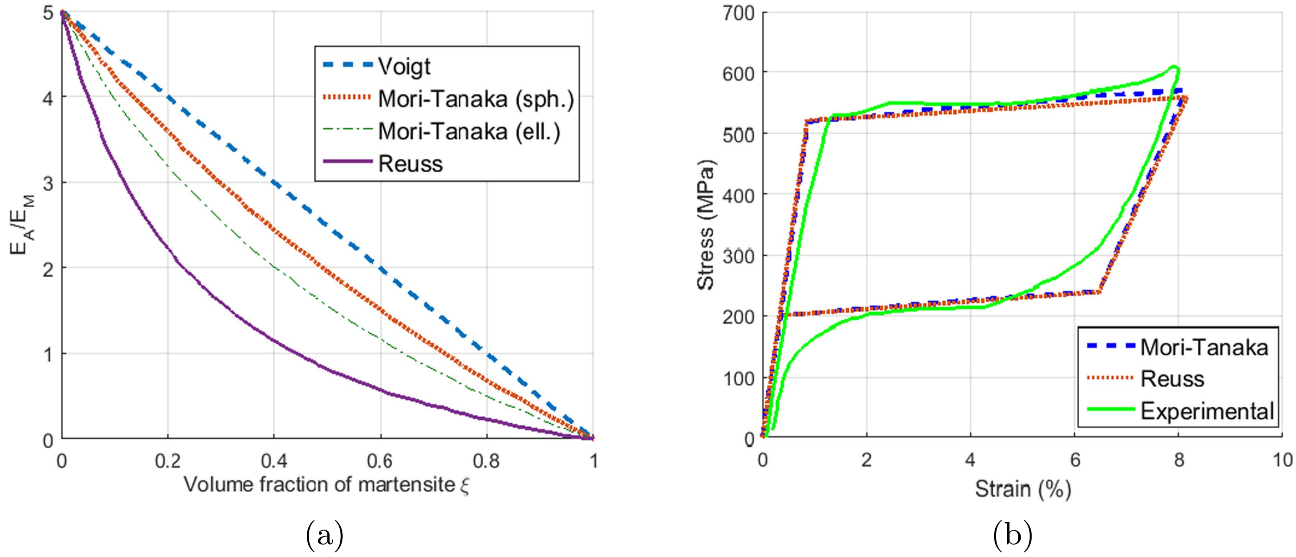


**Figure 1.** Comparison and validation of different homogenization schemes used for the determination of an equivalent SMA Young's modulus (Auricchio and Sacco 1997). (a) Evolution of the normalized equivalent Young's modulus with respect to Young's modulus of martensite during phase transformation for $E_A/E_M = 5$. (b) Validation of the Mori–Tanaka and Reuss schemes for a Ni–Ti SMA.

orientation direction $\boldsymbol{N}$ whereby

$$\varepsilon^{\text{ine}} = q\boldsymbol{N}, \text{ where } q = \|\varepsilon^{\text{ine}}\| \text{ and } \|\boldsymbol{N}\| = 1. \tag{8}$$

This expression leads to a rate equation for $\varepsilon^{\text{ine}}$ similar to (7) where $\dot{\varepsilon}^{\text{tr}}$ and $\dot{\varepsilon}^{\text{ori}}$ are given by

$$\dot{\varepsilon}^{\text{tr}} = \dot{q}\boldsymbol{N} \text{ and } \dot{\varepsilon}^{\text{ori}} = q\dot{\boldsymbol{N}}. \tag{9}$$

An interpretation of the above equation is that the amount of martensite is only influenced by pure phase transformation, while the average spacial alignment of the martensite variants is governed by pure reorientation. More recently, Chemisky *et al* (2011) proposed an additive split of the inelastic strain into transformation and twin accommodation contributions, given by $\xi\bar{\varepsilon}^{\text{tr}}$ and $\xi\bar{\varepsilon}^{\text{twn}}$. A common limitation of these models is the assumption of small perturbations. In an attempt to address this limitation, finite strain models that distinguish reorientation and detwninning processes were proposed by Thamburaja (2005) and Thamburaja *et al* (2005). The numerical implementation for this work, however, was carried out using an explicit time integration procedure, which raises issues of stability and dependence of time increments on mesh size for convergence. This dependence can result in prohibitive computation times for finely meshed structures or those subjected to a lengthy loading program. A further limitation is the common disregard for dislocation slip and the formation of martensite pinned by plasticity. This was addressed in the work of Yu *et al* (2014b, 2015). In particular, Yu *et al* (2015) separated the total SMA inelastic strain into a recoverable transformation part $\varepsilon^{\text{tr}}_{\text{rec}}$, an irrecoverable transformation part $\varepsilon^{\text{tr}}_{\text{irr}}$ due to the presence of trapped martensite, a reorientation part $\varepsilon^{\text{reo}}$ and a plastic part $\varepsilon^{\text{pl}}$. Considering 24 possible martensite variants, the authors defined $\varepsilon^{\text{reo}}$ as follows:

$$\varepsilon^{\text{reo}} = \sum_{j>i}^{24}\sum_{i=1}^{23}\lambda^{ij}g^{\text{tr}}(\boldsymbol{P}^i - \boldsymbol{P}^j), \tag{10}$$

where $g^{\text{tr}}$ is the shearing magnitude related to phase transformation, and $\lambda^{ij}$ is the amount of deformation induced during the transition from the $j$th to the $i$th martensite variants, for which the orientation tensors are noted $\boldsymbol{P}^j$ and $\boldsymbol{P}^i$ respectively. The detwinning strain was defined as follows:

$$\varepsilon^{\text{det}} = \sum_{j=1}^{24}\xi^j(\lambda^j - \lambda^j_0)\boldsymbol{P}^{\text{det}}_j, \tag{11}$$

where $\xi^j$ is the total volume fraction of the $j$th martensite variant, $\lambda^j - \lambda^j_0$ is the transformation fraction between the two sub-variants, and $\boldsymbol{P}^{\text{det}}_j$ is the orientation tensor for the $j$th detwinning system. The microscopic forms of (10) and (11) are analytically and numerically ill-adapted to the analysis of polycrystalline SMAs. Therefore, the authors used the $\beta$-rule scale-transition initially proposed by Cailletaud and Pilvin (1994) and simplified by Yu *et al* (2013) to derive a constitutive model for SMA polycrystals. Under the assumption of uniform stress, the local stress $\boldsymbol{\sigma}$ in a given grain is obtained from the uniform macroscopic stress $\boldsymbol{\Sigma}$ as follows:

$$\boldsymbol{\sigma} = \boldsymbol{\Sigma} + D(\boldsymbol{E}_{\text{in}} - \varepsilon_{\text{in}}), \tag{12}$$

where $\boldsymbol{E}_{\text{in}}$ is the volume average inelastic strain in the polycrystal, and $D$ is a parameter that controls the heterogeneity of the stress field across grains. The use of a scalar $D$ in (12) suggests that the authors implicitly ignored possible anisotropy, which would have required replacing $D$ with a higher-order tensor. Because of the complexity of the inelastic deformation process in SMAs , the decomposition of inelastic strain into parts corresponding to different inelastic

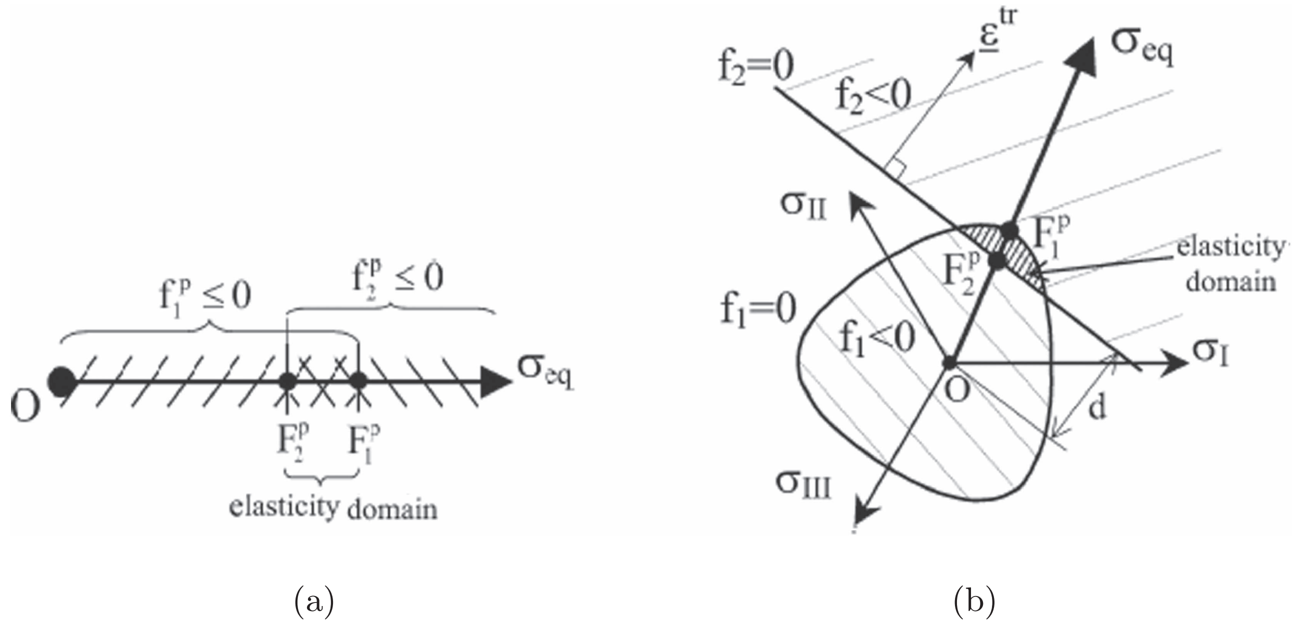


**Figure 2.** Comparison of the forward ($f_1$) and reverse ($f_2$) transformation onset surfaces for proportional and nonproportional loading cases according to (Bouvet *et al* 2004). (a) Proportional multiaxial loading case. (b) Nonproportional multiaxial loading case.

deformation mechanisms appears to be useful for proper description of the behavior of SMAs under complex loading.

Experimental results for SMAs subjected to nonproportional loading are reported by Šittner *et al* (1995) and Rogueda *et al* (1996) for Cu-based alloys, Lim and McDowell (1999), Helm and Haupt (2001) and Raniecki *et al* (2001) for NiTi, (Vivet and Lexcellent 1999) for biaxial tension on CuZnAl and (Bouvet *et al* 2002) for biaxial compression on CuAlBe. In order to account for the observations made in these papers, constitutive models for SMAs were developed to consider both phase transformation and martensite reorientation. Souza *et al* (1998) developed one of the first pseudoelastic constitutive models that account for nonproportional loading. The authors successfully simulated the experimental results of Šittner *et al* (1995) considering a rectangular tension–torsion path but the stress–strain response in shear was not captured properly. Panico and Brinson (2007) also used a square axial/shear stress path and compared the coupling between axial and shear responses in elasto-plastic materials to that in SMAs, which they found to be more pronounced. Building on experimental data and physical considerations, Bouvet *et al* (2004) proposed dual loading surfaces for phase transformation and reorientation where the loading surface for RT is perpendicular to the transformation strain (figure 2(b)). Numerical simulation using this model requires non-standard tracking of the two loading surfaces and the corresponding flow rules, which may be challenging.

Arghavani *et al* (2010) simulated the experimental results of Šittner *et al* (1995) and compared the simulations to earlier work by Auricchio and Petrini (2002) and Panico and Brinson (2007). The results of Panico and Brinson (2007) were found to be more accurate in shear while those of Arghavani *et al* (2010) were better in describing the shear versus axial strain behavior. Saleeb *et al* (2011) simulated the reorientation of martensite in response to combined tension and shear without providing experimental validation. The experimental observations of Grabe and Bruhns (2009) for NiTi were later simulated by Zaki (2012). More recently, Gu *et al* (2015) used the ZM model to simulate several sets of experimental data for SMAs subjected to square, rectangular, triangular and butterfly loading paths. The authors obtained good agreement with the experimental data of Šittner *et al* (1995) for CuZnAlMn, Bouvet *et al* (2002) and Bouvet *et al* (2004) for CuAlBe and Grabe and Bruhns (2009) for NiTi. The numerical simulations presented assume a limitation on the analytical ZM model, which leads to full orientation of martensite by the external stress as soon as martensite forms The authors further compared their results with those of Panico and Brinson (2007) and Arghavani *et al* (2010) for the case of rectangular loading. Figure 3(a) shows that Gu *et al* (2015) obtained better accuracy in simulating the axial versus shear strain behavior, which is not the case in pure axial behavior (see figure 3(b)). Figure 3(c) shows that the simulations of Gu *et al* (2015) are less accurate than those of Panico and Brinson (2007) but more so than Arghavani *et al* (2010) in describing pure shear in CuAlZnMn.

Bouvet *et al* (2004) considered the triangular loading path in figure 4(a), for which the simulation results were shown to agree to different degrees with experimental data as seen in figures 4(b), (c) and (d). Figure 4(b), in particular, shows significant deviation from experimental data.

Helm and Haupt (2003) simulated to good accord the experiments of Helm (2001) for a SMA subjected to a butterfly loading path. Later, Auricchio *et al* (2007b) simulated the behavior of a NiTi SMA subjected to five cycles of biaxial square and hourglass loading. Simulations involving an hourglass loading path were also proposed by Arghavani *et al*

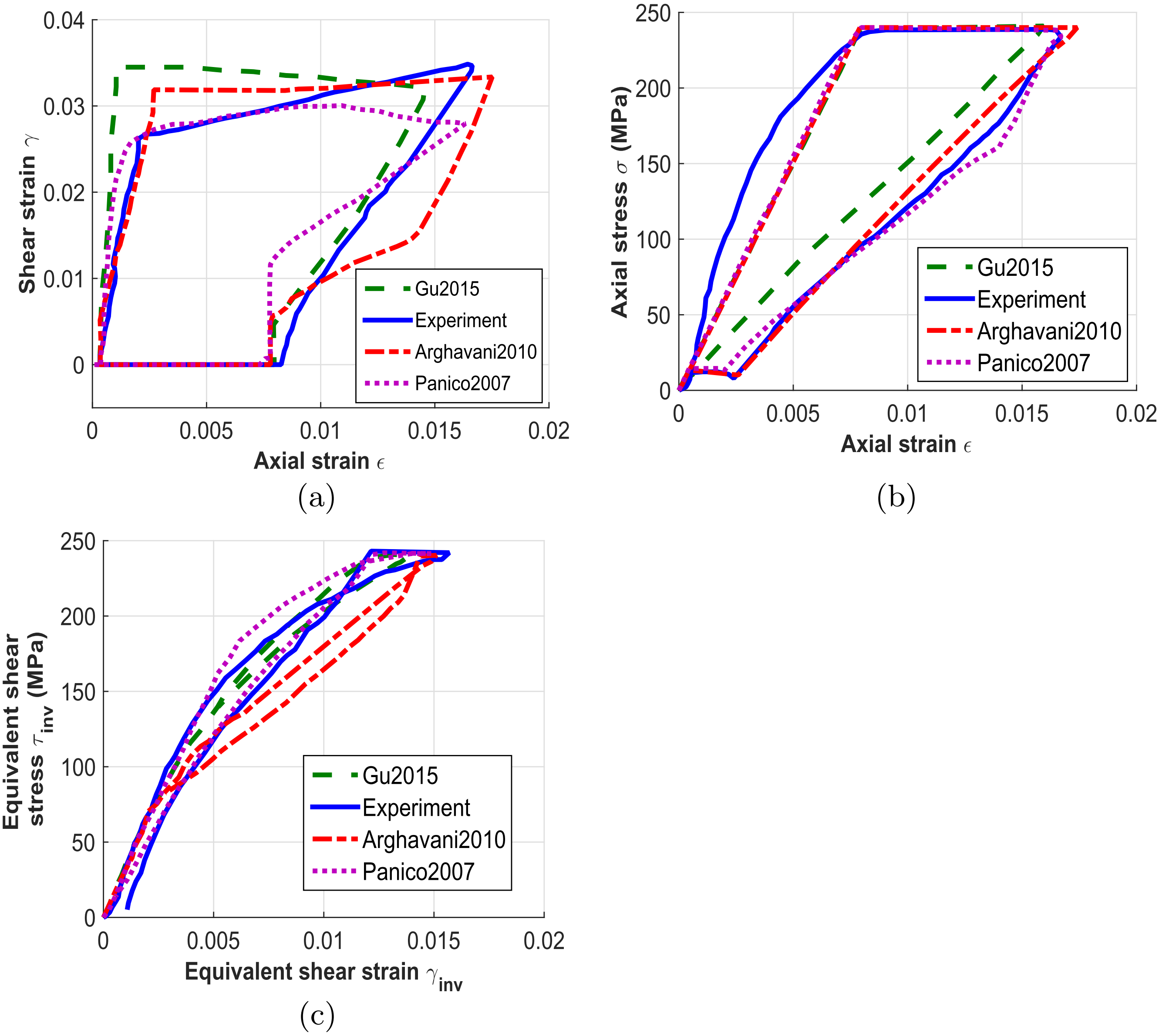


**Figure 3.** Comparison between the simulations of Gu *et al* (2015), Arghavani *et al* (2010), Panico and Brinson (2007) and the experimental data of Šittner *et al* (1995) for CuAlZnMn SMA. (a) Axial versus shear strain. (b) Axial stress–strain response. (c) Shear stress versus shear strain.

(2011). In this work, complete pseudoelastic strain recovery was achieved for a temperature $T = A_f + 37$ °C (see figure 5(a)), while the simulation for $T = M_f$ shows residual inelastic strain (see figure 5(b)) that can be recovered by heating. These simulations were not experimentally validated.

SMA simulations using circular nonproportional loading were carried out by Helm and Haupt (2003) and Mehrabi *et al* (2014b). The results of (Helm and Haupt 2003) reported in figure 6(b) show eight points where the direction of the transformation strain rate is abruptly modified because of stress redistribution in the material. The simulated stress response in figure 6(b) further displays a phase shift compared to the strain-controlled loading case in figure 6(a). Moreover, the model could not capture the deviation from an ideal circle observed in the experimental results of Lim and McDowell (1999). Such deviation was simulated by Saleeb *et al* (2011), in addition to the numerical observations of Helm and Haupt (2003).

More recently, Yu *et al* (2014b) properly investigated hourglass, butterfly and octagonal nonproportional tension-shear loading cases for SMAs capable of permanent plastic strain. In the special case of some SMAs such as Fe–Mn–Si, however, this feature becomes irrelevant since the martensite variants cannot be reoriented because of energy gaps between the variants that are higher than the plastic gliding energy.

## 4. TRIP, slip plasticity and training

Detwinning and plastic deformation are both dissipative and mostly shear-driven deformation processes. A key difference, however, is that the former mechanism occurs by lattice

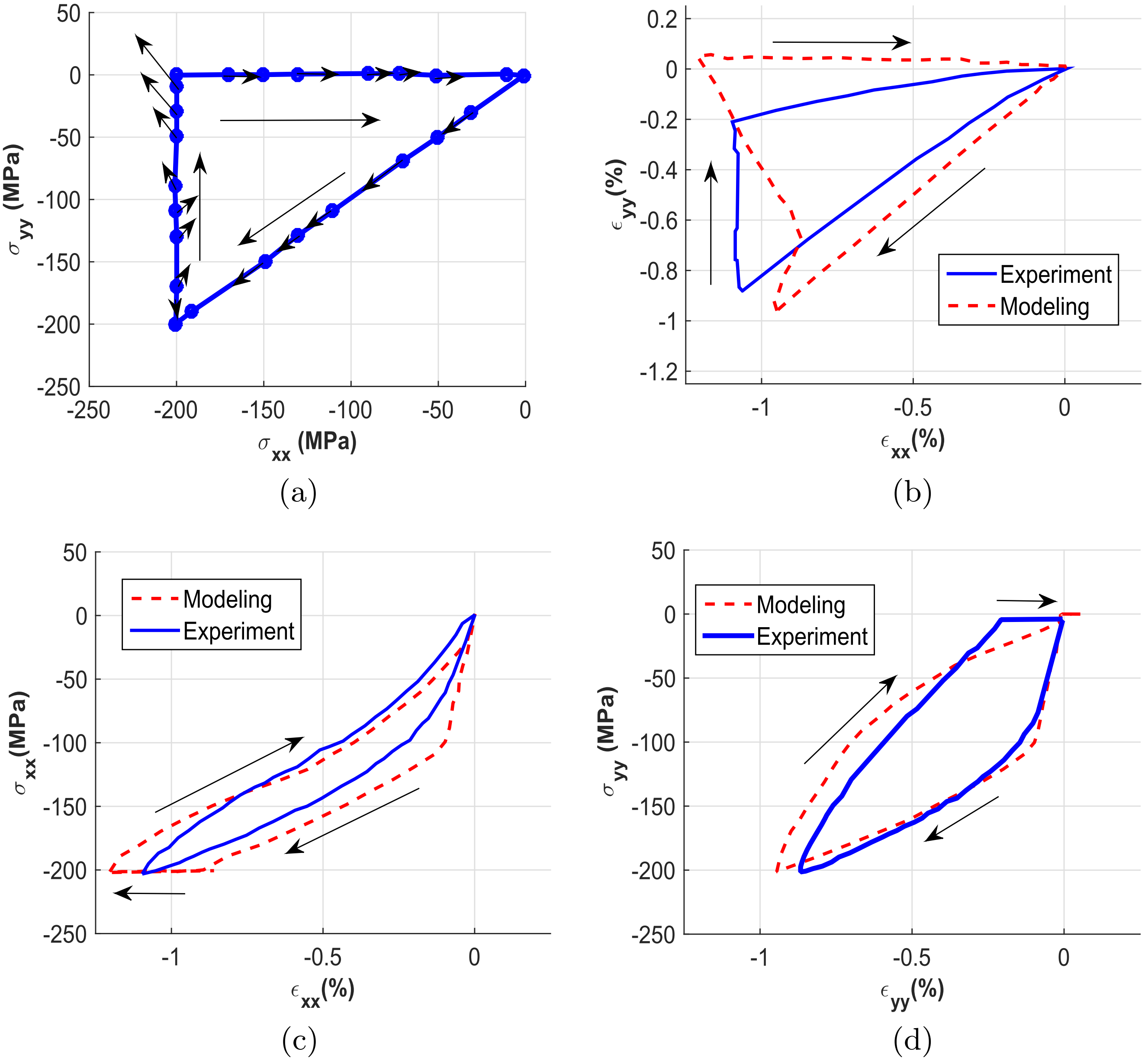


**Figure 4.** Simulation of SMA subjected to nonproportional biaxial compression tests at $T = 35$ °C (Bouvet *et al* 2004). (a) Triangular loading path for modeling. (b) $\epsilon_{11}$ versus $\epsilon_{22}$ behavior. (c) $\epsilon_{11}$ versus $\sigma_{11}$ behavior. (d) $\epsilon_{22}$ versus $\sigma_{22}$ behavior.

change without alteration to neighboring atoms, while the latter does involve such alteration. The resulting plastic strain cannot be recovered, unlike the strain due to phase transformation and detwinning. The experimental investigations of Strnadel *et al* (1995), Sehitoglu *et al* (2001) and Gall and Maier (2002) showed that plastic strain accumulates in pseudoelastic nitinol subjected to cyclic loading. Plastic deformation in this case does not require exceeding the yield strength of either phase but only that local stress fields at the austenite–martensite interface become sufficiently high to cause localized slip dislocations. Such plastic deformation is termed 'transformation-induced' or TRIP and the accompanying formation of residual stress fields is used to explain the observed stabilization of a fraction of martensite during unloading (Lexcellent and Bourbon 1996, Auricchio *et al* 2003, Yan *et al* 2003, Kumar and Lagoudas 2010). The activation of plasticity was found to interfere with forward phase transformation in Fe-based SMAs at higher temperatures (Kajiwara 1999) and with RT in NiTi (McKelvey and Ritchie 2001). Auricchio and Reali (2007) also showed that plastic deformation decreases the transformation stress in NiTi wires during cyclic loading (see figure 7(a)). Kato and Sasaki (2013) further showed that solutionized austenitic nitinol has a narrow temperature interval in which both phase transformation and TRIP are activated at the same critical stress but with a loss in shape memory effect exceeding 60%. During cyclic loading, plastic deformation was found to pin certain martensite variants and prevent their RT to austenite, thereby reducing the amount of recoverable inelastic strain. In Fe-based SMAs, Nishimura *et al* (1998) and Nishimura and

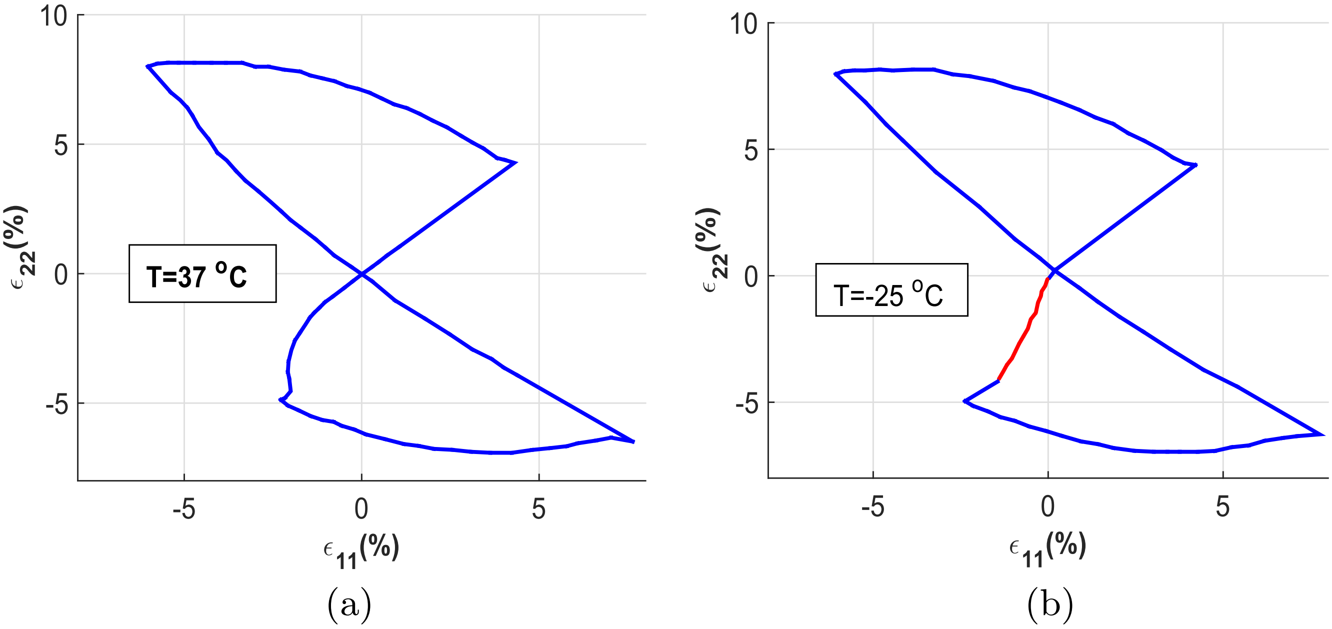


**Figure 5.** Simulation of the hourglass biaxial test (Arghavani *et al* 2011). (a) $\epsilon_{11}$ versus $\epsilon_{22}$ at $T = A_f + 37$ °C. (b) $\epsilon_{11}$ versus $\epsilon_{22}$ at $T = M_f$.

Tanaka (1998) showed that the relaxation of stress concentration at the tips of martensite plates by means of slip or martensite reorientation can prevent complete shape recovery even if the RT is completed. For Fe–30Mn–(6 − $x$)Si–$x$Al, $x$ = mass%, Koyama *et al* (2008) reported 4% recoverable strain, which could be improved by 0.3% and 3% respectively for $x = 1$ and $x = 3$ by means of training. Reversible TRIP was reported for the same alloy for $x = 0$ by Sawaguchi *et al* (2008) under alternating tension and compression. The competing effects of phase transformation and plasticity in Fe-based SMAs were recently investigated by Khalil *et al* (2013) who proposed a coupled constitutive model for the alloy and plotted the stress–temperature phase diagram shown in figure 7(b). The figure shows that plastic deformation in Fe-based SMAs is favored with increasing temperature and stress at the expense of phase transformation, with similar results reported by Hartl and Lagoudas (2009) for NiTi.

In modeling plastic deformation in SMAs, a common approach is to consider an additive split of the total strain $\varepsilon$ featuring a plastic strain term $\varepsilon^{\mathrm{pl}}$ such that the elastic strain tensor $\varepsilon^{\mathrm{el}}$ is given by

$$\boldsymbol{\varepsilon}^{\mathrm{el}} = \boldsymbol{\varepsilon} - \boldsymbol{\varepsilon}^{\mathrm{tr}} - \boldsymbol{\varepsilon}^{\mathrm{pl}} - \boldsymbol{\alpha}_{\mathrm{T}}(T - T_0), \tag{13}$$

where $\varepsilon^{\mathrm{tr}}$ is the transformation strain, $\boldsymbol{\alpha}_{\mathrm{T}}$ is the second-order matrix of thermal expansion coefficients and $T_0$ is a reference temperature. The evolution of strain due to plastic slip is usually accounted for by means of a generalized plasticity theory and associative flow rules. In this context, Yan *et al* (2003) used the von Mises isotropic hardening theory to describe plasticity in NiTi. Feng and Sun (2007) used a similar approach to analyze the shakedown of SMA structures. The authors found that depending on geometry, loading mode and constitutive relations, the load-bearing capacity of a SMA structure can be increased or reduced as a consequence of phase transformation. Hartl and Lagoudas (2009) proposed the following plastic flow rule:

$$\dot{\boldsymbol{\varepsilon}}^{\mathrm{pl}} = \frac{3}{2}\|\dot{\varepsilon}^{\mathrm{pl}}\|\frac{\mathrm{dev}(\boldsymbol{\sigma} - \boldsymbol{\beta})}{\|\boldsymbol{\sigma} - \boldsymbol{\beta}\|_{\mathrm{VM}}}, \tag{14}$$

where the back stress $\boldsymbol{\beta}$ is such that $\dot{\boldsymbol{\beta}}$ varies linearly with $\dot{\varepsilon}^{\mathrm{pl}}$. Zhou (2012) proposed a different plastic strain expression based on a linear hardening model whereby

$$\dot{\boldsymbol{\varepsilon}}^{\mathrm{pl}} = H(\sigma_{\mathrm{vm}}, \sigma_{\mathrm{y}})(\boldsymbol{S}^{\mathrm{pl}} - \boldsymbol{S}^{\mathrm{el}}) : \dot{\boldsymbol{\sigma}}. \tag{15}$$

In this equation, $H(\sigma_{\mathrm{vm}}, \sigma_{\mathrm{y}})$ is the Heaviside function that takes a value of 1 when the von Mises stress $\sigma_{\mathrm{vm}}$ is greater than the plastic yield strength $\sigma_{\mathrm{y}}$, zero otherwise, and $\boldsymbol{S}^{\mathrm{el}}$ and $\boldsymbol{S}^{\mathrm{pl}}$ are the elastic and plastic compliance tensors, respectively. Recently, Wang *et al* (2014a) used the PeierlsNabarro (PN) formulation with a sinusoidal series representation of generalized stacking fault energy to numerically investigate the dislocation slip in different SMAs. The authors obtained good agreement with the experimental results for Peierls stresses in NiTi, CuZn, $Ni_2TiHf$, $Ni_2FeGa$, $Co_2NiAl$ and $Co_2NiGa$. On the micromechanical scale, the crystalline structure needs to be considered. Body-centered cubic crystals display 24 slip systems formed by the 12 primary slip systems obtained from the six primary slip planes of type {110}, each presenting two slip directions of type ⟨111⟩, and the 12 secondary slip systems ⟨111⟩ (110) and ⟨111⟩ (112) (Franz *et al* 2009). In face-centered cubic structures, 12 slip systems form along the close-packed plane of type {111}, and in the ⟨110⟩ directions. Finally, in hexagonal close packed crystals, slip occurs only on the densely packed basal {0001} planes in the ⟨1120⟩ directions. Therefore there exists only three independent slip systems on the basal planes for random plasticity, except if additional slip or twin systems are activated.

In their micromechanical models, Wang *et al* (2008) considered only one [100] (001) slip system and eleven

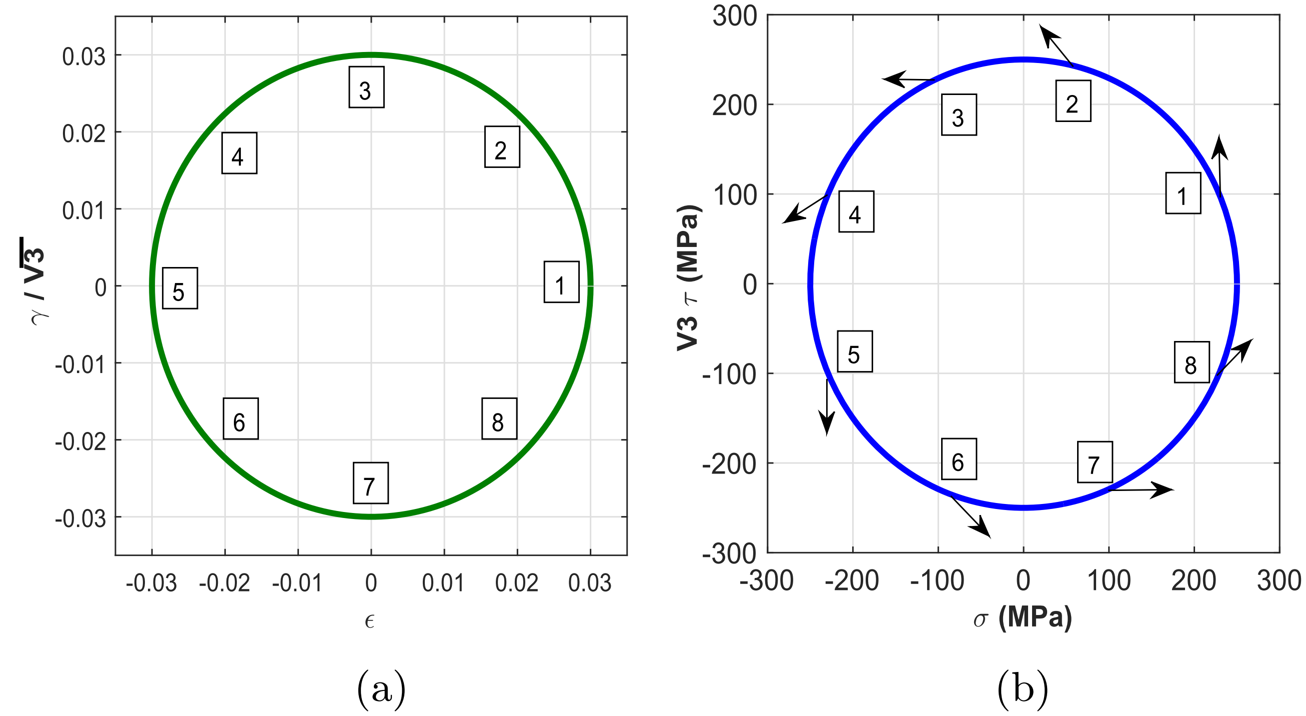


**Figure 6.** NiTi SMA subjected to circular loading (Helm and Haupt 2003). (a) Circular loading path. (b) Stress response to nonproportional circular loading.

deformation twinning modes. The average plastic strain rate in NiTi was expressed as follows:

$$\dot{\varepsilon}^{\mathrm{pl}} = (1-\xi)\boldsymbol{P}^{(s)}\dot{\gamma}^{(s)} + \sum_{i=1}^{11}\boldsymbol{P}^{(i)}\dot{\gamma}_{\mathrm{tw}}^{(i)}, \tag{16}$$

where $\boldsymbol{P}^{(s)}$ and $\boldsymbol{P}^{(i)}$ represent the directions of the shear caused by slip and twinning, $\dot{\gamma}^{(s)}$ is the shear rate of slip and $\dot{\gamma}_{\mathrm{tw}}^{(i)}$ is the shear rate of the $i$th twin system. The model was shown to capture the stabilization of martensite and the obstruction of reverse phase transformation due to plasticity. This approach is limited to a single slip system in martensite and ignores plastic slip in austenite. The limitation was addressed in the work of Yu *et al* (2012) who considered all 12 primary slip systems in the austenitic phase of NiTi and considered a rate of plastic strain given by

$$\dot{\varepsilon}^{\mathrm{pl}} = (1-\xi)\sum_{s=1}^{12}\boldsymbol{P}^{(s)}\dot{\gamma}^{(s)} \tag{17}$$

and proposed an associated plastic strain hardening energy given by the integral

$$\Phi_{\mathrm{pl}} = \int_0^{\mathrm{tr}}\sum_{s=1}^{12}R^{(s)}|(1-\xi)\dot{\gamma}^{(s)}|\mathrm{d}t, \tag{18}$$

where $R^{(s)}$ describes the isotropic slip resistance. This model does not consider plasticity in martensite and is only valid in a limited temperature range where plastic gliding in the product phase can be neglected. A more general approach was proposed by Yu *et al* (2014b) who considered 12 primary slip systems in austenite and 11 twinning systems in martensite.

With regard to TRIP in SMAs, Fischlschweiger and Oberaigner (2012) developed a mean-field model accounting for nonproportional loading in which the macroscopic TRIP strain is defined as follows:

$$\varepsilon^{\mathrm{pl}} = (1-\xi)\bar{\varepsilon}_{\mathrm{A}}^{\mathrm{pl}} + \xi\bar{\varepsilon}_{\mathrm{M}}^{\mathrm{tp}}, \tag{19}$$

where $\bar{\varepsilon}_{\mathrm{A}}^{\mathrm{pl}}$ and $\bar{\varepsilon}_{\mathrm{M}}^{\mathrm{pl}}$ are the average plastic strains in the austenite and martensite phases. In general, TRIP strain is commonly expressed in terms of parameters and variables related to the number of loading cycles. For example, Bo and Lagoudas (1999) proposed the following expression for the TRIP strain magnitude:

$$|\varepsilon^{\mathrm{tp}}| = \left[\left(\frac{d_0}{d_1}\right)^{r_1+1} + (r_1+1)\left(\frac{\sigma}{d_1}\right)^{r_1}\zeta^{\mathrm{dtw}}\right]^{\frac{1}{r_1+1}} - \frac{d_0}{d_1}, \tag{20}$$

where $d_0$ is the resistance to plastic deformation, $d_1$ accounts for strain hardening, $\zeta^{\mathrm{dtw}}$ is the accumulated volume fraction of martensite considered proportional to the number of cycles, and $r_1$ controls the rate of plastic strain. In this work, the magnitude of plastic strain was found to decrease during cyclic torsional loading without considering the saturation of plastic strain observed by Strnadel *et al* (1995). This limitation was addressed by Lagoudas and Entchev (2004) who considered TRIP strain to be proportional to the rate of accumulated detwinned martensite volume fraction $\zeta^{\mathrm{dtw}}$ such that

$$\dot{\varepsilon}^{\mathrm{tp}} = \dot{\zeta}^{\mathrm{dtw}}\boldsymbol{\Lambda}^{\mathrm{tp}}, \tag{21}$$

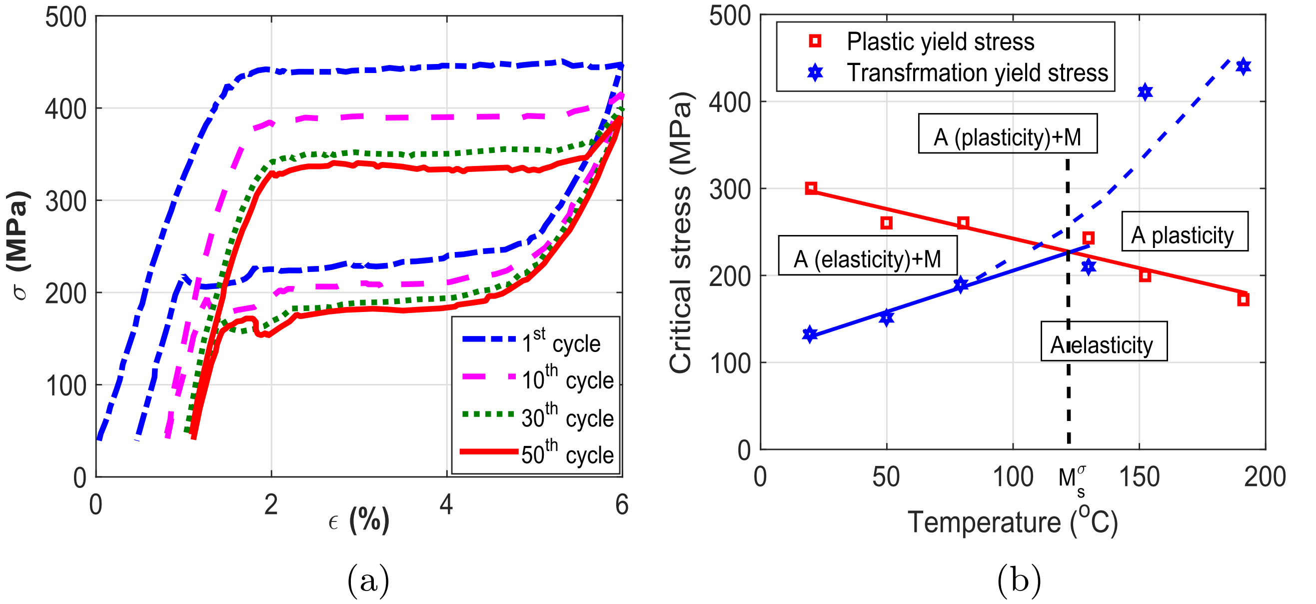


**Figure 7.** Cyclic stress–strain behavior and phase diagram in presence of plastic deformation. (a) Influence of plastic deformation on phase transformation stress and residual strain (Auricchio and Reali 2007). (b) Stress–temperature diagram for an Fe-based SMA Khalil *et al* (2013).

where the flow direction $\Lambda^{\rm tp}$ takes different values for forward and reverse phase transformations, as follows:

$$\Lambda^{\rm tp}_{\rm fwd} = \sqrt{\frac{3}{2}}C_1^{\rm tp}\frac{\mathrm{dev}(\boldsymbol{\sigma}+\boldsymbol{\beta})}{\mathrm{dev}(\boldsymbol{\sigma}+\boldsymbol{\beta}):\mathrm{dev}(\boldsymbol{\sigma}+\boldsymbol{\beta})}\exp\left(-\frac{\zeta^{\rm dtw}}{C_2^{\rm tp}}\right),$$
$$\Lambda^{\rm tp}_{\rm rev} = \sqrt{\frac{3}{2}}C_1^{\rm tp}\frac{\mathrm{dev}(\varepsilon^{\rm tr}_{\rm max})}{\varepsilon^{\rm tr}_{\rm rev}:\varepsilon^{\rm tr}_{\rm rev}}\exp\left(-\frac{\zeta^{\rm dtw}}{C_2^{\rm tp}}\right). \tag{22}$$

In these expressions, the parameters $C_1^{\rm tp}$ and $C_2^{\rm tp}$ govern number of cycles to saturation and the saturation rate, and $\varepsilon^{\rm tr}_{\rm rev}$ is the transformation strain on load reversal. An alternative expression for the TRIP direction during forward phase transformation was proposed by Hartl *et al* (2010) who defined the direction tensor $\Lambda^{\rm tp}$ as

$$\Lambda^{\rm tp} = f^{\rm tp}(\bar{\sigma})\mathrm{sgn}(\dot{\xi})\frac{3}{2}\frac{\mathrm{dev}(\boldsymbol{\sigma})}{\sigma_{\rm vm}}, \tag{23}$$

where $f^{\rm tp}$ is a quadratic function of the von Mises effective stress. Expressions in (22) are similar to those in (Lim and McDowell 1994), with the only difference that $\zeta^{\rm dtw}$ is replaced with the total volume fraction of martensite. They were recently modified by Chemisky *et al* (2014) to account for cyclic actuation of high temperature shape memory alloys (HTSMAs) with the assumption that TRIP strain may not always saturate. The modified equations are given by

$$\Lambda^{\rm tp}_{\rm fwd} = \sqrt{\frac{3}{2}}\frac{\mathrm{dev}(\boldsymbol{\sigma})}{\|\mathrm{dev}(\boldsymbol{\sigma})\|}w_1\left(C_0^{\rm tp}+C_1^{\rm tp}\exp\left(-\frac{\zeta^{\rm dtw}}{C_2^{\rm tp}}\right)\right)\frac{H^{\rm cur}}{H^{\rm sat}},$$
$$\Lambda^{\rm tp}_{\rm rev} = \sqrt{\frac{3}{2}}\frac{\mathrm{dev}(\varepsilon^{\rm tr}_{\rm rev})}{\|\varepsilon^{\rm tr}_{\rm rev}\|}(1-w_1)\times\left(C_0^{\rm tp}+C_1^{\rm tp}\exp\left(-\frac{\zeta^{\rm dtw}}{C_2^{\rm tp}}\right)\right)\frac{H^{\rm cur}}{H^{\rm sat}}, \tag{24}$$

where $C_0^{\rm tp}$ is a parameter that accounts for ratcheting effects, $w_1$ is the ratio of the TRIP strain generated during forward transformation to the one obtained in a complete loading cycle and $H^{\rm cur}$ is the transformation strain magnitude, which takes a maximum value $H^{\rm sat}$. In their micromechanical model, Yu *et al* (2013) and Yu *et al* (2014a) neglected the dislocation plasticity but considered the TRIP to occur by friction slip along the 24 systems at the interfaces between the austenite and martensite variants. The same approach was used by Yu *et al* (2015) who additionally considered the reorientation-induced plastic (ROIP) and defined the following rates of TRIP strain $\varepsilon^{\rm tp}$ and ROIP strain $\varepsilon^{\rm rp}$:

$$\varepsilon^{\rm tp} = \sum_{i=1}^{24}\gamma_i^{\rm tp}\boldsymbol{P}^i,$$
$$\varepsilon^{\rm rp} = \sum_{i=1}^{24}\bar{\gamma}_i^{\rm rp}\boldsymbol{P}^i, \tag{25}$$

where $\gamma_i^{\rm tp}$ is the TRIP magnitude and $\bar{\gamma}_i^{\rm rp}$ is the effective ROIP magnitude at the interface between austenite and the $i$th martensite twin system. The plastic deformation and martensitic transformation are dissipative processes that can influence the mechanical response of SMAs by means of thermomechanical coupling.

Hartl and Lagoudas (2009) introduced a plastic back stress tensor $\boldsymbol{\beta}$ that modifies the phase transformation conditions by shifting the critical transformation stress such that the effective stress tensor in the transformation flow rule becomes

$$\boldsymbol{\sigma}^{\rm tr}_{\rm eff} = \boldsymbol{\sigma}+\boldsymbol{\beta}. \tag{26}$$

The following Gibbs free energy term was consequently introduced to account for the influence of back stress and the coupling between phase transformation and plasticity:

$$G_\alpha^{\rm pl} = -\frac{1}{\rho}\left[(\boldsymbol{\sigma} - \boldsymbol{\beta}) : \boldsymbol{\varepsilon}^{\rm pl} + \frac{\boldsymbol{\beta} : \boldsymbol{\beta}}{2H_\alpha}\right] - \dot{\xi}\boldsymbol{\beta} : \boldsymbol{\Lambda}^{\rm tr}, \tag{27}$$

where $H_\alpha$ is the kinematic hardening modulus of phase $\alpha = \{{\rm A, M}\}$. Auricchio *et al* (2007a) and Auricchio and Reali (2007) introduced a simpler expression considering kinematic hardening and explicit coupling between plasticity and phase transformation given by

$$\frac{H_{\rm pl}}{2}\ \|\boldsymbol{\varepsilon}^{\rm pl}\|^2 - A_{\rm cpl}\,{\rm dev}(\boldsymbol{\varepsilon}^{\rm tr}) : \boldsymbol{\varepsilon}^{\rm pl}, \tag{28}$$

where $H_{\rm pl}$ controls the evolution of residual inelastic strain and $A_{\rm cpl}$ is a material parameter. The authors simulated the saturation of plastic strain (see figure 8(b)) as well as the degradation of the mechanical response of the material (see figure 8(c)). An alternative expression for the strain energy density $\Psi_\alpha^{\rm hd}$ due to plastic deformation of the different phases was proposed by Frémond (1987), Savi *et al* (2002) and Paiva *et al* (2005) such that

$$\rho\Psi_\alpha^{\rm hd} = \frac{1}{2}K_\alpha(\gamma_{\rm pl})^2 + \frac{1}{2}H_\alpha(\mu_{\rm pl})^2, \tag{29}$$

where $\alpha$ represents either austenite or martensite that can be twinned or detwinned in tension or compression, $K_\alpha$ and $H_\alpha$ are hardening parameters and $\gamma_{\rm pl}$ and $\mu_{\rm pl}$ are linear functions of the plastic strain and phase fractions. Zaki *et al* (2010b) modified the ZM model to account for plastic deformation considering linear kinematic hardening in NiTi where plastic deformation is governed by the condition

$$\left\|\boldsymbol{\sigma} - \frac{2}{3}H_{\rm pl}\boldsymbol{\varepsilon}^{\rm pl}\right\|_{\rm VM} \leqslant \sigma_{\rm y}, \tag{30}$$

$\sigma_{\rm y}$ being the yield strength. The results in figure 9 show that plastic deformation was simulated better at ambient temperature than in the pseudoelastic range ($T = 40$ °C). The problem in the above equations is that the dissipation due to plasticity and its interaction with phase transformation is assumed to be linear, which is not consistent with experimental observations. Following Jemal *et al* (2009), Khalil *et al* (2012) considered plastic yielding in Fe-SMAs to occur exclusively in the austenitic phase. They accounted for nonlinear hardening using the following intergranular and intragranular interaction energies:

$$\begin{aligned}\Phi_{\rm intergranular} &= \frac{1}{2}\frac{H_{\rm grn}}{(n_{\rm g}+1)}(\boldsymbol{\varepsilon}^{\rm ine} : \boldsymbol{\varepsilon}^{\rm ine})^{n_{\rm g}+1},\\ \Phi_{\rm intragranular} &= \frac{H_{\rm v}}{(n_{\rm v}+1)}\xi^{n_{\rm v}+1}\\ &\quad + (1-\xi)\frac{H_{\rm s}}{(n_{\rm s}+1)}\gamma^{n_{\rm s}+1} - \frac{H_{\rm sv}}{(n_{\rm sv}+1)}(\xi\gamma)^{n_{\rm sv}+1}\end{aligned} \tag{31}$$

where $H_{\rm v}$, $H_{\rm s}$, and $H_{\rm sv}$ are parameters that govern hardening due to phase transformation, plastic gliding and the interaction between martensite variants and slip systems, $H_{\rm grn}$ accounts for interactions between grains, and $n_{\rm g}$, $n_{\rm v}$, $n_{\rm s}$ and $n_{\rm sv}$ are hardening exponents. Using the experimental data of Baruj *et al* (2010), the authors concluded that only phase transformation occurs at low temperature while plasticity is activated at high temperature and both processes are simultaneously active in the intermediate temperature range. The nonlinear stress–strain curve was accurately simulated during loading (see figure 10). However, the model does not account for nonlinear unloading at elevated temperature or for residual martensite trapped by plastic slip. The amount of martensite pinned by the residual mechanical fields that develop during cyclic loading was modelled by Auricchio *et al* (2003) by means of an irrecoverable martensite volume fraction $\xi_{\rm irr}$ given by

$$\xi_{\rm R} = \xi_{\rm u}[1 - \exp(-b_{\rm u}\gamma^{\rm AM})], \tag{32}$$

where $\xi_{\rm u}$ is the maximum value of $\xi$ achievable by training, $b_{\rm u}$ measures the training ability of the material, and $\gamma^{\rm AS}$ is given by $\dot{\gamma}^{\rm AS} = |\dot{\xi}_\sigma|$. The authors validated their numerical results against the experimental data of Castellano (2000) as shown in figure 11. In this figure, exponential variations of the residual martensite volume fraction $\xi_{\rm irr}$ and forward transformation start stress $\sigma_{\rm s}^{\rm AS}$ are observed with the accumulation of forward and RT strains, $g^{\rm AS}$ and $g^{\rm SA}$, which stabilize after 20 cycles for $\xi_{\rm R}$ and $\sigma_{\rm s}^{\rm AS}$. It can be noted that the results in figure 11(b) are less accurate that those in figure 11(a). An alternative expression for $\xi_{\rm irr}$ was proposed by Yan *et al* (2003) and Zhou (2012), given by the following relation:

$$\xi_{\rm irr} = \frac{\|\boldsymbol{\varepsilon}^{\rm pl}\|}{\varepsilon_{\rm crit}^{\rm pl}}, \tag{33}$$

where $\varepsilon_{\rm crit}^{\rm pl}$ is a critical value of the magnitude of plastic strain $\|\boldsymbol{\varepsilon}^{\rm pl}\|$. More recently, Chemisky *et al* (2014) expressed the rate of the volume fraction $\xi_{\rm irr}$ in HTSMAs as

$$\dot{\xi}_{\rm irr} = \begin{cases} wC_1^{\rm R}\exp\left(-\dfrac{\zeta^{\rm dtw}}{C_2^{\rm R}}\right)\dot{\zeta}^{\rm dtw} & \text{for } \dot{\xi} > 0,\\[2ex] (1-w)C_1^{\rm R}\exp\left(-\dfrac{\zeta^{\rm dtw}}{C_2^{\rm R}}\right)\dot{\zeta}^{\rm dtw} & \text{for } \dot{\xi} < 0,\end{cases} \tag{34}$$

where $w$ and $C_2^{\rm R}$ are material parameters and $C_1^{\rm R}$ is a function of the effective stress. An exponential variation of $\xi_{\rm irr}$ was also proposed by Yu *et al* (2014a) who considered an explicit additive split of the total martensite volume fraction into recoverable and irrecoverable parts, $\xi_{\rm rec}$ and $\xi_{\rm irr}$, where $\xi_{\rm irr}$ varies exponentially with $\xi_{\rm rec}$.

The development of residual stress fields and pinned martensite during cyclic loading allows autonomous shape recovery of SMAs during temperature-driven phase transformations, which gives rise to the well known TWSME (Bo and Lagoudas 1999, Lexcellent *et al* 2000, Lagoudas and Entchev 2004, Paiva *et al* 2005, Falvo *et al* 2008). Unlike one-way shape memory, TWSME is an acquired behavior in SMAs, with early work on the subject due to Perkins (1974), Miyazaki *et al* (1981), Liu and McCormick (1990), Rogueda *et al* (1991) and Stalmans *et al* (1992). The TWSME is generally induced by means of a so-called 'training' process consisting in subjecting the material to cyclic loading at temperatures lower than $M_0^{\rm f}$ or greater than $T > A_0^{\rm f}$ (Schroeder and Wayman 1977, Cingolani *et al* 1995, Pons

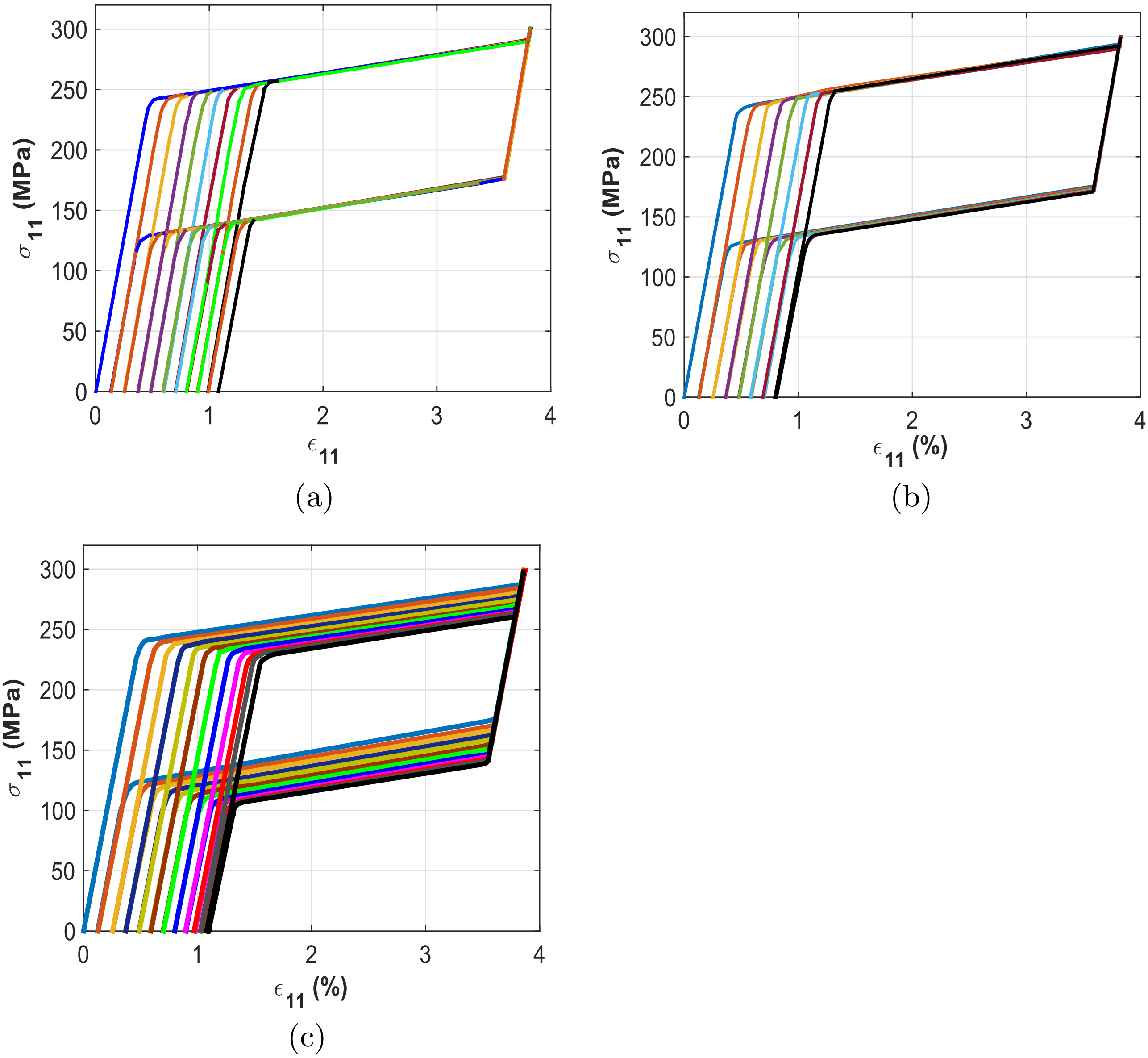


**Figure 8.** Cyclic stress–strain curves considering coupling between phase transformation and plasticity (Auricchio *et al* 2007a). (a) Tensile loading cycles for $H_{pl} = 0$ MPa, $A_{cpl} = 0$ MPa and $T = 298$ K. (b) Tensile loading cycles for $H_{pl} = 1.5 \times 10^4$ MPa, $A_{cpl} = 0$ MPa and $T = 298$ K. (c) Tensile loading cycles for $H_{pl} = 1.5 \times 10^4$ MPa, Acpl $= 2 \times 10^3$ MPa and $T = 298$ K.

*et al* 1999). It can also be induced by deformation of SIM at $T > M_s$ (Delaey *et al* 1974) or by the creation of precipitates in the material (Oshima and Naya 1978, Amengual *et al* 1995, Guilemany and Fernández 1995). The physical mechanism responsible for the development of TWSME in trained SMAs was explained by Perkins and Sponholz (1984), Contardo (1988), Tadaki *et al* (1988), Lovey *et al* (1995) and De Araujo (1999) as follows: unrecovered strain at the end of each loading cycle accumulates during training until saturation; the resulting permanent dislocations, defects and residual stress stabilize a fraction of the martensite plates that are then identically recreated during subsequent transformations, thus producing macroscopic strain. This allows a trained SMA to switch configurations between stable austenite and oriented martensite phases by heating or cooling without requiring additional external loading. If the orientation of martensite during cooling is facilitated by external stress, the resulting behavior is called assisted two-way shape memory effect (ATWSME) or superthermal effect. The adjunction of external stress favors the nucleation of oriented martensite variants, cooling the material then produces macroscopic inelastic strain that is recoverable by heating above $A_f$ (Kim 2004, 2005). Models for TWSME were proposed, among others, by Rogueda *et al* (1991), Hebda and White (1995), Bo and Lagoudas (1999), Lexcellent *et al* (2000), Auricchio *et al* (2003) and Zaki and Moumni (2007b). Lexcellent *et al* (2000) extended the model of Leclercq and Lexcellent (1996) by adding a training energy term $\Phi_{ed}$ derived under the assumption that $\Phi_{ed}$ is constant for constant stress $\sigma_{ed}$ and equal to zero for non-trained SMA or for

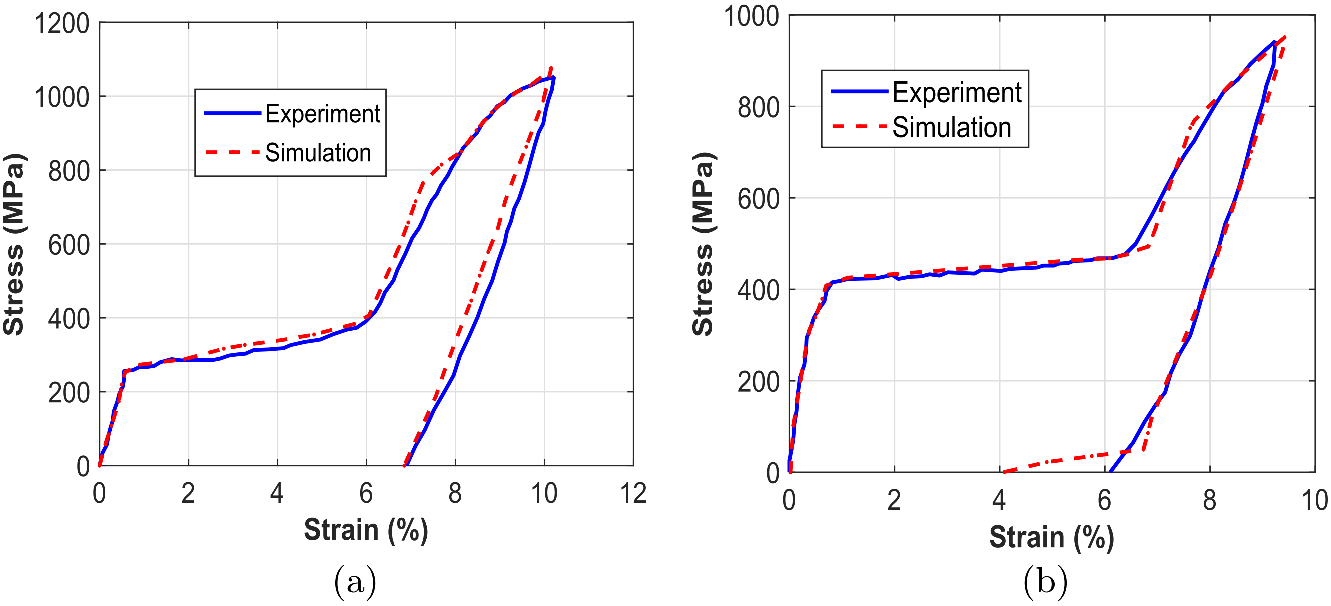


**Figure 9.** Simulated versus experimental stress–strain behavior considering plastic deformation in NiTi. The simulated curves are shown in dash–dot line (Zaki *et al* 2010b). (a) Ambient temperature. (b) $T = 40$ °C.

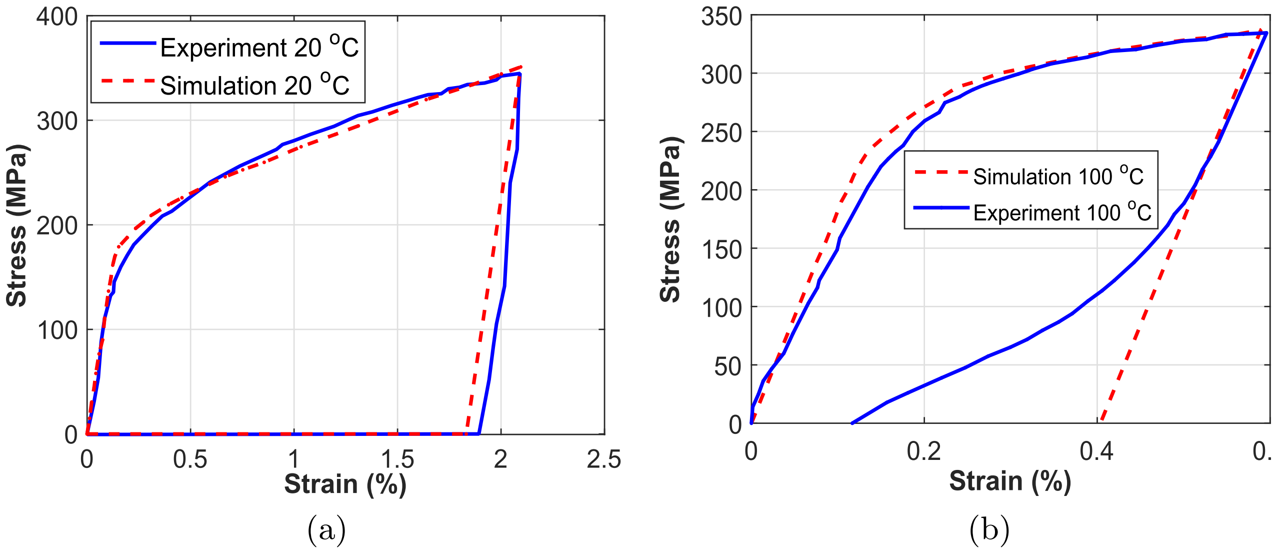


**Figure 10.** Simulation of martensite transformation and plastic deformation in austenitic iron-based SMAs (Khalil *et al* 2012). (a) Comparison between experimental and simulated stress–strain curves in tension at 20 °C for Fe–Mn31.6–Si6.45–C0.018. (b) Comparison between experimental and simulated stress-strain curves in tension at 100 °C for Fe–Mn28–Si6–Cr5.

$\sigma_{ed} = 0$. From these considerations an empirical form of $\Phi_{ed}$ was proposed as follows:

$$\Phi_{ed} = \Phi_{ed}^{sat}\left(\frac{a\sigma_{ed}}{1 + a\sigma_{ed}}\right), \tag{35}$$

where the parameters $\Phi_{ed}^{sat}$ and $a$ are determined based on the experimental work of Bourbon *et al* (1995). The model was validated against experimental data as shown in figure 12. This attempt, however, shows non negligible discrepancies compared to experimental results due to exceedingly high sensitivity to stress variation. To account for the cyclic deformation and TWSME, Zaki and Moumni (2007b) adapted the ZM model of Zaki and Moumni (2007a) by inserting new parameter $\boldsymbol{B}$ representing the internal stress that allows the martensite orientation in the absence of external mechanical loading. More precisely, the authors added the '$-\frac{2}{3}\xi\boldsymbol{B} : \varepsilon_r$' to the Helmholtz free energy term to simulate the TWMSE of NiTi. The results were not validated against experimental data. possible degradation of constitutive models in cyclic loadings due to the cumulative plastic

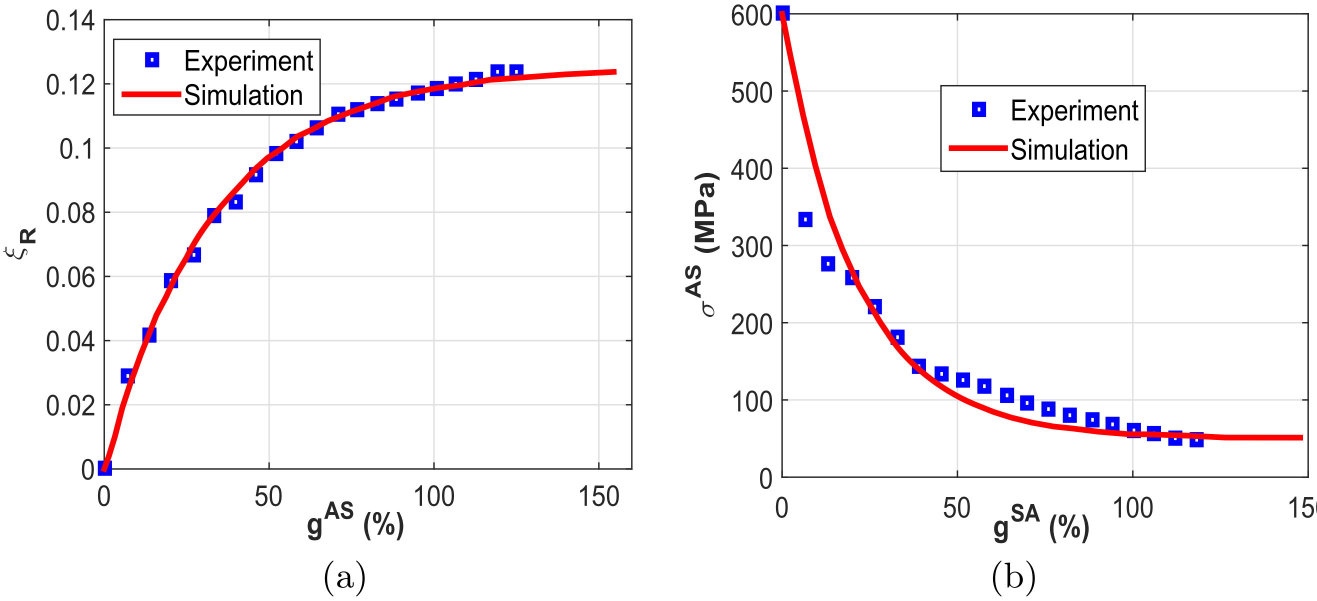


**Figure 11.** Degradation of SMA behavior due to cyclic loading (Auricchio *et al* 2003). (a) Evolution of $\xi_R$ with $g^{AS}$. (b) Evolution of $\sigma_s^{AS}$ with $g^{AS}$.

gliding. Therefore engineering applications requiring high mechanical loading should consider the plastic deformation.

## 5. Thermomechanical coupling

The forward phase transformation is accompanied with a release of latent heat and is therefore exothermic, while the RT is endothermic. The heat exchanged during phase transformation can result in self-heating or self-cooling of the alloy, depending on the transformation direction, with immediate consequences on the phase transformation process (Shaw and Kyriakides 1995, Zhu and Zhang 2007, Morin 2011). Indeed, the generation of heat during forward transformation can stabilize austenite by increasing its temperature, thus increasing the stress required to further proceed with the transformation (Ortin and Planes 1989). On the other hand, the release of latent heat during RT stabilizes the martensite phase thereby decreasing the RT stress. This behavior is further influenced by dissipation due to phase transformation and inelastic deformation of the SMA and by conditions influencing the exchange of heat with the surroundings, including the loading rate. The influence of strain rate on the critical stresses for phase transformation and on the size of the pseudoelastic hysteresis appears to have been first reported by Van Humbeeck and Delaey (1981) for Cu-based SMAs and by Mukherjee *et al* (1985) for NiTi alloys. A justification was later provided by Leo *et al* (1993), McCormick *et al* (1993), Shaw and Kyriakides (1995), and He and Sun (2010) who showed that SMA samples submerged in water require a significantly higher strain rate to display measurable variation in the size of hysteresis compared to samples in air, which motivated the conclusion that rate dependence was not a manifestation of viscous effects but rather a consequence of thermomechanical coupling. The isothermal experiments of Grabe and Bruhns (2008) and Heller *et al* (2009) and the numerical simulation results of Morin *et al* (2011a) further support this conclusion. Thermodynamics can be written as follows: thermodynamics gives the total dissipation $D_p$ as follows: in existing SMA models, thermomechanical coupling is commonly accounted for considering latent heat and intrinsic dissipation due to phase transformation as heat sources (Auricchio and Sacco 2001, Zhu and Zhang 2007, Chemisky *et al* 2011, Morin *et al* 2011a, 2011b, Yu *et al* 2014b, Yin *et al* 2014). A thermal energy density $\Phi_T$ is also defined in terms of the specific heat $C_p$ of the SMA and incorporated in the expression of the free energy density of the material:

$$\Phi_T = \rho C_p \left( T - T_0 - T \ln\left(\frac{T}{T_0}\right)\right), \tag{36}$$

where $\rho$ is the mass density and $T_0$ is a reference temperature. Morin *et al* (2011a) and Moussa *et al* (2012) utilized the following expression for the rate of energy dissipation density:

$$D = \boldsymbol{\sigma} : \dot{\varepsilon} - (\dot{L} + \dot{T}s) - \frac{\boldsymbol{q}\,\boldsymbol{\nabla} T}{T} \geqslant 0, \tag{37}$$

where $\boldsymbol{\sigma}$ is the stress tensor, $\dot{\varepsilon}$ is the total strain rate, $\dot{T}$ is the temperature rate, $s$ is entropy, $\boldsymbol{q}$ is the heat influx vector and $L$ is the energy Lagrangian used in the ZM model (Zaki and Moumni 2007a, 2007b). Like in (Bernardini and Pence 2002) and (Anand and Gurtin 2003), the authors divided $D$ into an intrinsic mechanical part $D_1$ and a thermal dissipation part $D_2$, which are assumed to be independently positive and given by

$$\begin{aligned} D_1 &= \boldsymbol{\sigma} : \dot{\varepsilon} - (\dot{L} + \dot{T}s) = A_\xi \dot{\xi} + \boldsymbol{A}_{\mathrm{ori}} : \dot{\varepsilon}^{\mathrm{ori}}, \\ D_2 &= -\frac{\boldsymbol{q}\,\boldsymbol{\nabla} T}{T}, \end{aligned} \tag{38}$$

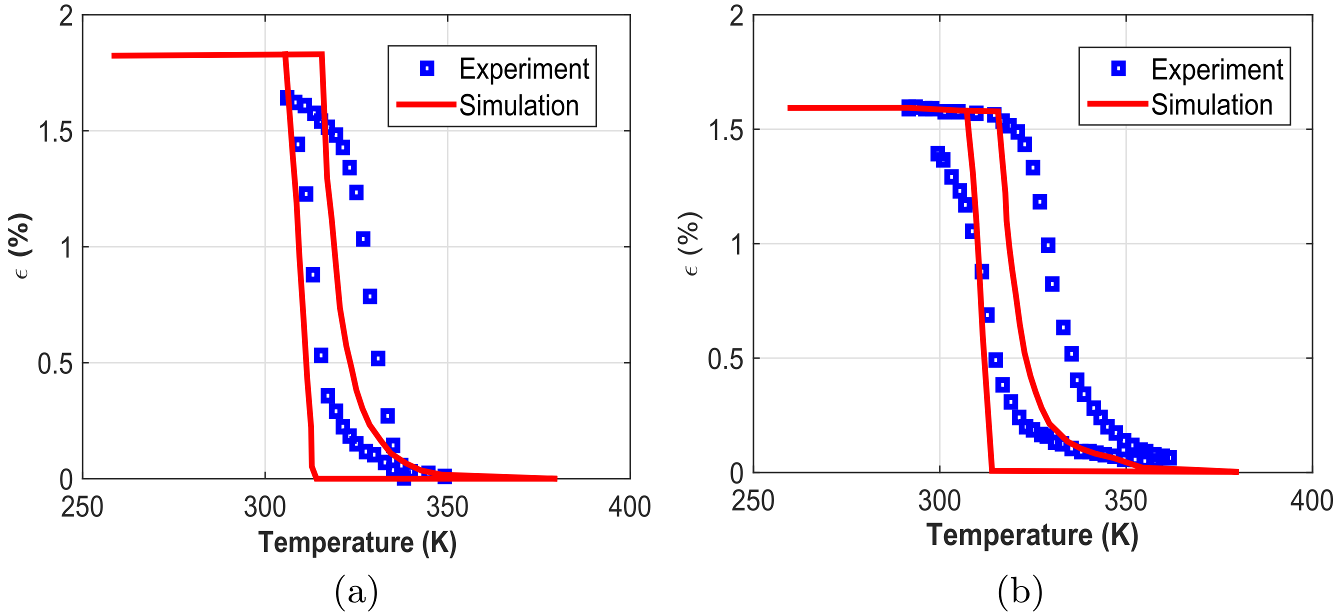


**Figure 12.** Modeling of the TWSME for different levels of applied stress (Lexcellent *et al* 2000). (a) $\sigma_{\mathrm{ed}} = 65$ MPa. (b) $\sigma_{\mathrm{ed}} = 144$ MPa.

where $A_\xi$ and $\boldsymbol{A}_{\mathrm{ori}}$ are the thermodynamic forces driving martensite transformation and orientation, respectively. Considering $A_\xi$ and $\boldsymbol{A}_{\mathrm{ori}}$ as sub-gradients of the homogeneous dissipation potential in the ZM model and neglecting the heat generation due to martensite orientation, the heat equation and thermal boundary conditions in a region $\Omega$ of the SMA were defined by the authors as

$$\begin{cases} \rho C_{\mathrm{p}}\dot{T} - \mathrm{div}(k_{\mathrm{T}}\,\boldsymbol{\nabla}T) = T\dfrac{\partial C_{\mathrm{p}}(T)}{\partial T}\dot{\xi} \\ \quad +[a_1(1-\xi) + a_2\xi]|\dot{\xi}| \ \text{ in } \ \Omega, \\ \boldsymbol{q}^{\mathrm{T}}.\,\boldsymbol{n} = h(T - T_{\mathrm{ext}}) \text{ at the boundary } \ \partial\Omega, \\ T_{(t=0)} = T_{\mathrm{ext}}, \end{cases} \tag{39}$$

where $h$ is the heat convection coefficient, $T_{\mathrm{ext}}$ is the ambient temperature, $k_{\mathrm{T}}$ is the heat conduction coefficient, $\boldsymbol{n}$ is an outward unit vector normal to the boundary $\partial\Omega$, and $a_1$ and $a_2$ are material parameters. In the above heat equation, only phase transformation appears as a source of dissipative heat while reorientation is disregarded. An expression equivalent to $D_1$ in (38) was also derived by Panico and Brinson (2007) and Christ and Reese (2009). Thamburaja and Nikabdullah (2009) and Thamburaja (2010) further dissociated the forward and reverse behaviors and obtained

$$\begin{aligned} c\dot{T} - \mathrm{div}(k_{\mathrm{T}}(\boldsymbol{\nabla}T)) &= \overline{H}_{\mathrm{AM}}\frac{T}{T_0}\dot{\xi} - 3\kappa\alpha_{\mathrm{T}}\dot{\varepsilon}^{\mathrm{el}}_{kk}T \\ &+ A_{\mathrm{fwr}}\dot{\xi}_{\mathrm{fwr}} + A_{\mathrm{rev}}\dot{\xi}_{\mathrm{rev}} + r, \end{aligned} \tag{40}$$

where $\kappa$ is the bulk modulus of the material, $\overline{H}_{\mathrm{AM}}$ is the transformation latent heat, $r$ is the heat supply per unit reference volume, and $A_{\mathrm{fwr}}$ and $A_{\mathrm{rev}}$ are the thermodynamic forces for forward and RTs. The following relation between $\overline{H}_{\mathrm{AM}}$ and $A_\xi$ was established by Chang *et al* (2006):

$$\overline{H}_{\mathrm{AM}} = A_\xi - T\frac{\partial A_\xi}{\partial T}, \tag{41}$$

where the Voigt model is used to determine an effective thermal expansion coefficient $\alpha_{\mathrm{T}}$ for the SMA and the Reuss model is used to determine an equivalent conductivity $k_{\mathrm{T}}$. Equations similar to (40) were derived by Zaki *et al* (2010a) and Peigney and Seguin (2013) and by Depriester *et al* (2014) who further considered thermoelastic contributions. Auricchio *et al* (2008) simulated a thin SMA sample taking into account the influence of thermomechanical coupling. They neglected heat conduction based on the small cross-section of the sample. The simulation shows that the slope of the transformation stress plateau increases with the loading rate, while the hysteresis size remains constant. More recently, Christ and Reese (2009) simulated the adiabatic thermomechanical behavior of a SMA strip using experimental data from Helm and Haupt (2002). The strip was subjected to prescribed initial temperature $T_0 = 302$ K at both ends. A maximum displacement $u_{\max} = 2$ mm was applied to a long, thin strip ($l = 100$ mm; $b = 12$ mm and $t = 4$ mm) and held for 10 s before unloading. The results at the centroïd of the sample show a dependence of the stress–strain curve, martensite volume fraction and temperature distribution on the loading rate. Figure 13(a) shows that the maximum temperature increased by 21 K when the stretching rate is increased from $\dot{u} = 2 \times 10^{-4}$ mm s$^{-1}$ to $\dot{u} = 2 \times 10^{-2}$ mm s$^{-1}$. Moreover, the forward transformation finish stress $\sigma^{\mathrm{f}}_{\mathrm{AM}}$ increased by 150 MPa (figure 13(b)) and the maximum martensite volume fraction decreased from 0.95 for $\dot{u} = 2 \times 10^{-4}$ mm s$^{-1}$, to 0.91 for $\dot{u} = 2 \times 10^{-3}$ mm s$^{-1}$, and 0.8 for $\dot{u} = 2 \times 10^{-2}$ mm s$^{-1}$ (figure 13(c)). These results agree with the experimental observations of Leo *et al* (1993), Matsuzaki *et al* (2001) and Pieczyska *et al* (2006). The numerical results of Morin *et al*

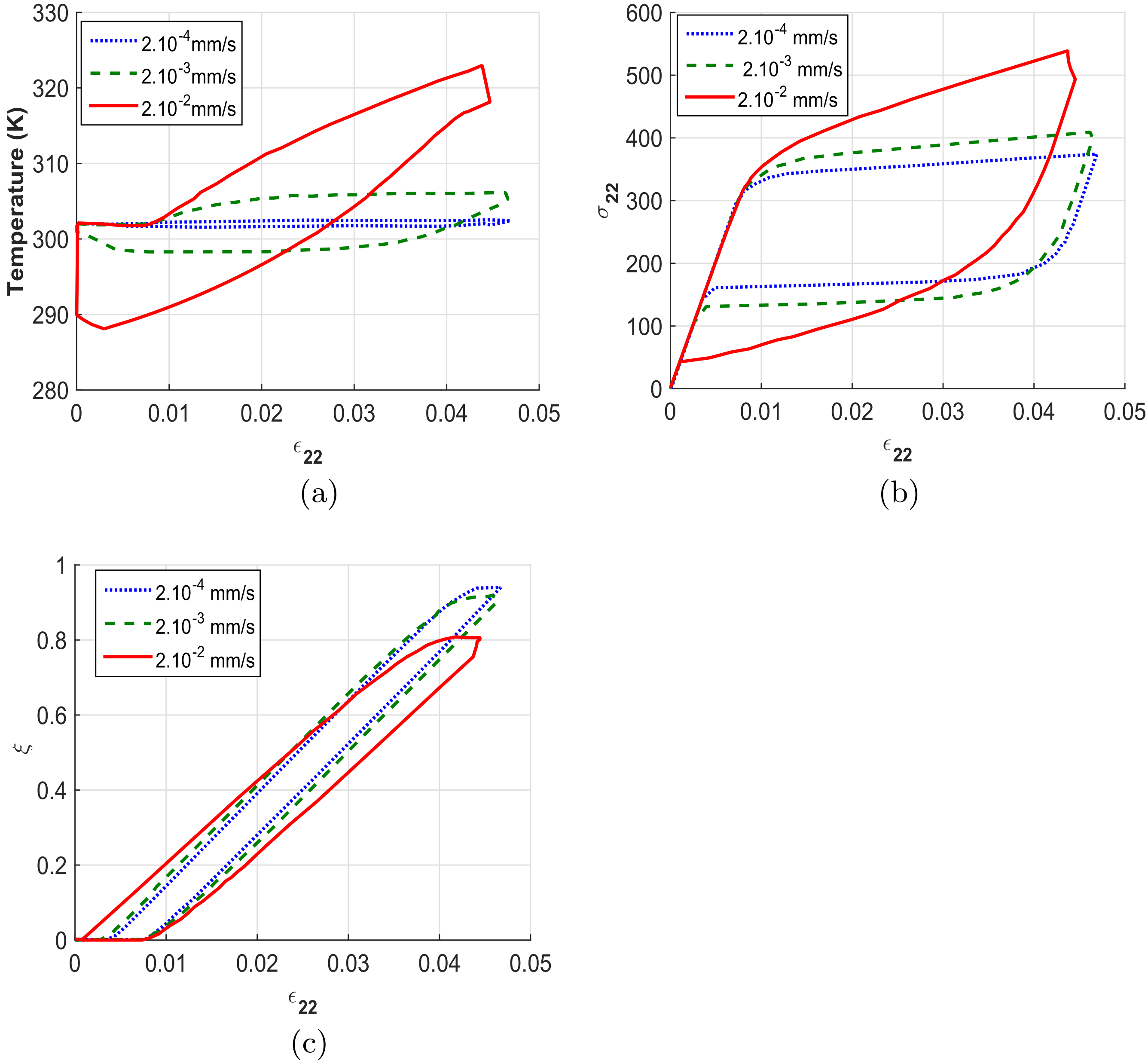


**Figure 13.** Adiabatic pseudoelasticity of NiTi for different loading rates (Christ and Reese 2009). (a) $T$ versus $\epsilon_{22}$. (b) $\sigma_{22}$ versus $\epsilon_{22}$. (c) $\xi$ versus $\epsilon_{22}$.

(2011a) show similar variation trends for the stress–strain and temperature-strain curves for loading rates of $4 \times 10^{-5}$ mm s$^{-1}$, $4 \times 10^{-4}$ mm s$^{-1}$ and $4 \times 10^{-2}$ mm s$^{-1}$. However, unlike in Christ and Reese (2009), the variation in hysteresis size was found to follow a bell-shaped curve with the increase in strain rate. Recently, Yu *et al* (2014a) successfully simulated the effects of loading rate observed experimentally by Morin *et al* (2011a) and Sun *et al* (2012b). Mirzaeifar *et al* (2011) proposed a 3D model considering thermomechanical coupling to investigate the effect of latent heat and the heat flux resulting from the temperature nonuniformity. The authors were able to simulate quasi-static and dynamic solicitations for SMA bars and wires considering the influence of loading rate, size and ambient condition effects. More recently, Hashemi *et al* (2015) obtained results similar to those in figure 13(b) but with near-constant hysteresis size.

The above models disregard localized dissipation that accompany the formation of Lüders-like phase transformation fronts in SMAs. The nucleation and propagation of these fronts at different loading rates and ambient thermal conditions were considered by e.g. Iadicola and Shaw (2004) who further considered the influence of material self-heating on the number of transformation fronts. Overall, accounting for thermomechanical coupling is required in presence of sufficiently high loading rates, for which the intensity of the heat exchange with the surroundings is not sufficient to maintain a relatively constant temperature in the SMA during phase transformation. In such case, the variation in temperature has implications on the size of the hysteresis loop, which is linked to the density of energy dissipation in a loading cycle and thereby to structural and functional fatigue of SMAs. It is worth noting that the behavior of SMAs at high loading rates, which is affected by thermomechanical coupling, appears not to be properly described by existing models.

## 6. Tension–compression asymmetry

The stress–strain behavior of SMAs is known to display tensile–compressive asymmetry (Wasilewski 1971, Lieberman *et al* 1975, Vacher and Lexcellent 1991, Chumljakov and Starenchenko 1995, Patoor *et al* 1995, Jacobus *et al* 1996, Gall *et al* 1997, Liu *et al* 1998). Buchheit and Wert (1994) explained this asymmetry by the unidirectional nature of phase transformation for individual martensite variants. Gall *et al* (2001a) demonstrated that the asymmetric critical transformation stress and hardening behavior in NiTi originate at the single crystal level from differences in the formation and detwinning of corresponding martensite variant pairs. The authors found that the [111] crystals in compression cannot develop as much uniaxial strain as in tension. In the case of NiTi SMAs, the asymmetry gives rise to lower recoverable strain as well as higher transformation stress and steeper transformation plateau in compression compared to tension (see figure 14(a)). The degree of asymmetry is influenced by texture in polycrystalline NiTi, whereas in single crystals it is mostly affected by the size of precipitates (Gall and Sehitoglu 1999). An influence of temperature was also observed by Orgéas and Favier (1995) who reported higher asymmetry with increasing temperature (see figure 14(b)). The authors found the same transformation energy density same in tension and compression and concluded that the asymmetry is unrelated to the Bauschinger effect or to anisotropy. In iron-based SMAs, Nishimura *et al* (1996) experimentally determined the slope of the phase transformation boundary in the stress–temperature diagram of Fe66Cr9Ni5Mn14Si6 (wt%) to be $0.85\ \mathrm{MPa\ K^{-1}}$ in tension and $-1.13\ \mathrm{MPa\ K^{-1}}$ in compression. The corresponding asymmetric forward transformation start stresses were plotted by Nishimura *et al* (1999) for different temperatures (see figure 14(c)). Similar results were reported for NiTi by Raniecki *et al* (2001) as shown in figure 14(d). To model the asymmetric behavior of SMAs, the von Mises effective stress $\sigma_{\mathrm{vm}}$ and/or stain commonly used to define phase transformation surfaces is substituted with expressions sensitive to changes in the loading direction, which typically feature the first or third invariants of the stress and strain tensors. Gillet *et al* (1998) and Raniecki and Lexcellent (1998) developed some of the earliest models that account for tension–compression asymmetry. Bouvet *et al* (2002) proposed the following effective stress used in defining the phase transformation surfaces:

$$\overline{\sigma}_{\mathrm{eff}} = \sigma_{\mathrm{vm}} f(y_\sigma), \tag{42}$$

where $f$ is a function of the third stress invariant $y_\sigma$ given by

$$y_\sigma = \frac{27}{2}\frac{\det(\boldsymbol{\sigma}^{\mathrm{d}})}{(\sigma_{\mathrm{vm}})^3}, \tag{43}$$

in which $\boldsymbol{\sigma}^{\mathrm{d}}$ the deviatoric part of the stress tensor. The function $f$ was defined as follows:

$$f(y_\sigma) = \cos\left[\frac{\cos^{-1}(1 - a(1 - y_\sigma))}{3}\right], \tag{44}$$

to guarantee the convexity of the loading surface for all values of the parameter $a$ between 0, for which $\overline{\sigma}_{\mathrm{eff}} = \sigma_{\mathrm{vm}}$, and 1, for which the asymmetry is maximum. The parameter $a$ was expressed in terms of the uniaxial tensile and compressive transformation stresses, $\sigma^{\mathrm{t}}$ and $\sigma^{\mathrm{c}}$, as

$$a = \frac{1}{2}\left[1 - \cos\left(3\cos^{-1}\left(\frac{\sigma^{\mathrm{t}}}{\sigma^{\mathrm{c}}}\right)\right)\right]. \tag{45}$$

The above expression of the equivalent stress was later used by Lexcellent *et al* (2006), Thiebaud *et al* (2007), Taillard *et al* (2008) and Saint-Sulpice *et al* (2009). Saint-Sulpice *et al* (2009) successfully simulated the experimental observations of asymmetric behavior reported by Raniecki and Lexcellent (1998). Thiebaud *et al* (2007) used (44) to simulate the asymmetric distribution of the martensite volume fraction in a plate subjected to bending as shown in figure 15. Raniecki *et al* (2001) proposed the following alternative expression for $f$, in which $f(0) = 0$ for $y_\sigma = 0$ corresponds to pure shear:

$$f(y_\sigma) = h - c\exp[-d(y_\sigma + 1)]. \tag{46}$$

The parameters $c$, $d$ and $h$ in this equation take the respective values 0.37, 0.78 and 1.17 for NiTi, and can be modified to achieve different degrees of asymmetry. Vieille *et al* (2007) suggested an alternative expression of the effective stress given by

$$\overline{\sigma}_{\mathrm{eff}} = \sqrt{3J_2}\left(1 + \frac{27}{2}b\frac{J_3}{(3J_2)^{3/2}}\right), \tag{47}$$

where the degree of asymmetry is controlled by the single parameter $b$. The von Mises stress is obtained for $b = 0$, while both $b = 1$ and $b = 2$ correspond to maximum asymmetry where the loading surface becomes an equilateral triangle in the deviatoric stress space. Auricchio and Petrini (2004) and Evangelista *et al* (2009) defined the following asymmetric loading function for phase transformation:

$$F(\boldsymbol{X}) = \sqrt{2J_2} + m\frac{J_3}{J_2} - R, \tag{48}$$

where $J_2$ and $J_3$ are the second and third invariants of the deviatoric part of the relative stress $\boldsymbol{X}$ given by

$$\boldsymbol{X} = \boldsymbol{\sigma} - \boldsymbol{\beta}. \tag{49}$$

In the above the equation, $\boldsymbol{\beta}$ is analogous to back stress in plasticity, and $R$ and $m$ are material parameters given by

$$R = 2\sqrt{\frac{2}{3}}\frac{\sigma^{\mathrm{c}}\sigma^{\mathrm{t}}}{\sigma^{\mathrm{c}} + \sigma^{\mathrm{t}}} \text{ and } m = \sqrt{\frac{27}{2}}\frac{\sigma^{\mathrm{c}} - \sigma^{\mathrm{t}}}{\sigma^{\mathrm{c}} + \sigma^{\mathrm{t}}}. \tag{50}$$

The convexity of the loading surface is insured for $m \leqslant 0.46$. In contrast to the observations of Orgéas and Favier (1995), the simulated asymmetry was more pronounced during martensite detwinning than during phase transformation in the range $A_{\mathrm{s}} < T < A_{\mathrm{f}}$, and nearly disappeared in the

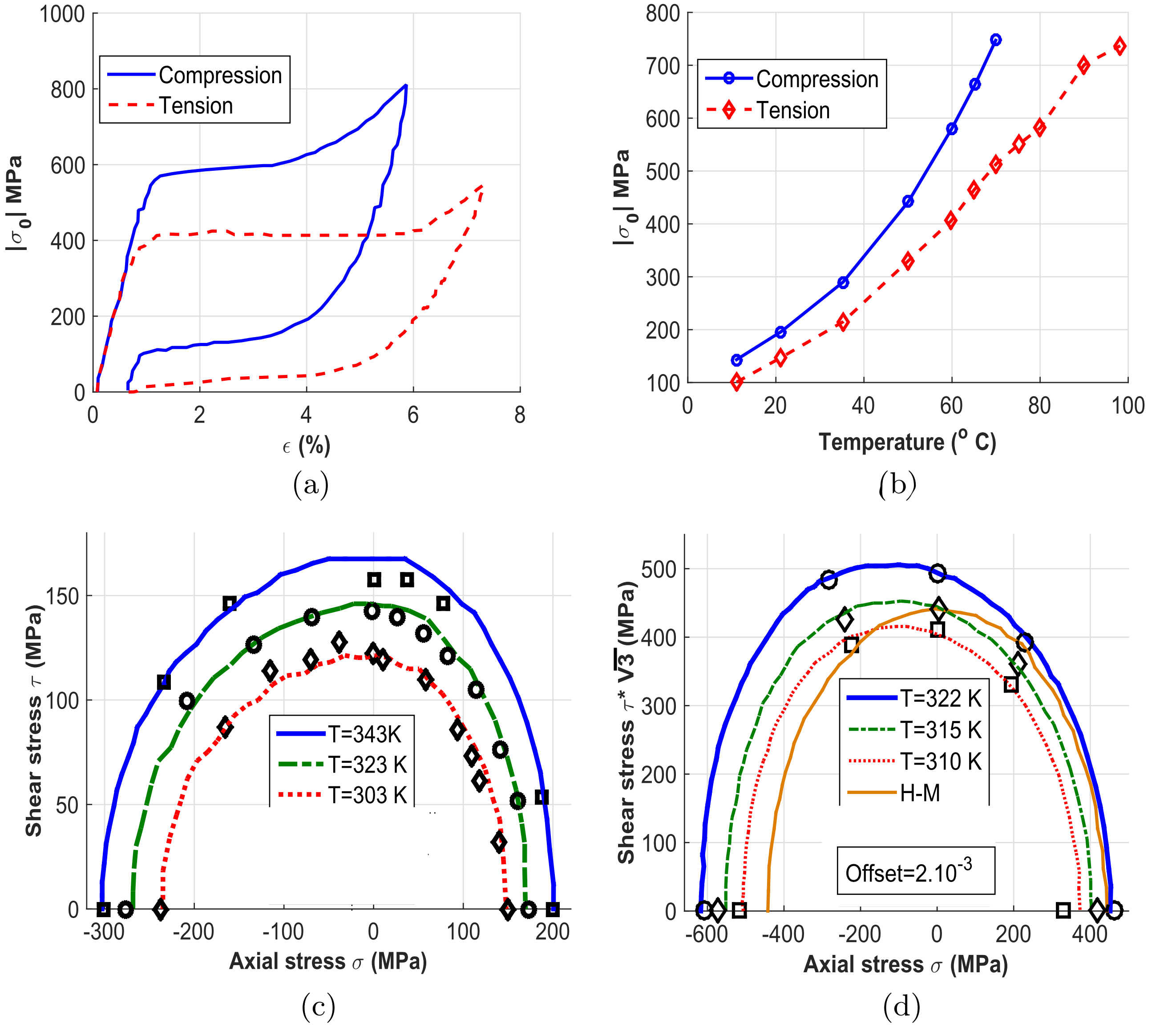


**Figure 14.** Experimental observations of asymmetry in the behavior of NiTi and Fe-based SMAs. (a) Tension and compression tests using equiatomic NiTi at $T = 60$ °C (Orgéas and Favier 1995). (b) Influence of temperature on the transformation stresses in NiTi (Orgéas and Favier 1995). (c) Martensite transformation start curves in terms of shear versus normal stress for Fe66Cr9Ni5Mn14Si6 (wt%) (Nishimura *et al* 1998). (d) Forward phase transformation surfaces for NiTi at different transformation temperatures. The von Mises curve is in dotted line (Raniecki *et al* 2001).

pseudoelastic domain. A similar approach was used by Christ and Reese (2009) where $R = k\sqrt{\frac{2}{3}}$, $k$ being half the height of the hysteresis loop. Considering the asymmetry in equivalent stress may be insufficient for proper simulation of SMA behavior and an asymmetric equivalent transformation strain may be needed. Bouvet *et al* (2004) and Saint-Sulpice *et al* (2009) considered asymmetric rate equations for the transformation stress where

$$\begin{cases} \varepsilon^{\mathrm{tr}}_{\mathrm{eq}} = \|\varepsilon^{\mathrm{tr}}\| \dfrac{f(-y_\varepsilon)}{f(-1)}, \\ y_\varepsilon = 4\dfrac{\det(\varepsilon^{\mathrm{tr}})}{\|\varepsilon^{\mathrm{tr}}\|}, \end{cases} \tag{51}$$

and $f$ is given by (44). This model introduces asymmetric equivalent values of of $\boldsymbol{\sigma}$ and $\varepsilon^{\mathrm{tr}}$ in the expression of the free energy, and $\varepsilon^{\mathrm{tr}}$ in the formulation of the constraints on the state variables. More recently, the following effective transformation strain at saturation was proposed by Zaki *et al* (2011) using a mathematical framework proposed by Raniecki and Mróz (2008):

$$\varepsilon^{\mathrm{tr}}_{\mathrm{eff}} = \sqrt[3]{\kappa_{\mathrm{ori}}\left(J_2^{3/2} - \rho_{\mathrm{ori}} J_3\right)}\,, \tag{52}$$

where

$$\kappa_{\mathrm{ori}} = \left[\left(\frac{3}{4}\right)^{\frac{3}{2}} - \frac{\rho_{\mathrm{ori}}}{4}\right]^{-1},$$
$$\rho_{\mathrm{ori}} = \frac{3\sqrt{3}}{2}\frac{(r^3 - 1)}{r^3 + 1} \text{ and } r = \frac{\gamma^{\mathrm{t}}}{\gamma^{\mathrm{c}}}, \tag{53}$$

$\gamma^{\mathrm{t}}$ and $\gamma^{\mathrm{c}}$ being the maximum transformation strains in tension and compression, respectively. The authors accurately

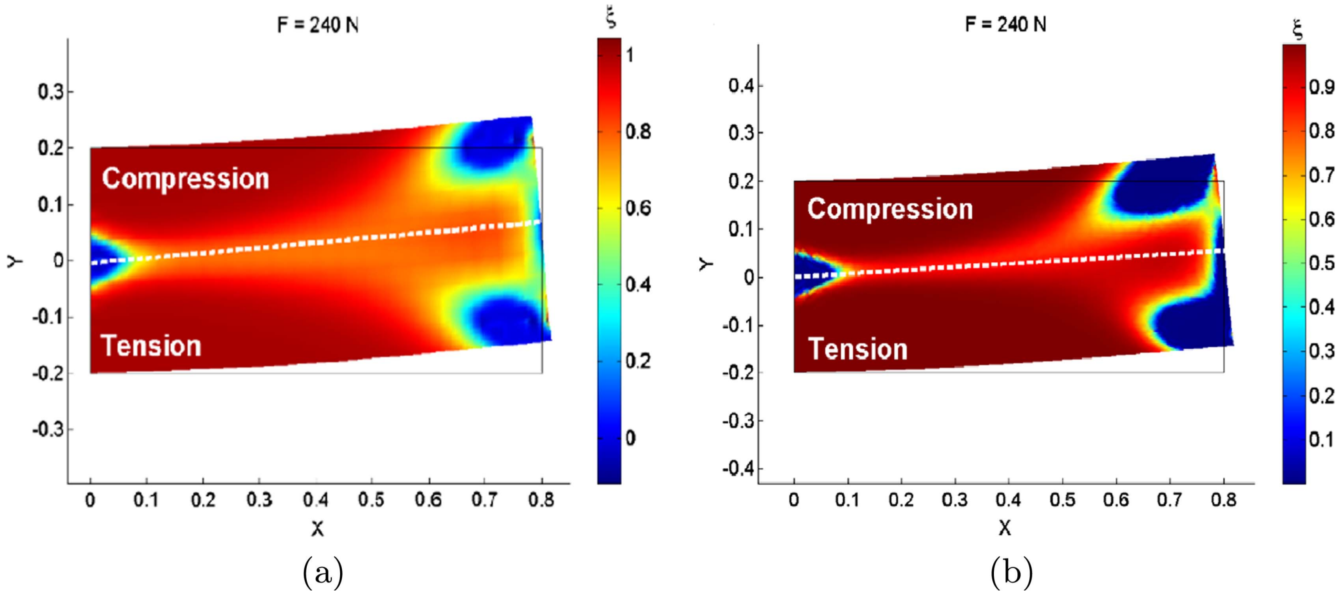


**Figure 15.** Distribution of the martensite volume fraction $\xi$ in a SMA plate using symmetric and asymmetric models (Thiebaud *et al* 2007). (a) Symmetric case with $a = 0$. (b) Asymmetric case with $a = 0.7$.

simulated the experimental results of Gall and Sehitoglu (1999). Peultier *et al* (2006, 2008) also accounted for asymmetric behavior in SMAs via a modified Prager formulation of the mean saturation strain given by

$$\bar{\varepsilon}^{\text{tr}}_{\text{sat}} = \kappa\left(1 + \rho\frac{J_3}{(J_2)^{\frac{3}{2}}}\right)^{\frac{1}{4}}. \tag{54}$$

This relation was later generalized by Chemisky *et al* (2011) as follows:

$$\bar{\varepsilon}^{\text{tr}}_{\text{sat}} = \kappa\left(1 + \rho\frac{J_3}{(J_2)^{\frac{3}{2}}}\right)^{\frac{1}{n}}, \tag{55}$$

where $\rho$ is no longer constrained in $[0, 1]$ and both $\rho$ and $\kappa$ are determined from simple tension and compression experiments using the equations

$$\kappa = \varepsilon^{\text{tr}}_{\text{tension}}\left(1 + \frac{\rho}{\upsilon}\right)^{-\frac{1}{n}},$$
$$\rho = \left(\frac{1-\omega}{1+\omega}\right)\upsilon \text{ and } \omega = \left(\frac{\gamma^{\text{c}}}{\gamma^{\text{t}}}\right)^{n}, \tag{56}$$

in which $\upsilon$ and $n$ are material parameters. The von Mises effective transformation strain is retrieved for $\rho = 0$ and (54) is obtained for $n = 4$. Auricchio *et al* (2009) used yet another expression for the scalar transformation strain in uniaxial loading equivalent to the 3D Prager–Lode $J_2/J_3$ norm and given by

$$\|\varepsilon^{\text{tr}}\| = (1 + c)|\varepsilon^{\text{tr}}| - c\varepsilon^{\text{tr}}, \tag{57}$$

where $c = 0.1$ for NiTi. The authors found that the asymmetry decreases with increasing temperature and nearly disappears above the austenite finish temperature, much like in (Evangelista *et al* 2009). However, none of these two paper attempted experimental validation of the reported results. A different approach was utilized by Thamburaja and Nikabdullah (2009) and Thamburaja (2010) who incorporated the asymmetry in the flow rule of the plastic strain, as follows:

$$\dot{\varepsilon}^{\text{p}} = \sqrt{\frac{3}{2}}(1 + \rho J_3)\sum_{i=1}^{2}\dot{\xi}_i \boldsymbol{P}^{(i)}, \tag{58}$$

where $\boldsymbol{P}^{(1)}$ and $\boldsymbol{P}^{(2)}$ are the flow directions for forward and RTs respectively, $J_3$ is the third stress invariant and $\rho$ is a material parameter. The asymmetric flow rule was successful in simulating the experimental results of Orgéas and Favier (1998).

The incorporation of tensile–compressive asymmetry in the simulation of SMAs by way of one of the methods described in this section allows higher fidelity in reproducing the actual behavior of these materials when analyzing SMA structures.

## 7. Hysteresis, internal loops and return-point memory

The hysteresis loop formed during phase transformation in SMAs is directly related to the coherency energy resulting from the motion of austenite–martensite and variant–variant interfaces (Müller and Seelecke 2001). In this context, Lexcellent *et al* (2008) discussed the validity of the criteria proposed by James and Zhang (2005) for the minimization of hysteresis width in alloys exhibiting first-order transition. From consideration of the free energy $\Phi$ given by Leclercq and Lexcellent (1996), Lexcellent *et al* (2008) drew the following conclusions:

(1) $\frac{\partial^2\Phi}{\partial\xi^2} = 0$ corresponds to the non-hysteretic Maxwell model and is applicable to single-crystal CuZnAl,

(2) $\frac{\partial^2\Phi}{\partial\xi^2} > 0$ reflects good cohabitation between the two phases and is applicable to modeling the non-hysteretic formation of *R*-phase in NiTi,
(3) $\frac{\partial^2\Phi}{\partial\xi^2} < 0$ suggests incompatibility between the two phases and is representative of the hysteretic transformation in NiTiZn.

Evidence of the hysteretic behavior in SMAs is provided by the existence of different sets of phase transformation temperatures and stresses during forward and reverse phase changes. In addition to the now well-established hysteretic behavior, the stress–strain response of SMAs was also found to display subloops when reloading through a point in the loading path from which there was previous unloading. Early models accounting for the formation of subloops are attributed to Huo and Müller (1993), Leclercq and Lexcellent (1996), Tanaka *et al* (1995), Gillet *et al* (1998) and Bekker and Brinson (1998). Different models for thermal hysteresis for SMAs in the $\varepsilon - T$ plan were developed by these authors.

For temperature-induced transformation, a major loop is formed for temperatures outside the interval $[M_f, A_f]$, whereas minor loops are created during cyclic temperature variation within the same interval. Early SMA models such as those of Tanaka (1986), Raniecki and Lexcellent (1994) and Boyd and Lagoudas (1996) describe thermal hysteresis within the framework of continuum thermodynamics using the same transformation criteria to describe major and minor loops. This approach, which considers a single modeling framework for both minor and major loops was largely abandoned in later models. In particular, Ivshin and Pence (1994) used the Duhem–Madelung hysteresis model to describe minor loops as homothetic reductions of the major loop. Accordingly, the variation of the martensite volume fraction in an internal loop was given by

$$\xi(T(t)) = \begin{cases} 1 - \left(\dfrac{1-\xi(t_j)}{1-\xi(T_{\rm maj}(t_j))}\right)(1-\xi_{\rm maj}(T(t))), & \text{for } \dot{\xi} > 0, \\ \dfrac{\xi(t_k)}{\xi(T_{\rm maj}(t_j))}\xi_{\rm maj}(T(t)), & \text{for } \dot{\xi} < 0, \end{cases} \quad (59)$$

where $t_j$ and $t_k$ are reversal times, $\xi$ is the martensite volume fraction for the current subloop and $\xi_{\rm maj}$ is the volume fraction for the major loop at temperature $T$. This approach, which only considers the last reversal point, could not predict the formation of minor loops near the start and finish points of phase transformation. An alternative approach was proposed by Ortín (1992) who adapted the Preisach hysteresis model for modeling SMAs. The material behavior was represented by means of an infinite number of Boolean hysteresis relays with operators $\gamma_{\alpha\beta}$ associated to weighting distribution functions $\mu(T_\alpha, T_\beta)$. The output $\xi$ is given by the number of '1-positioned' relays as follows:

$$\xi(T(t)) = \iint_{T_\alpha \geqslant T_\beta} \mu(T_\alpha, T_\beta)\gamma_{\alpha\beta}T(t)\mathrm{d}T_\alpha \mathrm{d}T_\beta, \quad (60)$$

where $\xi$ is a functional of the temperature history and $T_\alpha$ and $T_\beta$ are two temperatures. A challenge in this model is to determine the distribution function $\mu(T_\alpha, T_\beta)$, which must be redefined each time the loading direction changes for complex loading paths. Moreover, the Boolean relays are only representative for single crystals with one martensite variant and the model presents discontinuity issues in $\gamma_{\alpha\beta}$. These issues were addressed in the K–P hysteresis model of Krasnoselskii and Pokrovskii (1983) using a smooth hysteretic kernel function $k_s$. Moreover, the double integral in (60) is discretized and incremented with a linear thermal term to ensure the invertibility of $\xi$. This allows the simulation of complex and cyclic loadings but is not sufficient to capture the accumulation of plastic strain and the ensuing degradation of the stress–strain response (Webb *et al* 2000). More recently, Nascimento *et al* (2009) used a 1D thermal hysteresis model based on the limiting loop proximity ($L^2P$) proposed by de Almeida *et al* (2003) to simulate the formation of minor loops in SMA actuator wires. Like in (Nascimento *et al* 2004), the major loop was described by means of the following equation:

$$\varepsilon(T, \delta) = \frac{\xi_s}{\pi}\left[\arctan\left(\beta\left(\delta\frac{w}{2} + T_c - T\right)\right) + \frac{\pi}{2}\right] + \varepsilon_L, \quad (61)$$

where $\varepsilon_s$ is the hysteresis height, $w$ is the hysteresis width, $\varepsilon_L$ is the saturation strain and $\beta$ is the slope $\frac{\mathrm{d}\varepsilon}{\mathrm{d}T}$ at the critical temperature $T_c$ at the center of the loop. Minor loops are governed in this model by

$$\varepsilon(T) = \frac{\xi_s}{\pi}\left[\arctan\left(\beta\left(\delta\frac{w}{2} + T_c - T - T_{\rm pr}P(x)\right)\right) + \frac{\pi}{2}\right] + \varepsilon_L, \quad (62)$$

where $T_{\rm pr}$ is defined as a 'thermal distance' of the reversal point ($\varepsilon_L = \varepsilon_r$, $T = T_r$) to the major loop (see figure 16(a)) and is given by

$$T_{\rm pr} = \delta\frac{w}{2} + T_c - \frac{1}{\beta}\left(\tan\pi\left(\frac{\varepsilon - \varepsilon_r}{\varepsilon_s}\right) - \frac{\pi}{2}\right) - T_r, \quad (63)$$

$P(x)$ is a decreasing function that satisfies the conditions $P(0) = 1$ and $P(\infty) = 0$ with

$$x = \frac{(T - T_r)}{T_{\rm pr}}. \quad (64)$$

The comparison of numerical and experimental results for equiatomic Ni–Ti shows good agreement for $\sigma = 200$ MPa (see figure 16(b)). The authors also found that the hysteresis width decreases linearly with the applied stress, in contrast to some of the earlier models like (Huang and Xu 2005) where the size of thermal hysteresis was constant.

For pseudoelastic SMAs, hysteresis is described in the stress–strain space. In this regard, Müller (2012) distinguished three scenarios for pseudoelastic hysteresis in single crystals: unloading before complete forward transformation leading to internal recovery (figure 17(a)), reloading before full RT causing internal plastic yielding (figure 17(b)) and formation of internal loops when the partial loading/

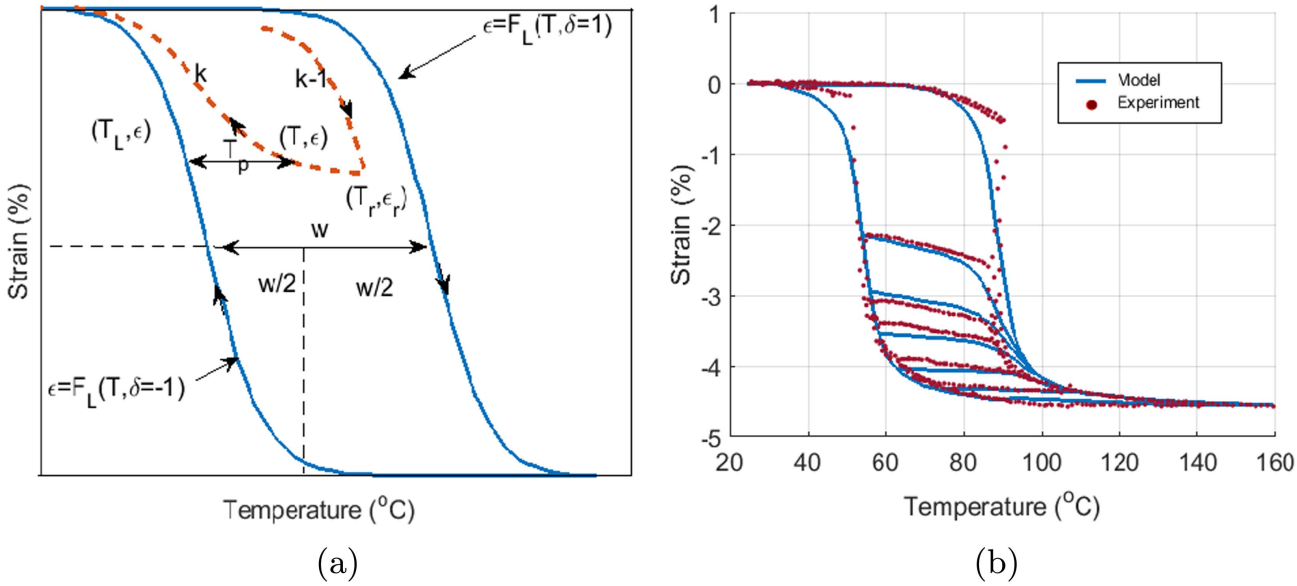


**Figure 16.** Simulation of thermal hysteresis in SMA wires using the $L^2P$ method (Nascimento *et al* 2009). (a) Representation of thermal hysteresis for a SMA wire actuator. (b) Simulation of hysteresis for a SMA wire actuator for $\sigma = 200$ MPa.

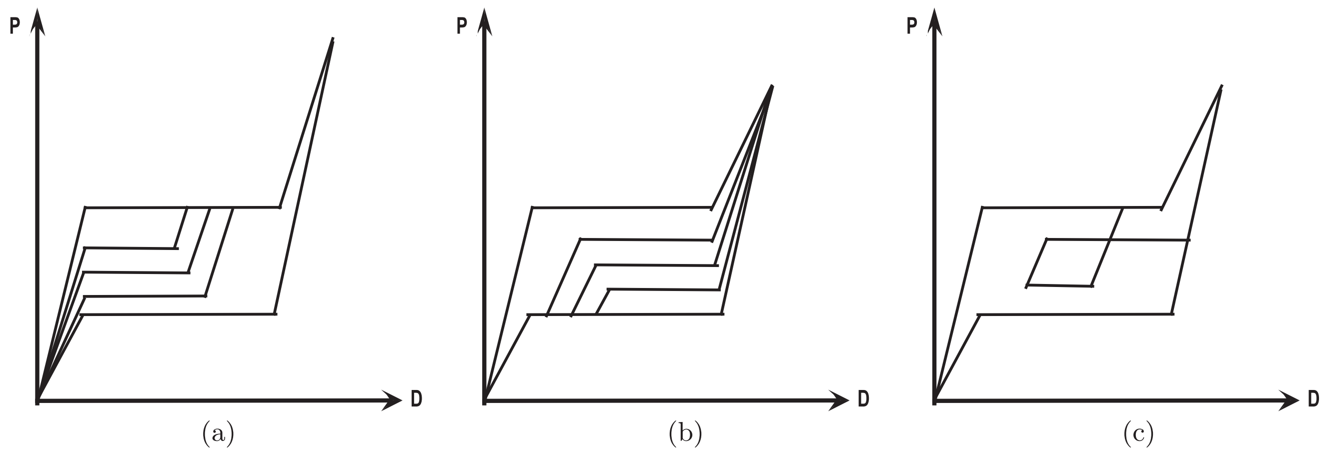


**Figure 17.** Pseudoelastic hysteresis in shape memory single crystals. (a) Internal recovery. (b) Internal yield. (c) Internal loop.

unloading takes place strictly within the major pseudoelastic loop (figure 17(c)). Gillet *et al* (1998) describes the sub-loops from the quantity of martensite formed during the previous forward transformation. The critical force for phase transformation was considered as a function of the martensite volume fraction at the end of the last direct transformation $\xi^*$

$$F_\xi^{\mathrm{crit}} = F_\xi^{\mathrm{max}}\,(1 - 2\xi^*), \tag{65}$$

Peultier *et al* (2006) extended (65) in such way that subloops are formed only when both the martensite volume fraction $\xi$ and equivalent mean transformation strain $\bar{\varepsilon}_{\mathrm{eq}}^{\mathrm{tr}}$ are less than their maximal values. They related the critical thermodynamic force for phase transformation $F_\xi^{\mathrm{crit}}$ in the subloop to that of the major loop ($F_\xi^{\mathrm{max}}$) by the relation

$$F_\xi^{\mathrm{crit}} = F_\xi^{\mathrm{max}}\left(1 - 2\frac{\xi^*\bar{\varepsilon}_{\mathrm{eq}}^{\mathrm{tr}*}}{\varepsilon_{\mathrm{L}}}\right), \tag{66}$$

where $\xi^*$ and $\bar{\varepsilon}_{\mathrm{eq}}^{\mathrm{tr}*}$ indicate the onset of the forward phase transformation loop, and $\varepsilon_{\mathrm{L}}$ is the maximum uniaxial transformation strain. Later, Chemisky *et al* (2011) generalized (66) by distinguishing minimum and maximum transformation thresholds for inner loops, $F_\xi^{\mathrm{min}}$ and $F_\xi^{\mathrm{max}}$, which they used to define two different critical thermodynamic forces, as follows, using the notion of memory point of Wack *et al* (1983):

$$F_\xi^{\mathrm{crit}} = \begin{cases} (1-\gamma_\xi)F_\xi^{\mathrm{min}} + \gamma_\xi F_\xi^{\mathrm{max}} + (1-\gamma_\xi)F_\xi^{\mathrm{mem}} \\ \quad +(B_{\mathrm{f}} - B)(T - T_0) - H_{\mathrm{s}}\bar{\varepsilon}_{\mathrm{eq}}^{\mathrm{tr}}, \ \mathrm{A} \to \mathrm{M}, \\ (1-\gamma_\xi)F_\xi^{\mathrm{min}} + \gamma_\xi F_\xi^{\mathrm{max}} - (1-\gamma_\xi)F_\xi^{\mathrm{mem}} \\ \quad +(B_{\mathrm{r}} - B)(T - T_0) - H_{\mathrm{s}}\bar{\varepsilon}_{\mathrm{eq}}^{\mathrm{tr}}, \ \mathrm{M} \to \mathrm{A}. \end{cases} \tag{67}$$

In these equations, $F_\xi^{\mathrm{mem}}$ is the memorized thermodynamic force at load reversal and $H_{\mathrm{s}}$, $B$, $B_{\mathrm{f}}$ and $B_{\mathrm{r}}$ are material parameters. The authors substituted $\xi^*$ in (66) by

$$\gamma_\xi = \frac{(\xi - \xi^*)}{(\xi^{\mathrm{obj}} - \xi^*)}, \tag{68}$$

where $\xi^{\mathrm{obj}} = 1$ for A $\rightarrow$ M and $\xi^{\mathrm{obj}} = 0$ for M $\rightarrow$ A. Bouvet *et al* (2004) also utilized the return point memory effect (RPME) notion of Ortín (1992) to describe the formation of inner loops in presence of complex loading cases. A reversal point RP, memorized as a maximum at the end of partial loading or as a minimum at the end of partial unloading, is 'forgotten' only when the loop is closed at the next RP. Extending this work, Saint-Sulpice *et al* (2009) developed a 3D model in which the evolution of the size $R(\xi)$ of the transformation surfaces is given by

$$R(\xi) = \begin{cases} R_{n-1}^{\min} + g_1(x)(R_{n-1}^{\max} - R_{n-1}^{\min}), & \mathrm{A} \rightarrow \mathrm{M}, \\ R_{n-1}^{\min} - \delta_{n-1}^{\min} + g_2(x)(R_n^{\max} - \delta_n^{\max} - R_{n-1}^{\min} + \delta_{n-1}^{\min}) + \delta(\xi), & \mathrm{M} \rightarrow \mathrm{A}. \end{cases} \tag{69}$$

In a given loop $n$, $\delta_n^{\max}$ and $\delta_n^{\min}$ are the values of the characteristic size $\delta$ of the elastic domain at the high and low memory points, $R_{n-1}^{\max}$ and $R_{n-1}^{\min}$ are the maximum and minimum values of $R(\xi)$, and $g_1(x)$ and $g_2(x)$ are logarithmic and polynomial functions of the variable $x$ given by

$$x = \frac{\xi - \xi_{n-1}^{\min}}{\xi_{n-1}^{\max} - \xi_{n-1}^{\min}}, \tag{70}$$

where $\xi_{n-1}^{\max}$ and $\xi_{n-1}^{\min}$ are the values of $\xi$ at the high and low reversal points respectively. The formation of minor loops during cyclic loading regimes is well established experimentally and has clear influence on the stress–strain–temperature behavior of SMAs as explained in this section. Accounting for minor loops is therefore important for proper simulation of cyclic SMA behavior.

## 8. Fracture of SMAs

The formation and propagation of cracks in SMAs is investigated in the literature using various experimental techniques such as electron microscopy (Maletta *et al* 2009, Ramaiah *et al* 2011), digital image correlation (Daly *et al* 2007), optical *in situ* observation (Creuziger *et al* 2008), infrared thermography (Gollerthan *et al* 2009), and synchrotron x-ray diffraction (Young *et al* 2013). Fracture is generally reported to take place in the martensite zone (MZ) either by cleavage, or by nucleation, growth and coalescence of microcracks (Gall *et al* 2001b, Olsen *et al* 2012). The martensite transformation ahead of the crack tip results in toughening of the SMA according to Daly *et al* (2007) who found that the region of SIM around the crack tip in thin NiTi sheets has a butterfly shape with two lobes oriented at 60° from the crack axis. These experimental observations cannot be accurately described using linear elastic fracture mechanics (LEFM) (Anderson (2005), p 44) and a correction such as Irwin's (Irwin 1960) is commonly introduced. Figure 18 illustrates the three main zones determined experimentally around the crack tip in a SMA, including the untransformed austenite zone (AZ), the partially transformed martensite zone (TZ) and the fully transformed martensite zone (MZ). In addition, if the local stress at the crack tip exceeds the yield limit, a plastic zone (PZ) develops within the MZ.

To account for SIM transformation, the stress field in the vicinity of the crack is usually assumed to be described by the stress intensity factor (SIF) $K_{\mathrm{I}}^{\mathrm{tip}}$ that controls the stress field near the crack tip. Yi *et al* (2001) used the superposition principle to describe fracture toughening in SMAs under plane strain mixed-mode loading. Using Eshelby inclusion and weight function methods, they expressed the remote and crack-tip energy release rates were taken follows:

$$G^{\infty} = [(K_{\mathrm{I}}^{\infty})^2 + (K_{\mathrm{II}}^{\infty})^2]\frac{1 - \nu^2}{E},$$
$$G^{\mathrm{tip}} = [(K_{\mathrm{I}}^{\mathrm{tip}})^2 + (K_{\mathrm{II}}^{\mathrm{tip}})^2]\frac{1 - \nu^2}{E}, \tag{71}$$

where $E$ is the Young's modulus, $\mu$ is Poisson's ratio, $K_{\mathrm{I}}^{\infty}$ and $K_{\mathrm{II}}^{\infty}$ are the remote SIFs for mode I and mode II loading, and $K_{\mathrm{I}}^{\mathrm{tip}}$ and $K_{\mathrm{II}}^{\mathrm{tip}}$ are those at the crack tip. The size of the TZ in this case is given by

$$R_{\mathrm{TZ}}(\theta) = \frac{1}{2\pi}\left[\frac{(G^{\infty} + G^{\mathrm{tip}})}{2(\sigma_{\mathrm{e}}^{\mathrm{c}})^2}\right] f_{\theta\vartheta}, \tag{72}$$

where $\sigma_{\mathrm{e}}^{\mathrm{c}}$ is a material parameter and $f_{\theta\vartheta}$ is a trigonometric function of the polar angle $\theta$ and the phase angle $\vartheta$ of the SIF $K = K_{\mathrm{I}} + \mathrm{i}K_{\mathrm{II}}$. However, the model is valid only for plane strain cases. Yan *et al* (2003) simulated an edge crack in a semi-infinite NiTi plate subjected to a stress intensity $K_{\mathrm{I}}^{\mathrm{app}} = 60\,\mathrm{MPa}\,\sqrt{\mathrm{m}}$. The authors found for plain strain loading case that for a normalized height with respect to $K_{\mathrm{I}}^{\infty}\sigma_{\mathrm{y}}$ of 2.1 for the TZ and only 0.12 for the PZ. Wang *et al* (2005b) used the constitutive model of Auricchio *et al* (1997) to show the formation of SIM near the notch in nitinol compact–tension specimens. The results show that $R_{\mathrm{TZ}}$ and $\xi$ are path-dependent and increase with the crack length and notch acuity. This simple model can only be used for cracks of fixed length. Using finite element analysis (FEA), Wang (2006) showed that an augmentation of the notch acuity decreases the transformation and yield stresses, and increases the stress and strain near the notch. In contrasts with Wang *et al* (2005b), $R_{\mathrm{TZ}}$ was found to decrease with the notch acuity, while $R_{\mathrm{MZ}}$ and $R_{\mathrm{PZ}}$ increased (see figure 19). Yan and

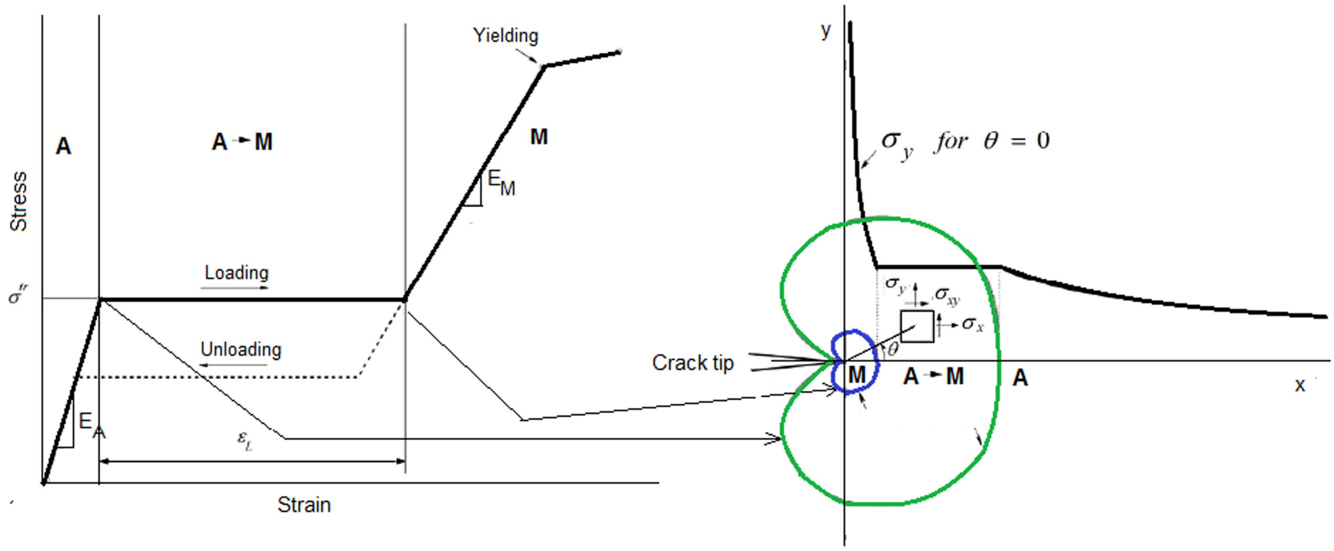


**Figure 18.** Schematic description of the SIM transformation zone near the crack tip of a superelastic NiTi SMA (Maletta 2012).

Mai (2006) studied the effect of non-deviatoric transformation strain on the fracture toughness of a pseudoelastic SMA and found that phase transformation with volume contraction tends to decrease the fracture toughness and increase brittleness, while transformation shear strain was found to increase toughness. The above models do not consider the effect of stress triaxility as in (Wang *et al* 2010). The authors analyzed stress distribution around the crack tip in NiTi using FEA. The simulations show unstable crack propagation in NiTi in plane strain conditions with high triaxiality and stable crack growth in plane stress conditions with low triaxiality. The authors used an apparent SIF that was obtained using the secant method applicable to common metals, thus disregarding the effect of phase transformation. Using the limit function of Panoskaltsis *et al* (2004), Freed and Banks-Sills (2007) generalized the expressions of $R_{TZ}$ and $R_{MZ}$ derived by Yi and Gao (2000) as follows:

$$K_I = \frac{K_I^{app} + K_I^{tip}}{2},$$
$$R_{MZ} = \frac{1}{2\pi}\left[\frac{K_I}{C_M(T - M_f)}\right]\left[\cos^2\frac{\theta}{2}\left(\tilde{\kappa} + 3\sin^2\frac{\theta}{2}\right)\right],$$
$$R_{TZ} = \frac{1}{2\pi}\left[\frac{K_I}{C_M(T - M_s)}\right]\left[\cos^2\frac{\theta}{2}\left(\tilde{\kappa} + 3\sin^2\frac{\theta}{2}\right)\right], \quad (73)$$

were $M_s$ and $M_f$ are the martensite start and finish temperatures, $\tilde{\kappa}$ is a parameter equal to 1 in plane stress and $(1 - 2\nu)^2$ in plane strain, $\theta$ is the crack tip angular coordinate and $C_M$ is a material parameter. The authors found that mismatch between the elastic moduli of austenite and martensite is beneficial for increasing the steady-state SIF. However, RT was found to decrease energy dissipation in the wake and therefore decrease the SIF. A limitation of this cohesive model is that it does not reflect the effects of mixed-mode deformation, where the direction of crack propagation may be complex. Xiong and Liu (2007) used the PZ correction of Irwin (1960) to show that as long as the crack half-length $a$ does not exceed $R_{PZ}$, the following relations hold:

$$R_{PZ} = \frac{2(\sigma^\infty)^2}{2\sigma_y^2 - (\sigma^\infty)^2},$$
$$K_I^\infty = \sigma^\infty\sqrt{\frac{2\pi a\sigma_y^2}{2\sigma_y^2 - (\sigma^\infty)^2}}, \quad (74)$$

where the plastic yield strength $\sigma_y$ is obtained from LEFM. The authors further used the flow rule of Tanaka (1986) to derive the following expressions of $R_{MZ}$ and $R_{TZ}$:

$$R_{MZ} = \left(\frac{\sigma^\infty}{\sigma^{tr}}\right)^2\left(\frac{T - M_s^0}{T - M_f^0}\right)^2\frac{a\sigma_y^2}{2\sigma_y^2 - (\sigma^\infty)^2} + \frac{R_{PZ}}{2},$$
$$R_{TZ} = a\left(\frac{\sigma^\infty}{\sigma^{tr}}\right)^2\frac{\sigma_y^2 + (\sigma^{tr})^2}{2\sigma_y^2 - (\sigma^\infty)^2}, \quad (75)$$

where $a$ is the crack half-length, $\sigma^{tr}$ is the transformation stress, $\sigma^\infty$ is the applied remote stress and $\sigma_y$ is the plastic yield strength. The results showed that the crack-tip SIF in NiMnGa increases significantly as the temperature approaches Ms. The crack-tip SIF was found to increase drastically with increased transformation interval. The above models, however, do not give quantitative information about the size of the fracture zone like in (Wang 2007). The authors simulated the decrease of the plastic yield strength and the fracture toughness at the notch tip in plane stress conditions. Figure 20 gives a comparison of the fracture process zone (FPZ) in a SMA with (MT-SMA) and without (NMT-SMA) martensite transformation based on two criteria: a critical equivalent strain $\varepsilon_{pc} = 0.01$ and a critical normal stress $\sigma_f = 1100$ MPa. A comparison of the FPZs shows that martensite transformation increases the apparent fracture toughness in NiTi by about 47%. From the work of Sun and Hwang (1998), Maletta and Furgiuele (2010) and Maletta and Furgiuele (2011) observed an increase of SIF and $R_{TZ}$ when the maximum transformation strain $\varepsilon_L$ increases. In

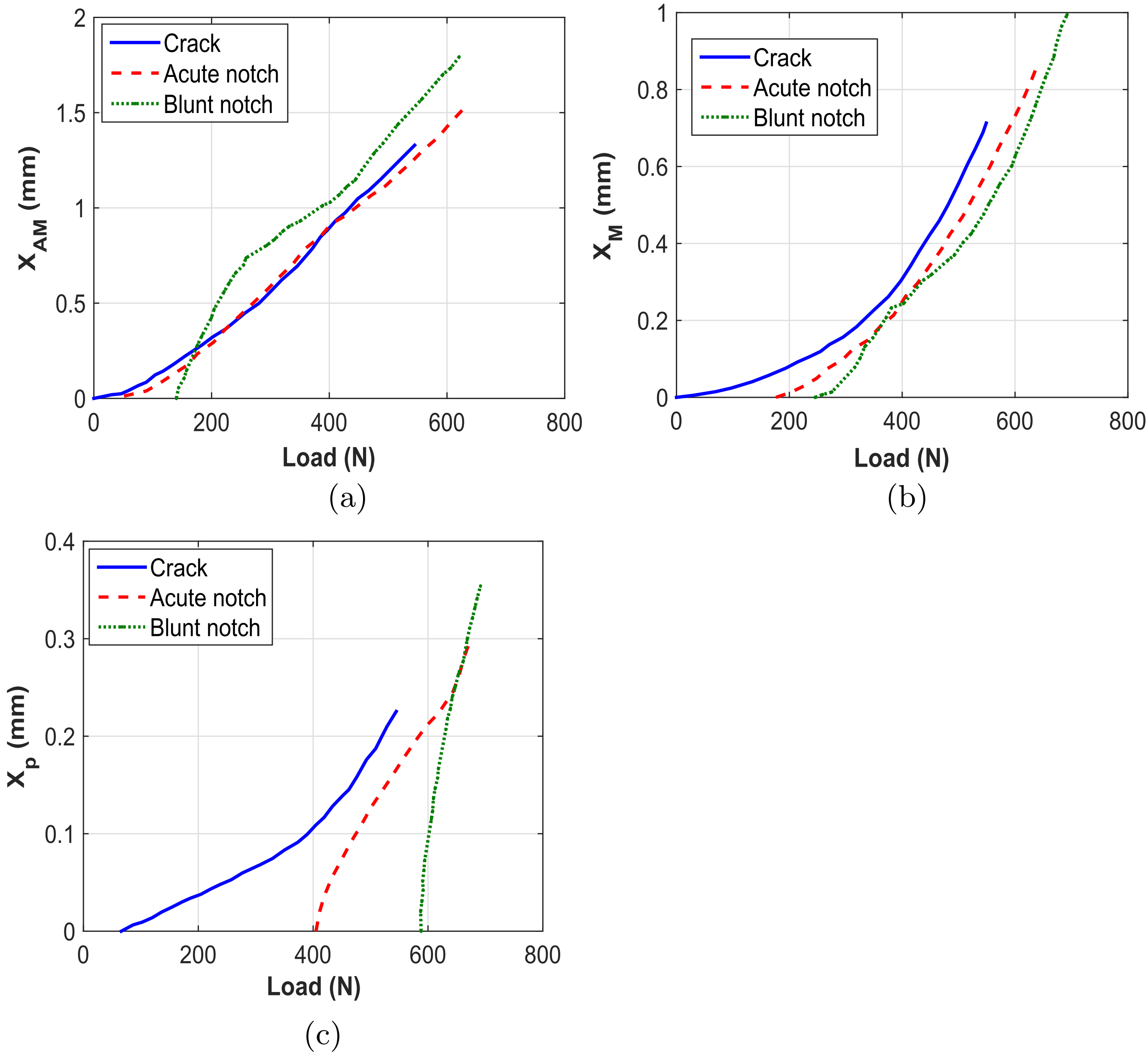


**Figure 19.** Evolution of the size of the TZ, MZ and PZ with notch acuity (Wang 2006). (a) Variation of $R_{TZ}$ with the load. (a) Variation of $R_{MZ}$ with the load. (c) Variation of $R_{PZ}$ with the load.

opposite, an increase in temperature was found to reduce the SIF, as confirmed by Sgambitterra *et al* (2014). From the modified relations for elastoplastic materials, the following expression of the SIF $K_{IA}$ in the AZ was obtained:

$$\begin{cases} K_{IA} = \sigma^{\infty}\sqrt{\pi(a + r^* - R_{TZ})}, \\ r^* = \dfrac{1}{2\pi}\left(\dfrac{K_I^{app}}{\sigma^{tr}}\right)^2. \end{cases} \tag{76}$$

Using this SIF expression, Maletta and Young (2011) obtained the following principal stresses in the AZ for $\theta = 0$:

$$\sigma_{A1}(r) = \sigma_{A2}(r) = \frac{K_{IA}}{\sqrt{2\pi(r + r^* - R_{TZ})}},$$
$$\sigma_{A3}(r) = b_{tc}\sigma_{A1}(r), \tag{77}$$

where $b_{tc} = 0$ for plane stress, $b_{tc} = 2\nu$ for plane strain and $r$ is a polar coordinate. Using the compatibility conditions, Maletta (2012) wrote the principal stress components $\sigma_{T1}(r)$ in the TZ and $\sigma_{M1}(r)$ MZ as functions of $\sigma_{A1}$. They defined the plane-stress SIF $K_{IM}$ in the MZ as follows:

$$K_{IM} = \lim_{r\to 0} \sigma_M\sqrt{2\pi r} = \frac{2(1 - \nu - b_{tc}\nu)K_{IA}}{(1 - b_{tc})(E_A/E_M) + (1 + b_{tc})(1 - 2\nu)}, \tag{78}$$

where $E_A$ and $E_M$ are the elastic moduli of austenite and martensite, respectively. This model is based on the assumption of small-scale yielding as well as zero plastic deformation in the MZ and a von Mises transformation criteria. It accounts only for mode I opening, which makes it

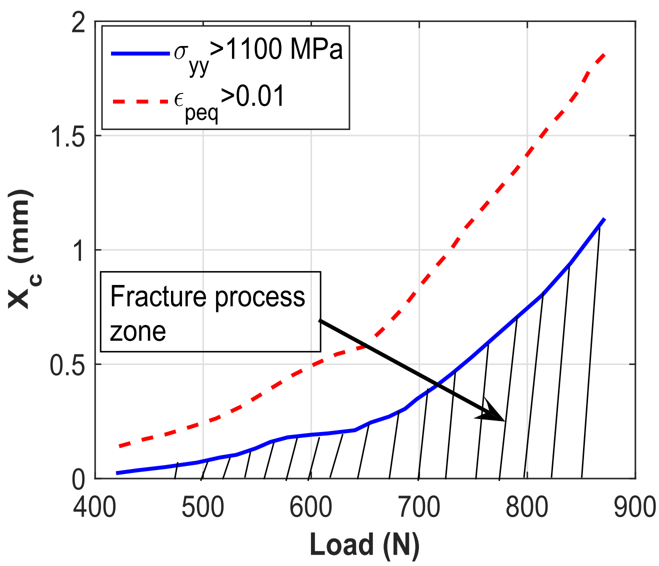


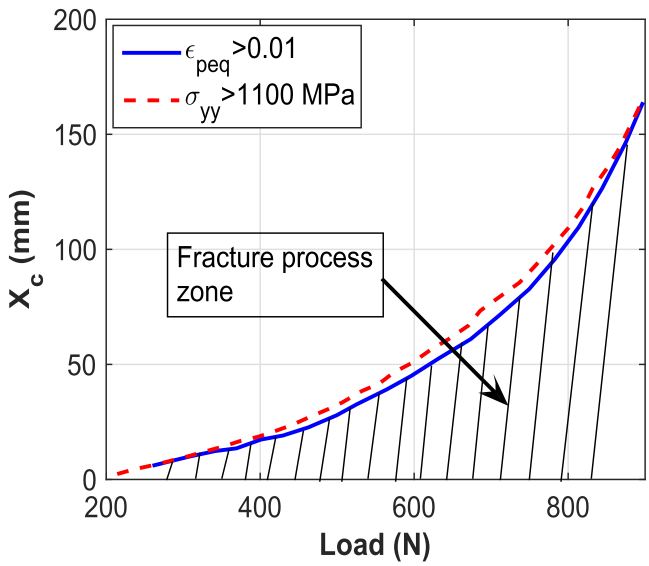


**Figure 20.** Change of FPZ size with the applied load in MT-SMA (a) and NMT-SMA (b) for $\varepsilon_{pc} = 0.01$ and $\sigma_f = 1100$ MPa (Wang 2007). (a) MT-SMA. (a) MT-SMA.

inapplicable for mixed-mode loading. Baxevanis and Lagoudas (2012) used the idea of Rice and Rosengren (1968) to show that in the absence of MZ the $J$-integral in mode I loading is related to the crack-tip opening displacement $\delta_{tip}$ and transformation stress $\sigma^{tr}$ by the relation

$$\begin{cases} J = \sigma^{tr}\delta_{tip}, \\ \delta_{tip} = \dfrac{8\sigma^{tr}a}{\pi E_A}\ln\left[\sec\left(\dfrac{\pi\sigma^{\infty}}{2\sigma^{tr}}\right)\right], \end{cases} \tag{79}$$

where $\sigma^{\infty}$ is the remote applied stress. The authors showed that an increase of the ratio $\frac{\sigma^{\infty}}{\sigma^{y}}$ leads to larger $R_{TZ}$, $R_{MZ}$, and $R_{PZ}$, while $J$ and $\delta_{tip}$ decrease. Baxevanis *et al* (2012) carried out plane strain FEM simulation of a stationary crack. The results show that SIM transformation reduces $R_{PZ}$ by 86% in mode I loading (figure 21(a)) and by 88% in mode II (see figure 21(b)). An increase in temperature from 80 °C to 110 °C was also found to reduce $R_{PZ}$ by 40% and $R_{TZ}$ by a factor of 5. Recently, Baxevanis *et al* (2014) noted an increase in fracture toughness due to RT in the wake of an advancing crack. The toughness increased with the augmentation of the ratio $\frac{E_M}{E_A}$ and Poisson's ratio $\nu$. Hazar *et al* (2013) and Hazar *et al* (2015) simulated the mode I steady-state edge crack propagation in NiTi. Hazar *et al* (2015) found larger MZ, crack face opening displacement and $\Delta J = J_{\infty} - J_{tip}$ in plane stress compared to plane strain. In contrast to many other models, the authors considered nonproportional loading and investigated the influence ofmartensite reorientation near the crack tip. The model is limited by the assumption of steady-state stable crack growth. Different SIFs are usually used for the remote and the crack tip stress fields. This allows to determine the size of the three characteristic zones near the crack tip: the PZ, the full transformed martensitic zone, the partially transformed zone, and the untransformed zone

In summary, the papers reviewed in this section deal with fracture in SMAs under quasi-static mechanical loading. The existing models are capable of capturing the formation of SIM near the crack tip, which provides increased fracture toughness and may enclose a plastic deformation zone. The possibility for RT in the wake of a growing crack is also considered in a small subset of these models. Notable limitations to current state of the art include the assumption of isothermal crack propagation and the restriction to relatively simple sample configurations and quasistatic loading. A possible venue for future work in this field may therefore involve accounting for thermomechanical coupling as well as cyclic and dynamic loading effects. A notable effort geared toward addressing these issues was recently proposed by Afshar *et al* (2015). The authors considered the influence of thermomechanical coupling on mixed-mode crack tip fields in analyzing an interface crack between a SMA and an elastic layer. The authors make the simplifying assumption of small-scale phase transformation near the tip.

## 9. Fatigue of SMAs

SMAs are commonly subjected to cyclic loading, which makes fatigue a critical design consideration. Fatigue of SMAs is characterized by a degradation of the SME and PE, in which case it is called functional, or by the initiation, coalescence and propagation of microcracks leading to failure, in which case it is called structural. For this latter fatigue type, experiments show the appearance of martensite ahead of the crack tips due to high stress concentration (Robertson *et al* 2007). The first experiments on the fatigue behavior of SMAs were carried out by Rachikger (1958) for CuAlNi, Melton and Mercier (1979) for NiTi and Sade *et al* (1985) for

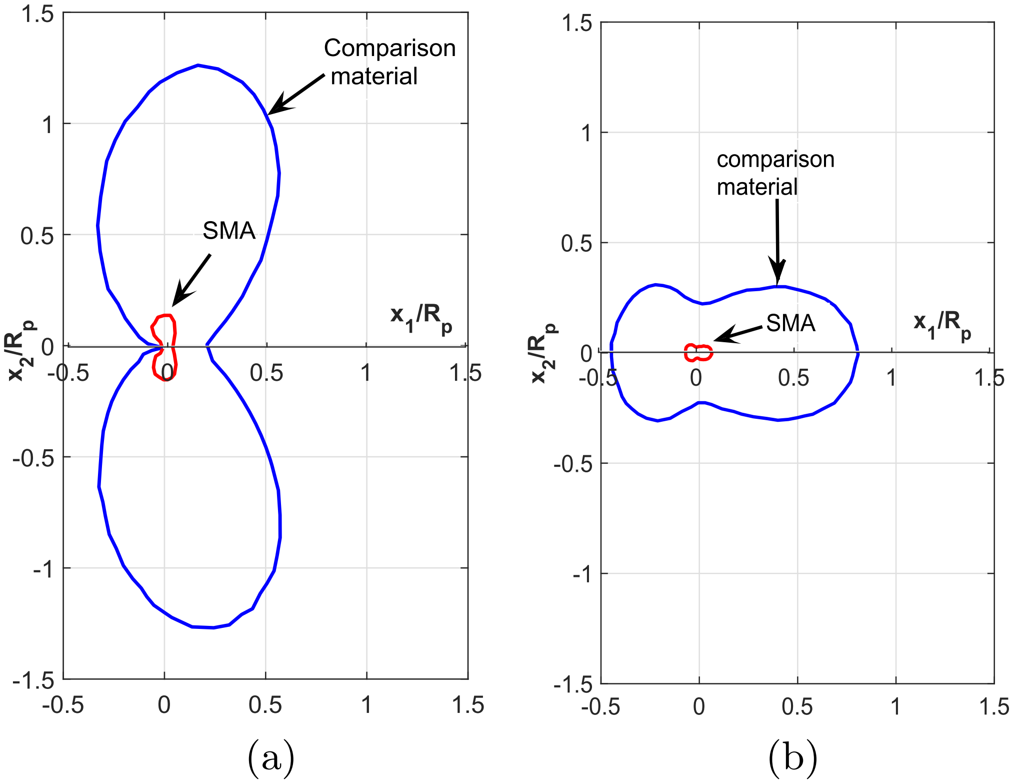


**Figure 21.** Comparison of the PZ size with and without transformation and their evolution with temperature (Baxevanis *et al* 2012). (a) Mode I. (b) Mode II.

CuAlZn. In addition to axial (Vaidyanathan *et al* 2000) and bending (Dolce and Cardone 2005) tests, other techniques were used, namely bending rotation fatigue (BRF) (Miyazaki *et al* 1999, Tobushi *et al* 2000) and torsional fatigue (Predki *et al* 2006, Casciati *et al* 2007). An overall decrease of fatigue life in NiTi is observed with increasing temperature (Miyazaki *et al* 1999) and with decreasing diameter in the case of NiTi wires (Wagner *et al* 2004, Chen and Schuh 2011). This was explained by McKelvey and Ritchie (2001) as a result of the lower fatigue crack growth rate in martensite compared to austenite, and was confirmed by the BRF test of Figueiredo *et al* (2009) where the fatigue life of stable austenite was estimated at about $1/100$ that of stable martensite. When both phases are present, the austenite–martensite interface can act as a supplementary crack initiation site, in addition to grain boundaries (Gloanec *et al* 2010). The fatigue life of NiTi was also found to decrease with increasing loading frequency (Sateesh *et al* 2014) and with the size of oxide and carbide inclusions (Rahim *et al* 2013, Kumar and Lasley 2014). Siredey *et al* (2005) found that the fatigue life in CuAlBe subjected to large strains as high as 10% is comparable to that of NiTi at 3% strain. Ueland and Schuh (2012) showed that oligrocrystalline CuZnAl has a fatigue life similar to that of NiTi, but higher than that of single-crystal and polycrystalline CuZnAl. Recently, Scirè Mammano and Dragoni (2014) obtained fatigue curves for NiTi wires under ‘constant stress’ or ‘constant stress with limited maximum strain’ that were similar in shape to those of common metals. The number of cycles to failure was found to decrease rapidly with the load amplitude in the low-cycle fatigue (LCF) region before approaching a horizontal line for a number of cycles to failure close to $5\times10^5$ in the high-cycle fatigue (HCF) region. Sedlák *et al* (2014) pointed out that the formation of *R*-phase enhances the fatigue life of NiTi springs. From their experimental data, McKelvey and Ritchie (2001) proposed a modified Paris power law (Paris 1964) to describe the evolution of the crack growth rate in terms of the maximum SIF $K_{\max}$ and its variation $\Delta K$, as follows:

$$\frac{\mathrm{d}a}{\mathrm{d}N} = \tilde{C}\,(K_{\max})^n\,(\Delta K)^p, \tag{80}$$

where $\tilde{C}$ is a scaling constant, and $n$ and $p$ are material parameters. However, this equation does not account for some of the experimental observations of the authors who found that fatigue crack growth in NiTi is sensitive not only to the microstructure but also to temperature. One of the rare fatigue life equations that consider thermal effects was proposed by Tobushi *et al* (2000). Tobushi *et al* (2000) established the following Manson–Coffin relation (Manson 1953, Coffin 1954) for low cycle BRF of NiTi to relate the strain amplitude $\varepsilon_a$ and number of cycles to failure $N_{\mathrm{f}}$:

$$\varepsilon_a N_{\mathrm{f}}^{\beta_{\mathrm{f}}} = \hat{\varepsilon}_a, \tag{81}$$

where $\beta_{\mathrm{f}} = 0.5$ and $\hat{\varepsilon}_a$ is the value of $\varepsilon_a$ for $N_{\mathrm{f}} = 1$. To account for the influence of temperature in a hydraulic environment, $\hat{\varepsilon}_a$ was written as

$$\hat{\varepsilon}_a = \alpha_{\mathrm{s}} \times 10^{-a_{\mathrm{s}}(T-M_{\mathrm{s}})}. \tag{82}$$

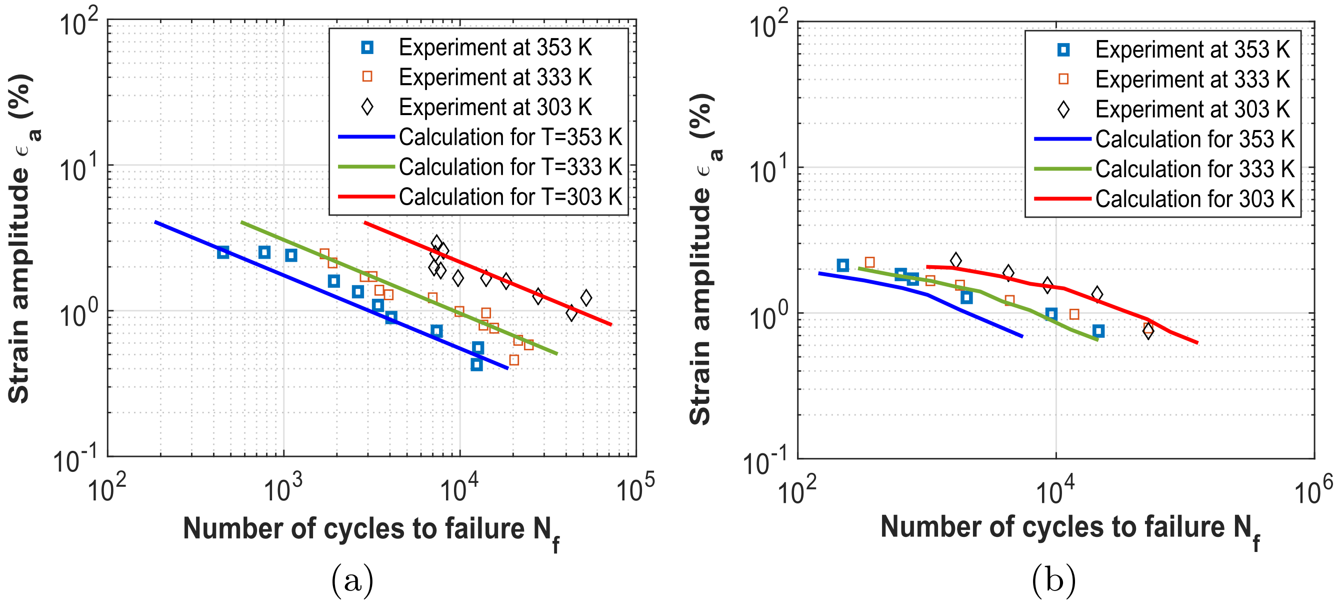


**Figure 22.** Calculated and experimental fatigue life of NiTi in water and air at $f = 500$ cpm (Tobushi *et al* 2000). (a) In water. (b) In air.

where $\alpha_s$ and $a_s$ are material parameters. In order to account for the temperature dependence of fatigue life in air, the author modified the formula obtained in water by replacing the temperature $T$ in (82) with $T + \Delta T$, where $\Delta T$ is a temperature increment given by

$$\Delta T = \left(\frac{f}{f_0}\right)^{c \log\left(\frac{\varepsilon_a}{\varepsilon_1}\right)} \times 10^{-h(T-T_1)}, \tag{83}$$

where $f_0$ is a reference frequency, $f$ is the testing frequency, and $c$, $\varepsilon_1$, $h$ and $T_1 = A_f - 3K$ are constants. The above equations are shown to properly fit the experimental results for LCF in nitinol in both air and water (figure 22). However, the authors did not account for the influence of loading frequency, which was later addressed by Young and Van Vliet (2005). For this purpose, a modified Manson–Coffin law was proposed to predict the *in vivo* LCF failure of pseudoelastic NiTi, considering the effects of radius of curvature, angle of curvature, wire diameter, strain amplitude, cyclic frequency, volume under strain, and specific heat of the surrounding environmental fluid. Unlike in (Pruett *et al* 1997), the influence of the loading frequency was considered by defining $\beta_f$ and $\hat{\varepsilon}_a$ as follows:

$$\begin{aligned} \hat{\varepsilon}_a &= -0.76 \ln(f) + 2.10(c_{p,e}/c_{p,NiTi}), \\ \beta_f &= 0.10(c_{p,e}/c_{p,NiTi}) \ln(f) - 0.75. \end{aligned} \tag{84}$$

where $c_{p,e}$ is the specific heat of the surrounding environment and $c_{p,NiTi}$ is that of NiTi. The strain amplitude for the RBF was given by

$$\varepsilon_a = \frac{2d}{2R + d}, \tag{85}$$

where $d$ is the specimen diameter and $R$ is the curvature radius of the deformed wire. Eggeler *et al* (2004) and Wagner *et al* (2004) analyzed the BRF of NiTi. However, they used the following expression of the surface strain:

$$\varepsilon_a = \frac{d}{2R}. \tag{86}$$

Runciman *et al* (2011) plotted the experimental strain-life diagram of nitinol tubing and attempted to normalize the fatigue data in tension, compression, bending and torsion. Figure 23(a) was obtained by replacing the strain amplitude $\varepsilon_a$ with the alternating equivalent strain $\Delta\bar{\varepsilon}/2$. Considering the transformation part $\frac{\Delta\bar{\varepsilon}_{tr}}{2}$ of $\Delta\varepsilon/2$, they obtained a 'universal' fit for a strain ratio $R_\varepsilon$ between $-1$ and 0.99 using the relation

$$\frac{\Delta\bar{\varepsilon}_{tr}}{2} = 61.7 N_f^{-1/2}, \tag{87}$$

as shown in figure 23(b). The obtained fit is satisfactory but not very accurate in torsion, tension/tension and bending. Kollerov *et al* (2013) proposed another modified Manson–Coffin equation using two structure-dependent coefficients $\varepsilon_{cr}$ and $\beta_f$:

$$N_f = \varepsilon_{cr}(1/\varepsilon_a)^{\beta_f}, \tag{88}$$

where $\varepsilon_{cr}$ is the critical deformation of the sample and $\beta_f$ is a function of the elastic modulus and transformation/reorientation stress. A good agreement was obtained between the calculated and experimental LCF curves, but HCF was not properly addressed. Based on the work of Auricchio *et al* (1997) and Olsen *et al* (2011), Wang *et al* (2014b) numerically predicted a decreasing fatigue life with the increase of notch acuity. Recently, Barrera *et al* (2014) extended the model of Souza *et al* (1998) to successfully simulate functional fatigue in SMAs including the training phase, stable regime and degradation. In a recent publication, Calhoun *et al* (2015) studied the fatigue life of SMA actuators subjected to cyclic superthermal loading. The authors adapted the critical plane model that was developed by Smith *et al* (1970) for low and intermediate-cycle fatigue life of common

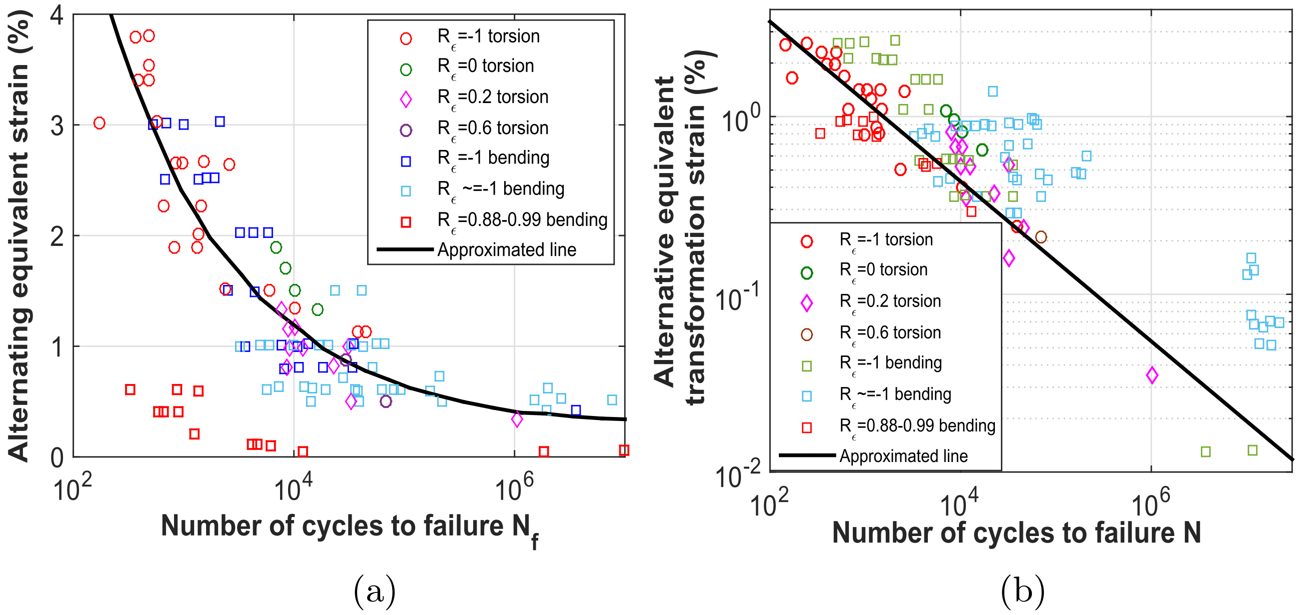


**Figure 23.** Multiaxial fatigue life of nitinol tubes (Runciman *et al* 2011). (a)$\frac{\Delta\bar{\varepsilon}}{2}$ versus $N_f$. (b) Strain versus fatigue life of NiTi tubes as $\frac{\Delta\bar{\varepsilon}_{tr}}{2}$ versus $N_f$.

metals for use with NiTi SMAs. The number of cycles to failure was related to the maximum normal stress $\sigma_{max}$ in the plane of the maximum principal strain $\varepsilon_a$ as follows:

$$\sigma_{max}\,\varepsilon_a = A\,(N_f)^{-b}, \tag{89}$$

where $A$ and $b$ are material parameters. The authors showed that the energy term $\sigma_{max}\,\varepsilon_a$ can be used to predict the fatigue life of SMAs subjected to pure mechanical loading and/or actuation conditions. Scirè Mammano and Dragoni (2015) investigated the fatigue behavior of NiTi wire and found that partial RT enhances its structural fatigue life. Using multi-factorial analysis, the interpolating function of $N_f$ was written as as a complete multilinear polynomial of the following form:

$$\begin{aligned} N_f = a\,.\,A + b\,.\,B + c\,.\,C + ab\,.\,AB \\ + ac\,.\,AC + bc\,.\,BC + abc\,.\,ABC, \end{aligned} \tag{90}$$

where $a$, $b$, $c$, $ab$, $ac$, $bc$, $abc$ are the respective regression coefficients of the coded factors $A$ for pre-stress, $B$ for heating rate, $C$ for degree of RT, and their interactions $AB$, $AC$, $BC$ and $ABC$. The authors found that the factor $C$ is dominant while $AC$ was less important. Indeed, incomplete RT ensures no fracture up to the considered 150 000 cycles, while full martensite-to-autenite phase change is characterized by a significant degradation of the functional and structural fatigue responses. Moumni *et al* (2009) and Moumni *et al* (2014) extended the ZM model to derive an energy-based LCF criterion and showed that the dissipated energy of the stabilized cycle $W_{sat}$ can be used to estimate the fatigue life $N_f$ of SMAs. Based on experimental data, the following relation was found between $W_{sat}$ and $N_f$:

$$W_{sat} = \alpha N_f^{\beta}, \tag{91}$$

where $\alpha = 11$ and $\beta = -0.377$ for NiTi. Most of the above fatigue life models neglect the evolution of the hysteresis energy during the first loading cycles. A notable exception is the work of Song *et al* (2015) who expressed the number of cycles to failure as follows:

$$N_f = N_{sat} + 1 + \frac{1 - \left[K_1 + K_3 \int_0^{N_{sat}} W_N\,\mathrm{d}N\right]}{K_2 + K_3 W_{sat}}, \tag{92}$$

where $W_N$ is the dissipated energy at the $N$th cycle that takes a value $W_{sat}$ at saturation where $N = N_{sat}$, and $K_1$, $K_2$ and $K_3$ are material parameters. It is worth noting that multiaxial fatigue behavior is usually disregarded, with the exception of few models including those where the dissipated energy is used as the relevant variable for predicting the number of cycles to failure (Moumni *et al* 2009, 2014, Song *et al* 2015). Moreover, the influence of thermomechanical coupling on fatigue life in SMAs has only started to be addressed (Zhang *et al* 2016).

Applications in the aerospace field are considered by McDonald Schetky (1991), Van Humbeeck (1999), Hartl and Lagoudas (2007), Bil *et al* (2013), Barbarino *et al* (2014), in the automotive field by Stoeckel (1990), Leo *et al* (1998), Predki *et al* (2008), Butera (2008), Bellini *et al* (2009), Cartmell *et al* (2012), Gheorghita *et al* (2014), in the biomedical field by Duerig *et al* (1999), Mantovani (2000), Machado and Savi (2003), Morgan (2004), Fischer *et al* (2004), Niinomi (2008), Ko *et al* (2011), Petrini and Migliavacca (2011), Vincent *et al* (2015), in petroleum engineering by Wang *et al* (2005a), Dai and Zhou (2006), Jee *et al* (2006), Druker *et al* (2014), in mini-actuators and micro-electromechanical systems by Krulevitch *et al* (1996), Kahn *et al* (1998), Fujita and Toshiyoshi (1998), Kohl (2004), Sun *et al* (2012a), Merzouki *et al* (2012), in paraseismic devices by DesRoches and Delemont (2002), Sharabash and Andrawes (2009), in railways by Maruyama *et al* (2008), Khalil *et al* (2012) and in civil engineering by Corbi (2003), Song *et al* (2006), Williams *et al* (2010), Cladera *et al* (2014).

## 10. Conclusion

The paper presents recent developments in modeling and simulation of advanced SMA effects such as the reorientation of martensite under multiaxial loading, training and two-way shape memory, plasticity and its coupling with the martensitic transformation, the role of thermomechanical coupling and tensile–compressive asymmetry, the evolution of elastic stiffness with phase transformation as well as the analysis and prediction of functional and structural fatigue and the investigation of static and propagating cracks and fracture. The present paper, together with the recently published work of Cissé *et al* (2016), is an attempt to summarize the output of several decades of research dedicated to the investigation of SMAs, which has tremendously improved our understanding of these materials. The models developed by the different research groups have matured over the years with each having its own advantages and shortcomings. It is also worth noting that the bulk of the available research work is dedicated to NiTi and Cu-based SMAs, which are consequently much better understood than the more recent yet very promising Fe-based alloys. Significant theoretical and experimental work is therefore needed to improve our understanding of these materials, which may include the establishment of accurate phase transformation diagrams in terms of stress and temperature, in which the presence of plastic deformation regions must be considered, as well as relevant analytical and numerical developments. The investigation of fatigue and fracture is another area where much still needs to be done and is therefore expected to be one of the focus areas for future research on SMAs.

## Acknowledgments

Dr Wael Zaki would like to acknowledge the financial support of Khalifa University through KUIRF level 2 research fund no. 210031.

## References

Afshar A, Ardakani S H, Hashemi S and Mohammadi S 2015 Numerical analysis of crack tip fields in interface fracture of SMA/elastic bi-materials *Int. J. Fract.* **195** 39–52

Amengual A, Cesari E and Pons J 1995 Characteristics of the two-way memory effect induced by thermomechanical cycling in Cu–Zn–Al single crystals *J. Phys.* IV **5** 871–6

Anand L and Gurtin M E 2003 Thermal effects in the superelasticity of crystalline shape-memory materials *J. Mech. Phys. Solids* **51** 1015–58

Anderson T L 2005 *Fracture Mechanics: Fundamentals and Applications* (Boca Raton, FL: CRC Press)

Arghavani J, Auricchio F, Naghdabadi R and Reali A 2011 On the robustness and efficiency of integration algorithms for a 3D finite strain phenomenological SMA constitutive model *Int. J. Numer. Methods Eng.* **85** 107–34

Arghavani J, Auricchio F, Naghdabadi R, Reali A and Sohrabpour S 2010 A 3D phenomenological constitutive model for shape memory alloys under multiaxial loadings *Int. J. Plast.* **26** 976–91

Auricchio F 1995 Shape-memory alloys: applications, micromechanics, macromodelling and numerical simulations *PhD Thesis* University of California Berkeley

Auricchio F, Bonetti E, Scalet G and Ubertini F 2014 Theoretical and numerical modeling of shape memory alloys accounting for multiple phase transformations and martensite reorientation *Int. J. Plast.* **59** 30–54

Auricchio F, Fugazza D and Desroches R 2008 Rate-dependent thermo-mechanical modelling of superelastic shape-memory alloys for seismic applications *J. Intell. Mater. Syst. Struct.* **19** 47–61

Auricchio F, Marfia S and Sacco E 2003 Modelling of SMA materials: training and two way memory effects *Comput. Struct.* **81** 2301–17

Auricchio F and Petrini L 2002 Improvements and algorithmical considerations on a recent three-dimensional model describing stress-induced solid phase transformations *Int. J. Numer. Methods Eng.* **55** 1255–84

Auricchio F and Petrini L 2004 A three-dimensional model describing stress–temperature induced solid phase transformations: solution algorithm and boundary value problems *Int. J. Numer. Methods Eng.* **61** 807–36

Auricchio F and Reali A 2007 A phenomenological one-dimensional model describing stress-induced solid phase transformation with permanent inelasticity *Mech. Adv. Mater. Struct.* **14** 43–55

Auricchio F, Reali A and Stefanelli U 2007a A phenomenological 3D model describing stress-induced solid phase transformations with permanent inelasticity *Topics on Mathematics for Smart Systems* pp 1–14

Auricchio F, Reali A and Stefanelli U 2007b A three-dimensional model describing stress-induced solid phase transformation with permanent inelasticity *Int. J. Plast.* **23** 207–26

Auricchio F, Reali A and Stefanelli U 2009 A macroscopic 1D model for shape memory alloys including asymmetric behaviors and transformation-dependent elastic properties *Comput. Methods Appl. Mech. Eng.* **198** 1631–7

Auricchio F and Sacco E 1997 A one-dimensional model for superelastic shape-memory alloys with different elastic properties between austenite and martensite *Int. J. Non-Linear Mech.* **32** 1101–14

Auricchio F and Sacco E 1999 A temperature-dependent beam for shape-memory alloys: constitutive modelling, finite-element implementation and numerical simulations *Comput. Methods Appl. Mech. Eng.* **174** 171–90

Auricchio F and Sacco E 2001 Thermo-mechanical modelling of a superelastic shape-memory wire under cyclic stretching-bending loadings *Int. J. Solids Struct.* **38** 6123–45

Auricchio F, Taylor R L and Lubliner J 1997 Shape-memory alloys: macromodelling and numerical simulations of the superelastic behavior *Comput. Methods Appl. Mech. Eng.* **146** 281–312

Barbarino S, Flores E S, Ajaj R, Dayyani I and Friswell M 2014 A review on shape memory alloys with applications to morphing aircraft *Smart Mater. Struct.* **23** 063001

Barrera N, Biscari P and Urbano M F 2014 Macroscopic modeling of functional fatigue in shape memory alloys *Eur. J. Mech.* A **45** 101–9

Baruj A, Bertolino G and Troiani H 2010 Temperature dependence of critical stress and pseudoelasticity in a Fe–Mn–Si–Cr pre-rolled alloy *J. Alloys Compd.* **502** 54–8

Baxevanis T, Chemisky Y and Lagoudas D 2012 Finite element analysis of the plane strain crack-tip mechanical fields in pseudoelastic shape memory alloys *Smart Mater. Struct.* **21** 094012
Baxevanis T and Lagoudas D 2012 A mode I fracture analysis of a center-cracked infinite shape memory alloy plate under plane stress *Int. J. Fract.* **175** 151–66
Baxevanis T, Landis C M and Lagoudas D C 2014 On the fracture toughness of pseudoelastic shape memory alloys *J. Appl. Mech.* **81** 041005
Bekker A and Brinson L 1998 Phase diagram based description of the hysteresis behavior of shape memory alloys *Acta Mater.* **46** 3649–65
Bellini A, Colli M and Dragoni E 2009 Mechatronic design of a shape memory alloy actuator for automotive tumble flaps: a case study *IEEE Trans. Ind. Electron.* **56** 2644–56
Bernardini D and Pence T J 2002 Models for one-variant shape memory materials based on dissipation functions *Int. J. Non-Linear Mech.* **37** 1299–317
Bil C, Massey K and Abdullah E J 2013 Wing morphing control with shape memory alloy actuators *J. Intell. Mater. Syst. Struct.* **24** 879–98
Bo Z and Lagoudas D C 1999 Thermomechanical modeling of polycrystalline SMAs under cyclic loading: III. Evolution of plastic strains and two-way shape memory effect *Int. J. Eng. Sci.* **37** 1175–203
Bourbon G, Lexcellent C and Leclercq S 1995 Modelling of the non isothermal cyclic behaviour of a polycrystalline CuZnAl shape memory alloy *J. Phys.* IV **5** 221–8
Bouvet C, Calloch S and Lexcellent C 2002 Mechanical behavior of a Cu–Al–Be shape memory alloy under multiaxial proportional and nonproportional loadings *J. Eng. Mater. Technol.* **124** 112–24
Bouvet C, Calloch S and Lexcellent C 2004 A phenomenological model for pseudoelasticity of shape memory alloys under multiaxial proportional and nonproportional loadings *Eur. J. Mech.* A **23** 37–61
Boyd J G and Lagoudas D C 1996 A thermodynamical constitutive model for shape memory materials: I. The monolithic shape memory alloy *Int. J. Plast.* **12** 805–42
Brinson L 1993 One-dimensional constitutive behavior of shape memory alloys: thermomechanical derivation with non-constant material functions and redefined martensite internal variable *J. Intell. Mater. Syst. Struct.* **4** 229–42
Brinson L and Lammering R 1993 Finite element analysis of the behavior of shape memory alloys and their applications *Int. J. Solids Struct.* **30** 3261–80
Buchheit T and Wert J 1994 Modeling the effects of stress state and crystal orientation on the stress-induced transformation of niti single crystals *Metall. Mater. Trans.* A **25** 2383–9
Butera F 2008 Shape memory actuators for automotive applications *Adv. Mater. Process.* **166** 37–40
Cailletaud G and Pilvin P 1994 Utilisation de modèles polycristallins pour le calcul par éléments finis *Rev. européenne des éléments finis* **3** 515–41
Calhoun C, Wheeler R, Baxevanis T and Lagoudas D 2015 Actuation fatigue life prediction of shape memory alloys under the constant-stress loading condition *Scr. Mater.* **95** 58–61
Cartmell M, Ak A and Ganilova O 2012 Applications for shape memory alloys in structural and machine dynamics *Nonlinear Dynamic Phenomena in Mechanics* (*Solid Mechanics and its Applications* vol 181) ed J Warminski *et al* (Netherlands: Springer) pp 115–58
Casciati F, Casciati S and Faravelli L 1999, 2007 Fatigue characterization of a Cu-based shape memory alloy *Proc. Estonian Academy of Sciences. Physics Mathmatics* vol 56 ((Estonian Academy Publishers) pp 207–17
Castellano M 2000 Project: Shape memory alloy devices for seismic protection of cultural heritage structures *Final Workshop of ISTECH Project (Ispra, Italy)*
Chang B-C, Shaw J A and Iadicola M A 2006 Thermodynamics of shape memory alloy wire: modeling, experiments, and application *Contin. Mech. Thermodyn.* **18** 83–118
Chemisky Y, Chatzigeorgiou G, Kumar P and Lagoudas D C 2014 A constitutive model for cyclic actuation of high-temperature shape memory alloys *Mech. Mater.* **68** 120–36
Chemisky Y, Duval A, Patoor E and Ben Zineb T 2011 Constitutive model for shape memory alloys including phase transformation, martensitic reorientation and twins accommodation *Mech. Mater.* **43** 361–76
Chen Y and Schuh C A 2011 Size effects in shape memory alloy microwires *Acta Mater.* **59** 537–53
Christ D and Reese S 2009 A finite element model for shape memory alloys considering thermomechanical couplings at large strains *Int. J. Solids Struct.* **46** 3694–709
Chumljakov J and Starenchenko S 1995 Stress induced martensitic transformation in aged titanium nickel single crystals *J. Phys.* IV **5** 803–7
Cingolani E, Yawny A and Ahlers M 1995 The two way shape memory effect in stabilized and pseudoelastically trained Cu–Zn–Al single crystals *J. Phys.* IV **5** 865–9
Cissé C, Zaki W and Ben Zineb T 2016 A review of constitutive models and modeling techniques for shape memory alloys *Int. J. Plast.* **76** 244–84
Cladera A, Weber B, Leinenbach C, Czaderski C, Shahverdi M and Motavalli M 2014 Iron-based shape memory alloys for civil engineering structures: an overview *Constr. Build. Mater.* **63** 281–93
Coffin L F Jr 1954 A study of the effects of cyclic thermal stresses on a ductile metal *Trans. ASME* **76** 931–50
Contardo L 1988 Etude des traitements d'éducation, de la stabilité et de l'origine de l'effet mémoire de forme double sens dans un alliage Cu–Zn–Al *PhD Thesis* Villeurbanne, INSA
Corbi O 2003 Shape memory alloys and their application in structural oscillations attenuation *Simul. Modelling Pract. Theory* **11** 387–402
Creuziger A, Bartol L, Gall K and Crone W 2008 Fracture in single crystal NiTi *J. Mech. Phys. Solids* **56** 2896–905
Dai P and Zhou L 2006 Investigation on the connecting strength of Fe–Mn–Si–C shape memory alloy pipe coupling *J. Mater. Sci.* **41** 3441–3
Daly S, Miller A, Ravichandran G and Bhattacharya K 2007 An experimental investigation of crack initiation in thin sheets of nitinol *Acta Mater.* **55** 6322–30
De Araujo C J 1999 Comportement cyclique de fils en alliage à mémoire de forme Ti–Ni–Cu: analyse électro-thermomécanique, dégradation et fatigue par cyclage thermique sous contrainte *PhD Thesis* INSA-Lyon
de Almeida L A L, Deep G S, Lima A M N and Neff H 2003 Limiting loop proximity hysteresis model *IEEE Trans. Magn.* **39** 523–8
Delaey L, Krishnan R, Tas H and Warlimont H 1974 Thermoelasticity, pseudoelasticity and the memory effects associated with martensitic transformations *J. Mater. Sci.* **9** 1521–35
Depriester D, Maynadier A, Lavernhe-Taillard K and Hubert O 2014 Thermomechanical modelling of a NiTi SMA sample submitted to displacement-controlled tensile test *Int. J. Solids Struct.* **51** 1901–22
DesRoches R and Delemont M 2002 Seismic retrofit of simply supported bridges using shape memory alloys *Eng. Struct.* **24** 325–32
Dolce M and Cardone D 2005 Fatigue resistance of SMA-martensite bars subjected to flexural bending *Int. J. Mech. Sci.* **47** 1693–717
Druker A V, Esquivel I, Perotti A and Malarria J 2014 Optimization of Fe–15Mn–5Si–9Cr–5Ni shape memory alloy for pipe and shaft couplings *J. Mater. Eng. Perform.* **23** 2732

Duerig T, Pelton A and Stöckel D 1999 An overview of nitinol medical applications *Mater. Sci. Eng.* A **273–275** 149–60
Eggeler G, Hornbogen E, Yawny A, Heckmann A and Wagner M 2004 Structural and functional fatigue of NiTi shape memory alloys *Mater. Sci. Eng.* A **378** 24–33
Evangelista V, Marfia S and Sacco E 2009 Phenomenological 3D and 1D consistent models for shape-memory alloy materials *Comput. Mech.* **44** 405–21
Falvo A, Furgiuele F and Maletta C 2008 Hysteresis modeling of two-way shape memory effect in NiTi alloys *Meccanica* **43** 165–72
Feng X-Q and Sun Q 2007 Shakedown analysis of shape memory alloy structures *Int. J. Plast.* **23** 183–206
Figueiredo A M, Modenesi P and Buono V 2009 Low-cycle fatigue life of superelastic NiTi wires *Int. J. Fatigue* **31** 751–8
Fischer H, Vogel B and Welle A 2004 Applications of shape memory alloys in medical instruments *Minimally Invasive Ther. Allied Technol.* **13** 248–53
Fischlschweiger M and Oberaigner E R 2012 Kinetics and rates of martensitic phase transformation based on statistical physics *Comput. Mater. Sci.* **52** 189–92
Ford D S and White S 1996 Thermomechanical behavior of 55Ni45Ti nitinol *Acta Mater.* **44** 2295–307
Franz G, Abed-Meraim F, Lorrain J-P, Ben Zineb T, Lemoine X and Berveiller M 2009 Ellipticity loss analysis for tangent moduli deduced from a large strain elastic-plastic self-consistent model *Int. J. Plast.* **25** 205–38
Freed Y and Banks-Sills L 2007 Crack growth resistance of shape memory alloys by means of a cohesive zone model *J. Mech. Phys. Solids* **55** 2157–80
Frémond M 1987 *C. R. Acad. Sci., Paris* II **304** 239–44
Fujita H and Toshiyoshi H 1998 Micro actuators and their applications *Microelectron. J.* **29** 637–40
Gall K and Maier H 2002 Cyclic deformation mechanisms in precipitated NiTi shape memory alloys *Acta Mater.* **50** 4643–57
Gall K and Sehitoglu H 1999 The role of texture in tension–compression asymmetry in polycrystalline NiTi *Int. J. Plast.* **15** 69–92
Gall K, Sehitoglu H, Anderson R, Karaman I, Chumlyakov Y I and Kireeva I V 2001a On the mechanical behavior of single crystal NiTi shape memory alloys and related polycrystalline phenomenon *Mater. Sci. Eng.* A **317** 85–92
Gall K, Sehitoglu H and Maier H 1997 Asymmetric stress–strain response in shape memory alloys *Plast* **97** 153–4
Gall K, Yang N, Sehitoglu H and Chumlyakov Y I 2001b Fracture of precipitated NiTi shape memory alloys *Int. J. Fract.* **109** 189–207
Gheorghita V, Gmpel P, Chiru A and Strittmatter J 2014 Future applications of Ni–Ti alloys in automotive safety systems *Int. J. Automot. Technol.* **15** 469–74
Gillet Y, Patoor E and Berveiller M 1998 Calculation of pseudoelastic elements using a non-symmetrical thermomechanical transformation criterion and associated rule *J. Intell. Mater. Syst. Struct.* **9** 366–78
Gloanec A-L, Cerracchio P, Reynier B, Van Herpen A and Riberty P 2010 Fatigue crack initiation and propagation of a TiNi shape memory alloy *Scr. Mater.* **62** 786–9
Gollerthan S, Young M, Neuking K, Ramamurty U and Eggeler G 2009 Direct physical evidence for the back-transformation of stress-induced martensite in the vicinity of cracks in pseudoelastic NiTi shape memory alloys *Acta Mater.* **57** 5892–7
Gong S, Li Z and Zhao Y 2011 An extended Mori–Tanaka model for the elastic moduli of porous materials of finite size *Acta Mater.* **59** 6820–30
Govindjee S and Kasper E P 1999 Computational aspects of one-dimensional shape memory alloy modeling with phase diagrams *Comput. Methods Appl. Mech. Eng.* **171** 309–26
Grabe C and Bruhns O 2008 On the viscous and strain rate dependent behavior of polycrystalline NiTi *Int. J. Solids Struct.* **45** 1876–95
Grabe C and Bruhns O 2009 Path dependence and multiaxial behavior of a polycrystalline NiTi alloy within the pseudoelastic and pseudoplastic temperature regimes *Int. J. Plast.* **25** 513–45
Gu X, Zaki W, Morin C, Moumni Z and Zhang W 2015 Time integration and assessment of a model for shape memory alloys considering multiaxial nonproportional loading cases *Int. J. Solids Struct.* **54** 82–99
Guilemany J and Fernández J 1995 Mechanism of two way shape memory effect obtained by stabilised stress induced martensite *J. Phys.* IV **05** 355–9
Hartl D and Lagoudas D 2009 Constitutive modeling and structural analysis considering simultaneous phase transformation and plastic yield in shape memory alloys *Smart Mater. Struct.* **18** 104017
Hartl D and Lagoudas D C 2007 Aerospace applications of shape memory alloys *Proc. Inst. Mech. Eng.* G **221** 535–52
Hartl D J, Chatzigeorgiou G and Lagoudas D C 2010 Three-dimensional modeling and numerical analysis of rate-dependent irrecoverable deformation in shape memory alloys *Int. J. Plast.* **26** 1485–507
Hashemi S, Ahmadian H and Mohammadi S 2015 An extended thermo-mechanically coupled algorithm for simulation of superelasticity and shape memory effect in shape memory alloys *Frontiers Struct. Civil Eng.* **9** 466–77
Hatcher N, Kontsevoi O Y and Freeman A 2009 Role of elastic and shear stabilities in the martensitic transformation path of NiTi *Phys. Rev.* B **80** 144203
Hazar S, Zaki W, Moumni Z and Anlas G 2013 Steady state crack growth in shape memory alloys *ASME 2013 Conf. on Smart Materials, Adaptive Structures and Intelligent Systems* (American Society of Mechanical Engineers) p V001T03A018
Hazar S, Zaki W, Moumni Z and Anlas G 2015 Modeling of steady-state crack growth in shape memory alloys using a stationary method *Int. J. Plast.* **67** 26–38
He Y and Sun Q 2010 Frequency-dependent temperature evolution in NiTi shape memory alloy under cyclic loading *Smart Mater. Struct.* **19** 115014
Hebda D A and White S R 1995 Effect of training conditions and extended thermal cycling on nitinol two-way shape memory behavior *Smart Mater. Struct.* **4** 298
Helbert G, Saint-Sulpice L, Chirani S A, Dieng L, Lecompte T, Calloch S and Pilvin P 2014 Experimental characterisation of three-phase NiTi wires under tension *Mech. Mater.* **79** 85–101
Heller L, Šittner P, Pilch J and Landa M 2009 Factors controlling superelastic damping capacity of SMAs *J. Mater. Eng. Perform.* **18** 603–11
Helm D 2001 Formgedächtnislegierungen: experimentelle untersuchung, phänomenologische modellierung und numerische simulation der thermomechanischen materialeigenschaften *PhD Thesis* Universität Gesamthochschule Kassel
Helm D and Haupt P 2001 Thermomechanical behavior of shape memory alloys *SPIE's 8th Annual Int. Symp. on Smart Structures and Materials* (International Society for Optics and Photonics) pp 302–13
Helm D and Haupt P 2002 Thermomechanical representation of the multiaxial behavior of shape memory alloys *SPIE's 9th Annual Int. Symp. on Smart Structures and Materials* (International Society for Optics and Photonics) pp 343–54
Helm D and Haupt P 2003 Shape memory behaviour: modelling within continuum thermomechanics *Int. J. Solids Struct.* **40** 827–49
Huang M and Brinson L 1998 A multivariant model for single crystal shape memory alloy behavior *J. Mech. Phys. Solids* **46** 1379–409

Huang W and Xu W 2005 Hysteresis in shape memory alloys. Is it always a constant? *J. Mater. Sci.* **40** 2985–6

Huo Y and Müller I 1993 Nonequilibrium thermodynamics of pseudoelasticity *Contin. Mech. Thermodyn.* **5** 163–204

Iadicola M A and Shaw J A 2004 Rate and thermal sensitivities of unstable transformation behavior in a shape memory alloy *Int. J. Plast.* **20** 577–605

Ikeda T, Nae F A, Naito H and Matsuzaki Y 2004 Constitutive model of shape memory alloys for unidirectional loading considering inner hysteresis loops *Smart Mater. Struct.* **13** 916

Irwin G 1960 Plastic zone near a crack and fracture toughness *Proc. 7th Sagamore Ordnance Materials Conf.* (Syracuse: Syracuse University Press) pp 63–78

Ivshin Y and Pence T J 1994 A thermomechanical model for a one variant shape memory material *J. Intell. Mater. Syst. Struct.* **5** 455–73

Jacobus K, Sehitoglu H and Balzer M 1996 Effect of stress state on the stress-induced martensitic transformation in polycrystalline Ni–Ti alloy *Metall. Mater. Trans.* A **27** 3066–73

James R and Zhang Z 2005 A way to search for multiferroic materials with unlikely combinations of physical properties *Magnetism and Structure in Functional Materials* (Berlin: Springer) pp 159–75

Jee K K, Han J and Jang W 2006 A method of pipe joining using shape memory alloys *Mater. Sci. Eng.* A **438** 1110–2

Jemal F, Bouraoui T, Ben Zineb T, Patoor E and Bradaï C 2009 Modelling of martensitic transformation and plastic slip effects on the thermo-mechanical behaviour of Fe-based shape memory alloys *Mech. Mater.* **41** 849–56

Kahn H, Huff M and Heuer A 1998 The TiNi shape-memory alloy and its applications for MEMS *J. Micromech. Microeng.* **8** 213

Kajiwara S 1999 Characteristic features of shape memory effect and related transformation behavior in Fe-based alloys *Mater. Sci. Eng.* A **273** 67–88

Kato H and Sasaki K 2013 Transformation-induced plasticity as the origin of serrated flow in an NiTi shape memory alloy *Int. J. Plast.* **50** 37–48

Khalil W, Mikolajczak A, Bouby C and Ben Zineb T 2012 A constitutive model for Fe-based shape memory alloy considering martensitic transformation and plastic sliding coupling: application to a finite element structural analysis *J. Intell. Mater. Syst. Struct.* **23** 1143–60

Khalil W, Saint-Sulpice L, Arbab Chirani S, Bouby C, Mikolajczak A and Ben Zineb T 2013 Experimental analysis of Fe-based shape memory alloy behavior under thermomechanical cyclic loading *Mech. Mater.* **63** 1–1

Kim H W 2004 A study of the two-way shape memory effect in Cu–Zn–Al alloys by the thermomechanical cycling method *J. Mater. Process. Technol.* **146** 326–9

Kim H W 2005 Investigation of a Cu–Zn–Al alloy with two-way shape memory effect by the cycled constrained heating/cooling technique *J. Mater. Sci.* **40** 211–2

Ko J, Jun M B, Gilardi G, Haslam E and Park E J 2011 Fuzzy PWM-PID control of cocontracting antagonistic shape memory alloy muscle pairs in an artificial finger *Mechatronics* **21** 1190–202

Kohl M 2004 *Shape Memory Microactuators* (Berlin: Springer)

Kollerov M, Lukina E, Gusev D, Mason P and Wagstaff P 2013 Impact of material structure on the fatigue behaviour of NiTi leading to a modified Coffin–Manson equation *Mater. Sci. Eng.* A **585** 356–62

Koyama M, Sawaguchi T, Ogawa K, Kikuchi T and Murakami M 2008 The effects of thermomechanical training treatment on the deformation characteristics of Fe–Mn–Si–Al alloys *Mater. Sci. Eng.* A **497** 353–7

Krasnoselskii M and Pokrovskii A 2012 *Systems with Hysteresis* (Berlin: Springer)

Krulevitch P, Lee A P, Ramsey P B, Trevino J C, Hamilton J and Northrup M A 1996 Thin film shape memory alloy microactuators *J. Microelectromech. Syst.* **5** 270–82

Kumar P K and Lagoudas D C 2010 Experimental and microstructural characterization of simultaneous creep, plasticity and phase transformation in Ti50Pd40Ni10 high-temperature shape memory alloy *Acta Mater.* **58** 1618–28

Kumar P K and Lasley C 2014 The influence of microcleanliness on the fatigue performance of nitinol *J. Mater. Eng. Perform.* **23** 2457

Lagoudas D, Hartl D, Chemisky Y, Machado L and Popov P 2012 Constitutive model for the numerical analysis of phase transformation in polycrystalline shape memory alloys *Int. J. Plast.* **32** 155–83

Lagoudas D C and Entchev P B 2004 Modeling of transformation-induced plasticity and its effect on the behavior of porous shape memory alloys: I. Constitutive model for fully dense SMAs *Mech. Mater.* **36** 865–92

Lagoudas D C, Entchev P B, Popov P, Patoor E, Brinson L C and Gao X 2006 Shape memory alloys: II. Modeling of polycrystals *Mech. Mater.* **38** 430–62

Lagoudas D C and Shu S G 1999 Residual deformation of active structures with SMA actuators *Int. J. Mech. Sci.* **41** 595–619

Leclercq S and Lexcellent C 1996 A general macroscopic description of the thermomechanical behavior of shape memory alloys *J. Mech. Phys. Solids* **44** 953–80

Leo D J, Weddle C, Naganathan G and Buckley S J 1998 Vehicular applications of smart material systems *5th Annual Int. Symp. on Smart Structures and Materials* (International Society for Optics and Photonics) pp 106–16

Leo P H, Shield T and Bruno O P 1993 Transient heat transfer effects on the pseudoelastic behavior of shape-memory wires *Acta Metall. Mater.* **41** 2477–85

Lexcellent C 2013 *Shape-Memory Alloys Handbook* (New York: Wiley)

Lexcellent C, Blanc P and Creton N 2008 Two ways for predicting the hysteresis minimisation for shape memory alloys *Mater. Sci. Eng.* A **481** 334–8

Lexcellent C and Bourbon G 1996 Thermodynamical model of cyclic behaviour of Ti–Ni and Cu–Zn–Al shape memory alloys under isothermal undulated tensile tests *Mech. Mater.* **24** 59–73

Lexcellent C, Boubakar M, Bouvet C and Calloch S 2006 About modelling the shape memory alloy behaviour based on the phase transformation surface identification under proportional loading and anisothermal conditions *Int. J. Solids Struct.* **43** 613–26

Lexcellent C, Leclercq S, Gabry B and Bourbon G 2000 The two way shape memory effect of shape memory alloys: an experimental study and a phenomenological model *Int. J. Plast.* **16** 1155–68

Liang C 1990 The constitutive modeling of shape memory alloys *PhD Thesis* Virginia Polytechnic Institute and State University

Liang C and Rogers C 1990 One-dimensional thermomechanical constitutive relations for shape memory materials *J. Intell. Mater. Syst. Struct.* **1** 207–34

Lieberman D, Schmerling M, Karz R and Perkins J 1975 *Shape Memory Effects in Alloys* (NY: Plenum Pub1. Co.) p 203

Lim J T and McDowell D L 1994 Degradation of an Ni–Ti alloy during cyclic loading *1994 North American Conf. on Smart Structures and Materials* (International Society for Optics and Photonics) pp 326–41

Lim T J and McDowell D L 1999 Mechanical behavior of an Ni–Ti shape memory alloy under axial-torsional proportional and nonproportional loading *J. Eng. Mater. Technol.* **121** 9–18

Liu Y and McCormick P 1990 Factors influencing the development of two-way shape memory in NiTi *Acta Metall. Mater.* **38** 1321–6

Liu Y, Xie Z, Van Humbeeck J and Delaey L 1998 Asymmetry of stress–strain curves under tension and compression for NiTi shape memory alloys *Acta Mater.* **46** 4325–38

Lovey F, Rodriguez P, Malarria J, Sade M and Torra V 1995 On the origin of the two way shape memory effect in Cu–Zn–Al alloys *J. Phys.* IV **5** 287–92

Machado L and Savi M 2003 Medical applications of shape memory alloys *Braz. J. Med. Biol. Res.* **36** 683–91
Maletta C 2012 A novel fracture mechanics approach for shape memory alloys with trilinear stress–strain behavior *Int. J. Fract.* **177** 39–51
Maletta C, Falvo A, Furgiuele F, Barbieri G and Brandizzi M 2009 Fracture behaviour of nickel–titanium laser welded joints *J. Mater. Eng. Perform.* **18** 569–74
Maletta C and Furgiuele F 2010 Analytical modeling of stress-induced martensitic transformation in the crack tip region of nickel–titanium alloys *Acta Mater.* **58** 92–101
Maletta C and Furgiuele F 2011 Fracture control parameters for NiTi based shape memory alloys *Int. J. Solids Struct.* **48** 1658–64
Maletta C and Young M 2011 Stress-induced martensite in front of crack tips in NiTi shape memory alloys: modeling versus experiments *J. Mater. Eng. Perform.* **20** 597–604
Manson S S 1953 *Behavior of Materials Under Conditions of Thermal Stress* NACA TN 2933
Mantovani D 2000 Shape memory alloys: properties and biomedical applications *JOM* **52** 36–44
Maruyama T, Kurita T, Kozaki S, Andou K, Farjami S and Kubo H 2008 Innovation in producing crane rail fishplate using Fe–Mn–Si–Cr based shape memory alloy *Mater. Sci. Technol.* **24** 908–12
Matsuzaki Y, Naito H, Ikeda T and Funami K 2001 Thermo-mechanical behavior associated with pseudoelastic transformation of shape memory alloys *Smart Mater. Struct.* **10** 884
McCormick P, Liu Y and Miyazaki S 1993 Intrinsic thermal-mechanical behaviour associated with the stress-induced martensitic transformation in NiTi *Mater. Sci. Eng.* A **167** 51–6
McDonald Schetky L 1991 Shape memory alloy applications in space systems *Mater. Des.* **12** 29–32
McKelvey A and Ritchie R 2001 Fatigue-crack growth behavior in the superelastic and shape-memory alloy nitinol *Metall. Mater. Trans.* A **32** 731–43
Mehrabi R, Kadkhodaei M and Elahinia M 2014a A thermodynamically-consistent microplane model for shape memory alloys *Int. J. Solids Struct.* **51** 2666–75
Mehrabi R, Kadkhodaei M and Elahinia M 2014b Constitutive modeling of tension–torsion coupling and tension–compression asymmetry in NiTi shape memory alloys *Smart Mater. Struct.* **23** 75021–35
Melton K and Mercier O 1979 Fatigue of NiTi thermoelastic martensites *Acta Metall.* **27** 137–44
Meraghni F, Chemisky Y, Piotrowski B, Echchorfi R, Bourgeois N and Patoor E 2014 Parameter identification of a thermodynamic model for superelastic shape memory alloys using analytical calculation of the sensitivity matrix *Eur. J. Mech.* A **45** 226–37
Merzouki T, Duval A and Ben Zineb T 2012 Finite element analysis of a shape memory alloy actuator for a micropump *Simul. Modelling Pract. Theory* **27** 112–26
Mirzaeifar R, Shakeri M, DesRoches R and Yavari A 2011 A semi-analytic analysis of shape memory alloy thick-walled cylinders under internal pressure *Arch. Appl. Mech.* **81** 1093–116
Miyazaki S, Mizukoshi K, Ueki T, Sakuma T and Liu Y 1999 Fatigue life of Ti-50 at% Ni and Ti–40Ni–10Cu (at%) shape memory alloy wires *Mater. Sci. Eng.* A **273** 658–63
Miyazaki S, Otsuka K and Suzuki Y 1981 Transformation pseudoelasticity and deformation behavior in a Ti–50.6 at%Ni alloy *Scr. Metall.* **15** 287–92
Morgan N 2004 Medical shape memory alloy applications the market and its products *Mater. Sci. Eng.* A **378** 16–23 *European Symp. on Martensitic Transformation and Shape-Memory*
Morin C 2011 A comprehensive approach for fatigue analysis of shape memory alloys *PhD Thesis* Palaiseau, Ecole Polytechnique
Morin C, Moumni Z and Zaki W 2011a A constitutive model for shape memory alloys accounting for thermomechanical coupling *Int. J. Plast.* **27** 748–67
Morin C, Moumni Z and Zaki W 2011b Influence of heat transfer on the thermomechanical behavior of shape memory alloys *Int. Rev. Mech. Eng.* **5** 329–39
Moumni Z 1995 Sur la modélisation du changement de phase à l'état solide *PhD Thesis* Ecole Nationale Supérieure des Ponts et Chaussées
Moumni Z, Zaki W and Maitournam H 2009 Cyclic behavior and energy approach to the fatigue of shape memory alloys *J. Mech. Mater. Struct.* **4** 395–411
Moumni Z, Zaki W and Maitournam H 2014 Cyclic behavior and energy approach of the fatigue of shape memory alloys *Vietnam J. Mech.* **31** 191–210
Moumni Z, Zaki W, Nguyen Q and Zhang W 2015 Modeling of materials capable of solid–solid phase transformation. Application to the analytical solution of the semi-infinite mode III crack problem in a phase-changing solid *Int. J. Non-Linear Mech.* **69** 146–56
Moussa M O, Moumni Z, Doaré O, Touzé C and Zaki W 2012 Non-linear dynamic thermomechanical behaviour of shape memory alloys *J. Intell. Mater. Syst. Struct.* **23** 1593–611
Mukherjee K, Sircar S and Dahotre N B 1985 Thermal effects associated with stress-induced martensitic transformation in a TiNi alloy *Mater. Sci. Eng.* **74** 75–84
Müller I 2012 Pseudo-elastic hysteresis in shape memory alloys *Physica* B **407** 1314–5
Müller I and Seelecke S 2001 Thermodynamic aspects of shape memory alloys *Math. Comput. Modelling* **34** 1307–55
Nascimento M, De Araújo C, de Almeida L, da Rocha Neto J and Lima A 2009 A mathematical model for the strain–temperature hysteresis of shape memory alloy actuators *Mater. Des.* **30** 551–6
Nascimento M M S, da Rocha Neto J S, de Lima A M N, de Almeida L A and de Araújo C J 2004 A model for strain–temperature loops in shape memory alloy actuators *Cep* **58109** 970
Niinomi M 2008 Mechanical biocompatibilities of titanium alloys for biomedical applications *J. Mech. Behav. Biomed. Mater.* **1** 30–42
Nishimura F and Tanaka K 1998 Phenomenological analysis of thermomechanical training in an Fe-based shape memory alloy *Comput. Mater. Sci.* **12** 26–38
Nishimura F, Watanabe N and Tanaka K 1996 Transformation lines in an Fe-based shape memory alloy under tensile and compressive stress states *Mater. Sci. Eng.* A **221** 134–42
Nishimura F, Watanabe N and Tanaka K 1998 Back stress and shape recoverability during reverse transformation in an Fe-based shape memory alloy *Mater. Sci. Eng.* A **247** 275–84
Nishimura F, Watanabe N, Watanabe T and Tanaka K 1999 Transformation conditions in an Fe-based shape memory alloy under tensile-torsional loads: martensite start surface and austenite start/finish planes *Mater. Sci. Eng.* A **264** 232–44
Olsen J, Zhang Z, Hals J and Lu H 2011 Effect of notches on the behavior of superelastic round-bar NiTi-specimens *Smart Mater. Struct.* **20** 025014
Olsen J, Zhang Z, Lu H and van der Eijk C 2012 Fracture of notched round-bar NiTi-specimens *Eng. Fract. Mech.* **84** 1–4
Orgéas L and Favier D 1995 Non-symmetric tension–compression behaviour of NiTi alloy *J. Phys.* IV **5** C8–605
Orgéas L and Favier D 1998 Stress-induced martensitic transformation of a NiTi alloy in isothermal shear, tension and compression *Acta Mater.* **46** 5579–91
Ortín J 1992 Preisach modeling of hysteresis for a pseudoelastic Cu–Zn–Al single crystal *J. Appl. Phys.* **71** 1454–61
Ortin J and Planes A 1989 Thermodynamics of thermoelastic martensitic transformations *Acta Metall.* **37** 1433–41

Oshima R and Naya E 1978 Reversible shape memory effect in a $\beta_1$ Cu–Zn alloy containing $\alpha$ precipitates *J. Japan Inst. Met.* **42** 463–9

Paiva A, Savi M A, Braga A M B and Pacheco P M C L 2005 A constitutive model for shape memory alloys considering tensile–compressive asymmetry and plasticity *Int. J. Solids Struct.* **42** 3439–57

Panico M and Brinson L 2007 A three-dimensional phenomenological model for martensite reorientation in shape memory alloys *J. Mech. Phys. Solids* **55** 2491–511

Panoskaltsis V, Bahuguna S and Soldatos D 2004 On the thermomechanical modeling of shape memory alloys *Int. J. Non-Linear Mech.* **39** 709–22

Paris P C 1964 The fracture mechanics approach to fatigue, fatigue—an interdisciplinary approach *Proc. 10th Sagamore Army Materials Research Conf. (Sagamore Conference Center, Raquette Lake, New York)* pp 107–32

Patoor E, El Amrani M, Eberhardt A and Berveiller M 1995 Determination of the origin for the dissymmetry observed between tensile and compression tests on shape memory alloys *J. Phys.* IV **5** 495–500

Peigney M and Seguin J 2013 An incremental variational approach to coupled thermo-mechanical problems in inelastic solids. Application to shape-memory alloys *Int. J. Solids Struct.* **50** 4043–54

Perkins J 1974 Residual stresses and the origin of reversible (two-way) shape memory effects *Scr. Metall.* **8** 1469–76

Perkins J and Sponholz R 1984 Stress-induced martensitic transformation cycling and two-way shape memory training in Cu–Zn–Al alloys *Metall. Trans.* A **15** 313–21

Petrini L and Migliavacca F 2011 Biomedical applications of shape memory alloys *J. Metall.* **2011** 501483

Peultier B, Ben Zineb T and Patoor E 2006 Macroscopic constitutive law of shape memory alloy thermomechanical behaviour. Application to structure computation by FEM *Mech. Mater.* **38** 510–24

Peultier B, Ben Zineb T and Patoor E 2008 A simplified micromechanical constitutive law adapted to the design of shape memory applications by finite element methods *Mater. Sci. Eng.* A **481** 384–8

Pieczyska E, Gadaj S, Nowacki W and Tobushi H 2006 Phase-transformation fronts evolution for stress-and strain-controlled tension tests in TiNi shape memory alloy *Exp. Mech.* **46** 531–42

Pons J, Masse M and Portier R 1999 Thermomechanical cycling and two-way memory effect induced in Cu–Zn–Al *Mater. Sci. Eng.* A **273** 610–5

Popov P and Lagoudas D C 2007 A 3D constitutive model for shape memory alloys incorporating pseudoelasticity and detwinning of self-accommodated martensite *Int. J. Plast.* **23** 1679–720

Predki W, Klönne M and Knopik A 2006 Cyclic torsional loading of pseudoelastic NiTi shape memory alloys: damping and fatigue failure *Mater. Sci. Eng.* A **417** 182–9

Predki W, Knopik A and Bauer B 2008 Engineering applications of NiTi shape memory alloys *Mater. Sci. Eng.* A **481-482** 598–601 *Proc. 7th European Symposium on Martensitic Transformations ESOMAT 2006*

Pruett J P, Clement D J and Carnes D L Jr 1997 Cyclic fatigue testing of nickel–titanium endodontic instruments *J. Endodontics* **23** 77–85

Qiu S, Clausen B, Padula S, Noebe R and Vaidyanathan R 2011 On elastic moduli and elastic anisotropy in polycrystalline martensitic NiTi *Acta Mater.* **59** 5055–66

Rachikger W 1958 A 'super-elastic' single crystal calibration bar *Br. J. Appl. Phys.* **9** 250

Rahim M, Frenzel J, Frotscher M, Pfetzing-Micklich J, Steegmüller R, Wohlschlögel M, Mughrabi H and Eggeler G 2013 Impurity levels and fatigue lives of pseudoelastic NiTi shape memory alloys *Acta Mater.* **61** 3667–86

Rajagopalan S, Little A L, Bourke M A M and Vaidyanathan R 2005 Elastic modulus of shape-memory NiTi from in situ neutron diffraction during macroscopic loading, instrumented indentation, and extensometry *Appl. Phys. Lett.* **86** 081901

Ramaiah K, Saikrishna C, Ranganath V, Buravalla V and Bhaumik S 2011 Fracture of thermally activated NiTi shape memory alloy wires *Mater. Sci. Eng.* A **528** 5502–10

Raniecki B and Lexcellent C 1994 $R_L$-models of pseudoelasticity and their specification for some shape memory solids *Eur. J. Mech.* A **13** 21–50

Raniecki B and Lexcellent C 1998 Thermodynamics of isotropic pseudoelasticity in shape memory alloys *Eur. J. Mech.* A **17** 185–205

Raniecki B and Mróz Z 2008 Yield or martensitic phase transformation conditions and dissipation functions for isotropic, pressure-insensitive alloys exhibiting sd effect *Acta Mech.* **195** 81–102

Raniecki B, Tanaka K and Ziółkowski A 2001 Testing and modeling of NiTi SMA at complex stress state-selected results of polish-Japanese research cooperation *Mater. Sci. Res. Int. Spec. Tech. Publ.* **2** 327–34

Reuss A 1929 Berechnung der fließgrenze von mischkristallen auf grund der plastizitätsbedingung für einkristalle *J. Appl. Math. Mech./Z. Angew. Math. Mech.* **9** 49–58

Rice J and Rosengren G 1968 Plane strain deformation near a crack tip in a power-law hardening material *J. Mech. Phys. Solids* **16** 1–2

Rizzoni R and Marfia S 2015 A thermodynamical formulation for the constitutive modeling of a shape memory alloy with two martensite phases *Meccanica* **50** 1121–45

Robertson S, Mehta A, Pelton A and Ritchie R 2007 Evolution of crack-tip transformation zones in superelastic nitinol subjected to in situ fatigue: a fracture mechanics and synchrotron x-ray microdiffraction analysis *Acta Mater.* **55** 6198–207

Rogueda C, Lexcellent C and Bocher L 1996 Experimental study of pseudoelastic behaviour of a CuZnAl polycrystalline shape memory alloy under tension–torsion proportional and non-proportional loading tests *Arch. Mech.- Arch. Mech. Stosow.* **48** 1025–45

Rogueda C, Vacher P, Lexcellent C, Contardo L and Guenin G 1991 Pseudoelastic behavior and two way memory effect in Cu–Zn–Al alloys *J. Phys.* IV **1** 409–14

Runciman A, Xu D, Pelton A R and Ritchie R O 2011 An equivalent strain Coffin–Manson approach to multiaxial fatigue and life prediction in superelastic nitinol medical devices *Biomaterials* **32** 4987–93

Sade M, Rapacioli R and Ahlers M 1985 Fatigue in Cu–Zn–Al single crystals *Acta Metall.* **33** 487–97

Saint-Sulpice L, Chirani S A and Calloch S 2009 A 3D super-elastic model for shape memory alloys taking into account progressive strain under cyclic loadings *Mech. Mater.* **41** 12–26

Saitoh K and Liu W K 2009 Molecular dynamics study of surface effect on martensitic cubic-to-tetragonal transformation in Ni–Al alloy *Comput. Mater. Sci.* **46** 531–44

Saleeb A, Padula Ii S and Kumar A 2011 A multi-axial, multimechanism based constitutive model for the comprehensive representation of the evolutionary response of SMAs under general thermomechanical loading conditions *Int. J. Plast.* **27** 655–87

Sateesh V, Senthilkumar P, Satisha and Dayananda G 2014 Low cycle fatigue evaluation of NiTi SESMA thin wires *J. Mater. Eng. Perform.* **23** 2429–36

Sato Y and Tanaka K 1988 Estimation of energy dissipation in alloys due to stress-induced martensitic transformation *Res. Mech.* **23** 381–93

Savi M A 2015 Nonlinear dynamics and chaos in shape memory alloy systems *Int. J. Non-Linear Mech.* **70** 2–19

Savi M A, Paiva A, Baeta-Neves A P and Pacheco P M 2002 Phenomenological modeling and numerical simulation of shape memory alloys: a thermo-plastic-phase transformation coupled model *J. Intell. Mater. Syst. Struct.* **13** 261–73

Sawaguchi T, Bujoreanu L-G, Kikuchi T, Ogawa K, Koyama M and Murakami M 2008 Mechanism of reversible transformation-induced plasticity of Fe–Mn–Si shape memory alloys *Scr. Mater.* **59** 826–9

Schroeder T and Wayman C 1977 The two-way shape memory effect and other training phenomena in Cu–Zn single crystals *Scr. Metall.* **11** 225–30

Scirè Mammano G and Dragoni E 2014 Effects of loading and constraining conditions on the thermomechanical fatigue life of NiTi shape memory wires *J. Mater. Eng. Perform.* **23** 2403

Scirè Mammano G and Dragoni E 2015 Effect of stress, heating rate, and degree of transformation on the functional fatigue of Ni–Ti shape memory wires *J. Mater. Eng. Perform.* **24** 2709–19

Sedlak P, Frost M, Benešová B, Ben Zineb T and Šittner P 2012 Thermomechanical model for NiTi-based shape memory alloys including *R*-phase and material anisotropy under multi-axial loadings *Int. J. Plast.* **39** 132–51

Sedlák P, Frost M, Kruisová A, Hiřmanová K, Heller L and Šittner P 2014 Simulations of mechanical response of superelastic NiTi helical spring and its relation to fatigue resistance *J. Mater. Eng. Perform.* **23** 2591–8

Sehitoglu H, Anderson R, Karaman I, Gall K and Chumlyakov Y 2001 Cyclic deformation behavior of single crystal NiTi *Mater. Sci. Eng.* A **314** 67–74

Sgambitterra E, Bruno L and Maletta C 2014 Stress induced martensite at the crack tip in NiTi alloys during fatigue loading *Fract. Struct. Integrity* **8** 167–73

Sharabash A M and Andrawes B O 2009 Application of shape memory alloy dampers in the seismic control of cable-stayed bridges *Eng. Struct.* **31** 607–16

Shaw J A and Kyriakides S 1995 Thermomechanical aspects of NiTi *J. Mech. Phys. Solids* **43** 1243–81

Siredey N, Hautcoeur A and Eberhardt A 2005 Lifetime of superelastic Cu–Al–Be single crystal wires under bending fatigue *Mater. Sci. Eng.* A **396** 296–301

Smith K, Topper T and Watson P 1970 A stress–strain function for the fatigue of metals (stress–strain function for metal fatigue including mean stress effect) *J. Mater.* **5** 767–78

Song D, Kang G, Kan Q, Yu C and Zhang C 2015 Damage-based life prediction model for uniaxial low-cycle stress fatigue of super-elastic NiTi shape memory alloy microtubes *Smart Mater. Struct.* **24** 085007

Song G, Ma N and Li H-N 2006 Applications of shape memory alloys in civil structures *Eng. Struct.* **28** 1266–74

Souza A C, Mamiya E N and Zouain N 1998 Three-dimensional model for solids undergoing stress-induced phase transformations *Eur. J. Mech.* A **17** 789–806

Stalmans R, Van Humbeeck J and Delaey L 1992 The two way memory effect in copper-based shape memory alloys—thermodynamics and mechanisms *Acta Metall. Mater.* **40** 2921–31

Stoeckel D 1990 Shape memory actuators for automotive applications *Mater. Des.* **11** 302–7

Strnadel B, Ohashi S, Ohtsuka H, Ishihara T and Miyazaki S 1995 Cyclic stress–strain characteristics of Ti–Ni and Ti–Ni–Cu shape memory alloys *Mater. Sci. Eng.* A **202** 148–56

Sun L, Huang W M, Ding Z, Zhao Y, Wang C C, Purnawali H and Tang C 2012a Stimulus-responsive shape memory materials: a review *Mater. Des.* **33** 577–640

Sun Q P and Hwang K C 1998 Singularity at the apex of a rigid wedge embedded in a nonlinear material *J. Appl. Mech. Trans. ASME* **55** 361–4

Sun Q P, Zhao H, Zhou R, Saletti D and Yin H 2012b Recent advances in spatiotemporal evolution of thermomechanical fields during the solid–solid phase transition *C. R. Méc.* **340** 349–58

Tadaki T, Otsuka K and Shimizu K 1988 Shape memory alloys *Annu. Rev. Mater. Sci.* **18** 25–45

Taillard K, Arbab Chirani S, Calloch S and Lexcellent C 2008 Equivalent transformation strain and its relation with martensite volume fraction for isotropic and anisotropic shape memory alloys *Mech. Mater.* **40** 151–70

Tanaka K 1986 A thermomechanical sketch of shape memory effect: one-dimensional tensile behavior *Res. Mech.* **18** 251–63

Tanaka K, Nishimura F, Hayashi T, Tobushi H and Lexcellent C 1995 Phenomenological analysis on subloops and cyclic behavior in shape memory alloys under mechanical and/or thermal loads *Mech. Mater.* **19** 281–92

Thamburaja P 2005 Constitutive equations for martensitic reorientation and detwinning in shape-memory alloys *J. Mech. Phys. Solids* **53** 825–56

Thamburaja P 2010 A finite-deformation-based phenomenological theory for shape-memory alloys *Int. J. Plast.* **26** 1195–219

Thamburaja P and Anand L 2001 Polycrystalline shape-memory materials: effect of crystallographic texture *J. Mech. Phys. Solids* **49** 709–37

Thamburaja P and Nikabdullah N 2009 A macroscopic constitutive model for shape-memory alloys: theory and finite-element simulations *Comput. Methods Appl. Mech. Eng.* **198** 1074–86

Thamburaja P, Pan H and Chau F 2005 Martensitic reorientation and shape-memory effect in initially textured polycrystalline Ti–Ni sheet *Acta Mater.* **53** 3821–31

Thiebaud F, Lexcellent C, Collet M and Foltete E 2007 Implementation of a model taking into account the asymmetry between tension and compression, the temperature effects in a finite element code for shape memory alloys structures calculations *Comput. Mater. Sci.* **41** 208–21

Tobushi H, Nakahara T, Shimeno Y and Hashimoto T 2000 Low-cycle fatigue of TiNi shape memory alloy and formulation of fatigue life *J. Eng. Mater. Technol.* **122** 186–91

Ueland S M and Schuh C A 2012 Superelasticity and fatigue in oligocrystalline shape memory alloy microwires *Acta Mater.* **60** 282–92

Vacher P and Lexcellent C 1991 Study of pseudoelastic behaviour of polycrystalline shape memory alloys by resistivity measurements and acoustic emission *Mech. Behav. Mater.* VI **3** 231–6

Vaidyanathan R, Dunand D and Ramamurty U 2000 Fatigue crack-growth in shape-memory NiTi and NiTi–TiC composites *Mater. Sci. Eng.* A **289** 208–16

Van Humbeeck J 1999 Non-medical applications of shape memory alloys *Mater. Sci. Eng.* A **273** 134–48

Van Humbeeck J and Delaey L 1981 The influence of strain-rate, amplitude and temperature on the hysteresis of a pseudoelastic Cu–Zn–Al single crystal *J. Phys.* IV **42** 1007–11

Vieille B, Michel J-F, Boubakar M L and Lexcellent C 2007 Validation of a 3D numerical model of shape memory alloys pseudoelasticity through tensile and bulging tests on cualbe sheets *Int. J. Mech. Sci.* **49** 280–97

Vincent M, Thiebaud F, Khalifa S B H, Engels-Deutsch M and Zineb T B 2015 Finite element analysis of a copper single crystal shape memory alloy-based endodontic instruments *J. Mater. Eng. Perform.* 1–2 doi:10.1007/s11665-015-1677-9

Vivet A and Lexcellent C 1999 Observations and analysis of martensitic phase transformation on CuZnAl single crystals *J. Phys.* IV **9** 411–8

Voigt W 1889 Ueber die beziehung zwischen den beiden elasticitätsconstanten isotroper Körper *Ann. Phys., Lpz.* **274** 573–87

Šittner P, Hara Y and Tokuda M 1995 Experimental study on the thermoelastic martensitic transformation in shape memory alloy polycrystal induced by combined external forces *Metall. Mater. Trans.* A **26** 2923–35

Šittner P, Heller L, Pilch J, Curfs C, Alonso T and Favier D 2014 Youngs modulus of austenite and martensite phases in superelastic NiTi wires *J. Mater. Eng. Perform.* **23** 2303–14

Wack B, Terriez J-M and Guelin P 1983 A hereditary type, discrete memory, constitutive equation with applications to simple geometries *Acta Mech.* **50** 9–37
Wagner M, Sawaguchi T, Kausträter G, Höffken D and Eggeler G 2004 Structural fatigue of pseudoelastic NiTi shape memory wires *Mater. Sci. Eng.* A **378** 105–9
Wagner M-X and Windl W 2008 Lattice stability, elastic constants and macroscopic moduli of NiTi martensites from first principles *Acta Mater.* **56** 6232–45
Wang G 2006 Effects of notch geometry on stress–strain distribution, martensite transformation and fracture behavior in shape memory alloy NiTi *Mater. Sci. Eng.* A **434** 269–79
Wang G 2007 Effect of martensite transformation on fracture behavior of shape memory alloy NiTi in a notched specimen *Int. J. Fract.* **146** 93–104
Wang G, Xuan F, Tu S and Wang Z 2010 Effects of triaxial stress on martensite transformation, stress–strain and failure behavior in front of crack tips in shape memory alloy NiTi *Mater. Sci. Eng.* A **527** 1529–36
Wang J and Sehitoglu H 2014 Martensite modulus dilemma in monoclinic NiTi-theory and experiments *Int. J. Plast.* **61** 17–31
Wang J, Sehitoglu H and Maier H 2014a Dislocation slip stress prediction in shape memory alloys *Int. J. Plast.* **54** 247–66
Wang L, Rong L, Yan D, Jiang Z and Li Y 2005a DSC study of the reverse martensitic transformation behavior in a shape memory alloy pipe-joint *Intermetallics* **13** 403–7
Wang X, Cao W, Deng C, Liu H, Pfetzing-Micklich J and Yue Z 2014b The effect of notches on the fatigue behavior in NiTi shape memory alloys *Mater. Sci. Eng.* A **610** 188–96
Wang X, Wang Y, Baruj A, Eggeler G and Yue Z 2005b On the formation of martensite in front of cracks in pseudoelastic shape memory alloys *Mater. Sci. Eng.* A **394** 393–8
Wang X, Xu B and Yue Z 2008 Micromechanical modelling of the effect of plastic deformation on the mechanical behaviour in pseudoelastic shape memory alloys *Int. J. Plast.* **24** 1307–32
Wasilewski R 1971 The effects of applied stress on the martensitic transformation in TiNi *Metall. Mater. Trans.* B **2** 2973–81
Webb G, Kurdila A and Lagoudas D 2000 Adaptive hysteresis model for model reference control with actuator hysteresis *J. Guid. Control Dyn.* **23** 459–65
Williams E A, Shaw G and Elahinia M 2010 Control of an automotive shape memory alloy mirror actuator *Mechatronics* **20** 527–34
Xiong F and Liu Y 2007 Effect of stress-induced martensitic transformation on the crack tip stress-intensity factor in Ni–Mn–Ga shape memory alloy *Acta Mater.* **55** 5621–9
Zhang Y *et al* 2016 Energy-based fatigue model for shape memory alloys including thermomechanical coupling *Smart Mater. Struct.* **25** 035042
Yan W and Mai Y-W 2006 Theoretical consideration on the fracture of shape memory alloys *IUTAM Symp. on Mechanics and Reliability of Actuating Materials* (Berlin: Springer) pp 217–26
Yan W, Wang C H, Zhang X P and Mai Y-W 2003 Theoretical modelling of the effect of plasticity on reverse transformation in superelastic shape memory alloys *Mater. Sci. Eng.* A **354** 146–57
Yi S and Gao S 2000 Fracture toughening mechanism of shape memory alloys due to martensite transformation *Int. J. Solids Struct.* **37** 5315–27
Yi S, Gao S and Shen L 2001 Fracture toughening mechanism of shape memory alloys under mixed-mode loading due to martensite transformation *Int. J. Solids Struct.* **38** 4463–76
Yin H, He Y and Sun Q 2014 Effect of deformation frequency on temperature and stress oscillations in cyclic phase transition of NiTi shape memory alloy *J. Mech. Phys. Solids* **67** 100–28
Young J M and Van Vliet K J 2005 Predicting in vivo failure of pseudoelastic NiTi devices under low cycle, high amplitude fatigue *J. Biomed. Mater. Res.* B **72** 17–26
Young M, Gollerthan S, Baruj A, Frenzel J, Schmahl W W and Eggeler G 2013 Strain mapping of crack extension in pseudoelastic NiTi shape memory alloys during static loading *Acta Mater.* **61** 5800–6
Yu C, Kang G and Kan Q 2014a Study on the rate-dependent cyclic deformation of super-elastic NiTi shape memory alloy based on a new crystal plasticity constitutive model *Int. J. Solids Struct.* **51** 4386–405
Yu C, Kang G and Kan Q 2014b Crystal plasticity based constitutive model of NiTi shape memory alloy considering different mechanisms of inelastic deformation *Int. J. Plast.* **54** 132–62
Yu C, Kang G, Kan Q and Song D 2013 A micromechanical constitutive model based on crystal plasticity for thermo-mechanical cyclic deformation of NiTi shape memory alloys *Int. J. Plast.* **44** 161–91
Yu C, Kang G, Song D and Kan Q 2012 Micromechanical constitutive model considering plasticity for super-elastic NiTi shape memory alloy *Comput. Mater. Sci.* **56** 1–5
Yu C, Kang G, Song D and Kan Q 2015 Effect of martensite reorientation and reorientation-induced plasticity on multiaxial transformation ratchetting of super-elastic NiTi shape memory alloy: new consideration in constitutive model *Int. J. Plast.* **67** 69–101
Zaki W 2012 An efficient implementation for a model of martensite reorientation in martensitic shape memory alloys under multiaxial nonproportional loading *Int. J. Plast.* **37** 72–94
Zaki W, Morin C and Moumni Z 2010a A simple 1D model with thermomechanical coupling for superelastic SMAs *IOP Conf. Ser.: Mater. Sci. Eng.* 10012149
Zaki W and Moumni Z 2007a A three-dimensional model of the thermomechanical behavior of shape memory alloys *J. Mech. Phys. Solids* **55** 2455–90
Zaki W and Moumni Z 2007b A 3D model of the cyclic thermomechanical behavior of shape memory alloys *J. Mech. Phys. Solids* **55** 2427–54
Zaki W, Moumni Z and Morin C 2011 Modeling tensile–compressive asymmetry for superelastic shape memory alloys *Mech. Adv. Mater. Struct.* **18** 559–64
Zaki W, Zamfir S and Moumni Z 2010b An extension of the ZM model for shape memory alloys accounting for plastic deformation *Mech. Mater.* **42** 266–74
Zhao Y, Taya M, Kang Y and Kawasaki A 2005 Compression behavior of porous NiTi shape memory alloy *Acta Mater.* **53** 337–43
Zhou B 2012 A macroscopic constitutive model of shape memory alloy considering plasticity *Mech. Mater.* **48** 71–81
Zhu S and Zhang Y 2007 A thermomechanical constitutive model for superelastic SMA wire with strain-rate dependence *Smart Mater. Struct.* **16** 1696–707
Zhu Y, Zhang Y and Zhao D 2014 Softening micromechanical constitutive model of stress induced martensite transformation for NiTi single crystal shape memory alloy *Sci. China Phys. Mech. Astron.* **57** 1946–58